The physics of line-driven winds of hot massive stars

Front cover: “2010 NR37”, an artist’s impression of the night sky based on a composition of Hubble Space Telescope images. Painted by Michiel Muyres.

This research has been supported by:
Nederlandse Onderzoekschool voor Astronomie (NOVA).

The physics of line-driven winds of hot massive stars

ACADEMISCH PROEFSCHRIFT

ter verkrijging van de graad van doctor
aan de Universiteit van Amsterdam
op gezag van de Rector Magnificus
prof. dr. D. C. van den Boom
ten overstaan van een door het college voor promoties
ingestelde commissie,
in het openbaar te verdedigen in de Agnietenkapel
op vrijdag 12 november 2010, te 14:00 uur.

door

Lianne Emma Muijres

geboren te Sittard

Promotiecommissie:

Promotores:	Prof. dr. A. de Koter
	Prof. dr. N. Langer
Co-promotor:	dr. J. S. Vink
Overige leden:	Prof. dr. M.B.M. van der Klis
	Prof. dr. L. Kaper
	Prof. dr. H.F. Henrichs
	Prof. dr. L.B.F.M. Waters
	Prof. dr. H.J.G.L.M. Lamers
	dr. J. Puls

Faculteit der Natuurwetenschappen, Wiskunde en Informatica

The research reported in this thesis was carried out at the Astronomical Institute "Anton Pannekoek", at the Universiteit van Amsterdam, The Netherlands.

Por Ana Paula, Rafael, Roney, Danila, e Fernanda.
Todos nós temos a força para lutar
pelo nosso futuro, por um mundo melhor.
Nunca desistam!

Contents

1 Introduction

1.1 Massive stars in the universe

A starry night in the Chilean desert is one of the most beautiful views a person can see in her or his life. One is overwhelmed by the immensity of our galaxy (see Figure 1.1), and is intrigued by the presence of two of its satellites, the Large and Small Magellanic Cloud.

Galaxies are comprised of stars and clouds of gas. Stars that appear equally bright to the naked eye may either be nearby objects that are relatively dim or distant objects that are very luminous. The intrinsically brightest stars are the topic of this thesis. Their luminosities can be more than a million times that of our Sun, which is considered a nominal star. These stars are also the most massive ones, some of them starting their lives with perhaps more than a hundred times the mass of our Sun. Although spectacular objects, massive stars are rare. Depending on the adopted lower mass limit – usually eight solar masses – only some hundred thousands of such objects may exist in our galaxy, that overall contains approximately 10^{11} stars.

Why are we urged to understand these massive and luminous objects if they only comprise such a very small fraction of the stellar population? One compelling reason is that they are so extreme. They have short lifetimes – measured in millions of years rather than billions – and end their lives in a supernova explosion or gamma-ray burst, that can be seen throughout the universe. For the major part of their existence, their surface layers are extremely hot. Therefore, the many photons they emit are sufficiently energetic to heat-up, ionize, or facilitate chemical reactions in the gaseous material or microscopically small solid particles in their surroundings, called the interstellar medium.

Moreover their supernova explosions send shock waves through the interstellar medium, possibly triggering new epochs of star formation (e.g. Tenorio-Tagle & Bodenheimer 1988; Oey & Massey 1995). The material that is ejected in this explosion is enriched with chemical species produced in the star by nuclear fusion in its cen-

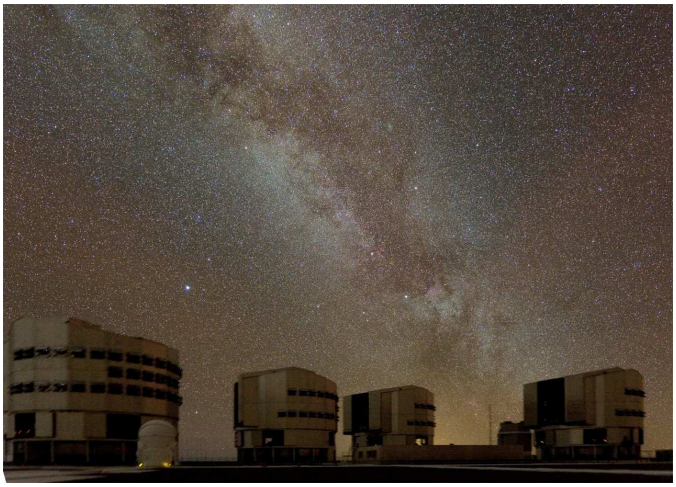

Figure 1.1: The Milky Way above Paranal in the Chilean Atacama desert where the most advanced European optical telescope, the Very Large Telescope (VLT) of the European Southern Observaty (ESO), was built. Courtesy: S. Deiries/ESO

ter but also elements with an atomic number higher than iron produced by neutron capture in the explosion. In this way, the ambient medium is enriched with these new elements. As a consequence, later generations of stars will be composed of a chemical mixture that contains a larger fraction of, for instance, metals.

It is not only through explosions that massive stars inject material into the interstellar medium. They do this – in a much milder way – during their entire lives, by powering a more or less spherical outflow of ionized gas. These outflows are called stellar winds. They create large bubbles around the stars by sweeping up the interstellar gas that is encountered (see Figure 1.2). Through these stellar winds, massive stars lose mass. This may severely affect their course of evolution – i.e. the way in which they change their physical state over time –, as well as the properties of their supernova explosions, and the nature of the compact object – a neutron star or black hole – that is left behind.

Beyond stellar physics, another reason to study these massive objects comes from considerations pertinent to the early universe. The mass distribution of the first generation of stars formed in our universe, some 400 million years after the Big Bang, is thought to be different from the present-day mass distribution. At these early times, massive stars dominated, with perhaps a sizable fraction of stars exceeding hundreds of solar masses (Abel et al. 2002; Bromm et al. 2002; Nakamura & Umemura 2002; Bromm & Larson 2004; Loeb et al. 2008). It is particularly interesting to ponder on the question of how much mass stars of the first generation might have lost through stellar winds, prior to their supernova explosions. If the time integrated mass loss is

small, or even negligible, they may have left black holes with masses of $\sim 10^2\,M_\odot$, that may have been pivotal in creating the first galaxies. If such first galaxies collided, these black holes might have merged and may be identified as the building blocks of the supermassive black holes detected in the centers of galaxies today (Kawakatu et al. 2005).

So, did these First Stars have stellar winds? If so, are the properties of these winds different from those of the massive stars of today? If they are not, it is extremely unlikely that massive black holes have been produced in the way described above, as the winds of massive stars in our galaxy are so powerful that these may strip 80–90 percent of the initial mass of such a star prior to its supernova explosion (Maeder & Meynet 1994).

The physics of stellar winds is the central theme of this thesis. A state-of-the-art method is presented that allows to determine the wind properties – notably the rate of mass loss and the terminal velocity at which this material is expelled from the star – of hot massive stars, given their global properties (for instance mass, luminosity, surface temperature) and surface chemical composition (for instance a metal-poor or a metal-rich mixture). In this first chapter, we will introduce stellar winds and present an overview of the studies presented in this thesis. We start by recapping some aspects of the evolution of massive stars (Sect. 1.2). Then, we briefly summarize some observed properties of massive star winds (Sect. 1.3). The driving mechanism of the winds of hot massive stars is described in Sect. 1.4. Finally, Sect. 1.5 provides an overview of the individual chapters of this thesis.

1.2 The evolution of massive stars

Most stars are in hydrostatic equilibrium. They obey a well defined relation between their mass M and luminosity L. Roughly, $L \propto M^\alpha$, where $1 < \alpha < 3$ (Kippenhahn & Weigert 1990). As the lifetime of a star τ is expected to be proportional to M/L this implies that $\tau \propto 1/M^{\alpha-1}$. It implies that, given a lifetime of 10 billion years for the Sun, a 100 $M_\odot$ star may live only on the order of a few million years.

During most of their life, massive stars produce their energy by thermonuclear burning of hydrogen to helium in their centers, where temperature and pressure are sufficiently high to overcome the strong repelling Coulomb forces between protons. The chain of reactions relevant for massive stars, in which eventually four protons are merged into one helium nucleus, involves catalyst species. These are carbon, nitrogen, and oxygen. Therefore, the chain of reactions is referred to as the CNO-cycle. This phase in the star's evolution encompasses about 90 percent of the total lifetime and lasts until all hydrogen is converted into helium in the stellar core. It is referred to as the main sequence phase of evolution, after which the star experiences a short contraction phase until hydrogen burning ignites in a shell around the helium

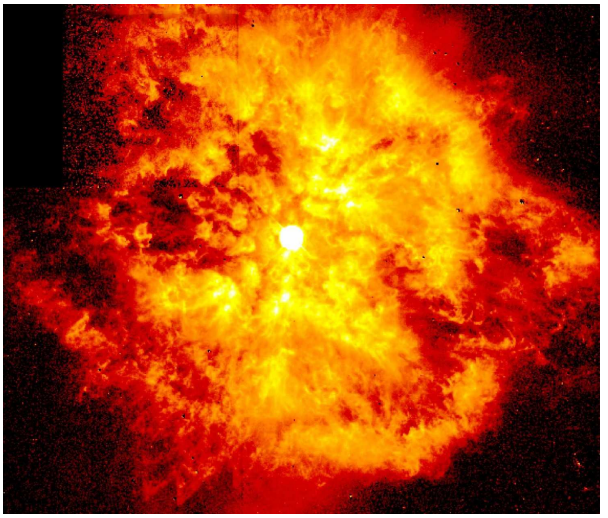

Figure 1.2: The M1-67 nebula surrounding WR 124: a Wolf-Rayet star, a massive star in a late evolutionary stage. The nebula with a diameter of about 2.3 parsec, is the result of the interaction of the stellar wind and material ejected in outbursts with the interstellar medium (Grosdidier et al. 1998; van der Sluys & Lamers 2003). The gas that we see here is ejected over at least tens of thousands of years. Courtesy: NASA, HST.

core. As a result the star expands and cools at the surface. The post main-sequence evolution of massive stars is complex and may involve many phases such as the blue supergiant, red supergiant, and the Wolf-Rayet phase. The evolutionary path the star follows, depends on many factors: e.g. its metal content, its mass, its rotational velocity, whether it is magnetic or not, and whether it is a single star or part of a multiple system.

In idealized circumstances, the initial conditions of the evolution completely determine the path the star takes. If the star does not form together with a companion, its mass, angular momentum and chemical composition fully specify what will happen to the star over time. The mass is a dominant parameter determining the total lifetime. Stars more massive than eight solar masses can prevent the carbon/oxygen core that develops after the main sequence has ended to become degenerate. This brings them on track to a supernova explosion. Lower mass stars, that do form degenerate cores, eject their outer layers and fade out as white dwarfs.

Rotation plays a more subtle role in the life of stars, at least at first sight. Through rotation the star may “feel” a slightly lower mass than it actually has, as the centrifugal forces associated with rotation help to balance gravity. Rotation, especially rapid rotation, induces internal mixing (see e.g. Maeder & Meynet 1996; Heger et al. 2000). Material from (close to) the core is dredged up to the surface – causing a change in

the chemical patterns as, for instance, products of CNO-cycle burning appear. Material from outside the core is dredged down into the core, delivering hydrogen, and prolonging the main sequence lifetime.

Interestingly, if the star is rotating with a significant fraction of its break-up velocity, i.e. the velocity at which the centrifugal force balances gravity at the stellar surface, the star may mix so efficiently that it becomes (quasi) chemically homogeneous (Maeder 1987; Langer 1991). Such stars evolve unlike normal (slowly or modestly rotating) stars, in that they do not inflate towards blue- or red supergiants. Rather they remain hot and compact. Massive stars in our galaxy may never experience such homogeneous evolution, because their stellar winds appear to be too strong. These winds not only carry away mass, but also angular momentum. In other words, galactic massive stars may spin down quite efficiently already in their main sequence stage. As we shall see below, stars with a chemical composition that is poor in metals have weaker winds (see e.g. Kudritzki et al. 1987; Kudritzki 2002; Vink & de Koter 2005). Such stars, if born rotating rapidly, may experience homogeneous evolution.

The chemically homogeneous evolving metal-poor stars have been proposed to be progenitors of long-duration gamma-ray bursts. These are very strong flashes of gamma-ray radiation. The current consensus is that long gamma-ray bursts may occur when a rapidly spinning massive star explodes as a supernova (see e.g. Hjorth et al. 2003). Studies of the progenitors of gamma-ray burts have been done by e.g. Hirschi et al. (2005); Yoon et al. (2006); Woosley & Heger (2006); Hirschi (2007).

An example of the behavior of a rapidly rotating metal-poor magnetic star of $40\,M_{\odot}$ in the Hertzsprung-Russell diagram – a plot of luminosity versus effective temperature– is shown by the grey curve in Fig. 1.3 (Yoon et al. 2006). This star remains hot during the course of its evolution since it evolves chemically homogeneous. In that same figure the evolution of a rapidly rotating $85\,M_{\odot}$ metal-poor star without internal magnetic fields is also presented (Hirschi 2007). This star becomes a cool supergiant, and spins down.

The third parameter controlling the evolution of stars is its chemical composition. Metal poor stars start their main sequence life being hotter than metal rich stars. The most important effect, however, is through the coupling between chemical composition and mass loss: both empirical and theoretical results show that the higher the metal content, the stronger the stellar wind (see e.g. Puls et al. 1996; Vink et al. 2001; Mokiem et al. 2007).

The mechanism that drives the wind is based on the absorption and scattering of photons in atomic transitions; the more complex atoms contribute stronger to the force, so the larger their abundance the higher the mass-loss rate. This rate scales in many cases with the metal content to the power ~ 0.7 (Vink et al. 2001; Krtička 2006; Mokiem et al. 2007). In other words, a massive star with a metal content ten

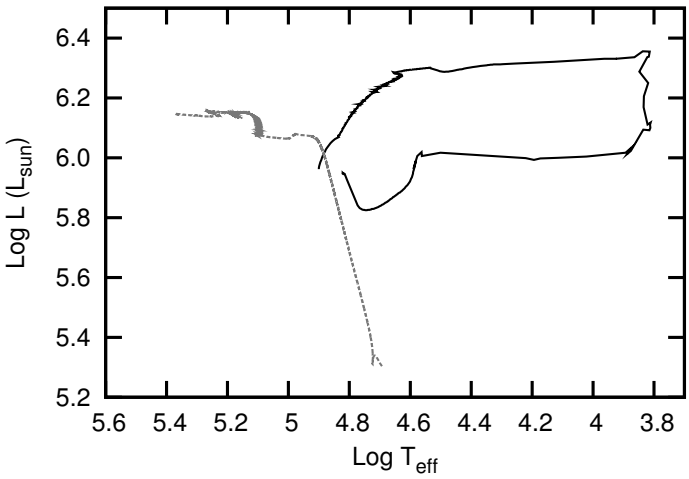

Figure 1.3: In this figure we present two different evolutionary tracks for low metallicity stars. The black track is that of a 85 $M_{\odot}$ star with an initial rotational velocity of 800 km/s from Hirschi (2007). The grey track is from Yoon et al. (2006). It belongs to a star with a mass of 40 $M_{\odot}$ and an initial rotational velocity of 555 km/s.

times lower than the Sun will lose mass at a rate 5 times lower than a star with the same properties but a solar chemical composition.

The effect of mass loss on the evolution of a massive star is twofold: the star becomes less massive and therefore the rate at which it burns nuclear fuel is affected, and the rotating star will spin down since the wind takes away angular momentum. During its life, a massive star in our galaxy may lose a significant fraction of its initial mass through its stellar wind, and almost all of its initial angular momentum. The mass-loss history of a star may also strongly impact the properties of its supernova explosion and the compact remnant it leaves behind.

Beside the effect of stellar winds, massive stars may also lose mass in eruptive processes (see e.g. Humphreys & Davidson 1994). These eruptive processes are not very well understood but tend to occur when the star becomes unstable by reaching either its critical rotation velocity, the so-called Eddington limit, i.e. when gravity is overcome by radiation forces at the surface, or a combination of both when the star reaches its Ω-Γ-limit (Maeder & Meynet 2000). Whether or not such eruptions depend on the metal content is unknown.

In the early universe, stars were very metal poor or practically metal free. The very first generation of stars or First Stars were formed from gas clouds containing almost only hydrogen and helium. Early on in their evolution, they may have produced small amounts of carbon, nitrogen and oxygen in their cores. These stars most likely do not

have a sufficient metal content to drive a stellar wind (Krtička & Kubát 2006). They may not lose any mass or angular momentum during their main sequence evolution if they do not suffer from mayor eruptive mass-loss events. In the later stages of their evolution, the (primary) carbon, nitrogen and oxygen produced at the center may surface due to internal mixing processes (Marigo et al. 2001, 2003; Yoon et al. 2006; Hirschi 2007). This happens in rapid rotators but also in slow rotators it could be the case (due to dredge up during the red supergiant phase). As a consequence the sum of the carbon, nitrogen and oxygen surface abundance may become higher than the total solar metal abundance. Will these enriched stars suffer from strong stellar winds? Their total metal content may be high but carbon, nitrogen and oxygen have a different atomic structure than elements like iron that are present in massive stars in our galaxy. Iron-like atoms are very efficient in driving a wind, more so than carbon, nitrogen and oxygen (Vink et al. 1999; Puls et al. 2000). The study of the wind properties of these CNO enriched very metal-poor stars is one of the subjects adressed in this thesis.

1.3 Observational properties of stellar winds

Hot massive stars reveal that they lose mass in several ways. For a detailed description of these signatures we refer to e.g. Lamers & Cassinelli (1999) or Kudritzki & Puls (2000), here we give a short overview. First, profiles of resonance lines of metal species such as carbon, nitrogen, oxygen, silicon and magnesium, located in the ultraviolet part of the spectrum, show shapes indicating a more or less spherical outflow of matter. These P Cygni lines probe up to about 10 stellar radii from the surface and are the most sensitive mass-loss rate ($\dot{M}$) diagnostics, allowing to measure rates as low as $10^{-9}\,M_{\odot}\mathrm{yr}^{-1}$. Second, recombination lines of hydrogen and helium in the optical and near-infrared parts of the spectrum are signatures of out-flowing gas close to the star (within ∼2 stellar radii). The hydrogen lines can probe mass-loss rates as low as $10^{-7}\,M_{\odot}\mathrm{yr}^{-1}$. Finally, continuum emission at infra-red or radio wavelengths provides a measure of the wind density, hence the mass-loss rate (Panagia & Felli 1975; Wright & Barlow 1975). Notably radio emission may originate from up to 30-100 stellar radii. As radio-fluxes tend to be weak for hot massive stars, only galactic objects can be studied in this way. The rates that can be measured probe the range of several times $10^{-7}\,M_{\odot}\mathrm{yr}^{-1}$ and up.

The best way to obtain an estimate of the terminal wind velocity is by measuring the location of the blue-edge of the absorption trough in saturated P Cygni profiles (see Figure 1.4). The blue-shifted region is caused by absorption of continuum photons in the gas in front of the stellar disk that is moving towards us. Though a simple measurement, a presence of turbulence in the outflow and photospheric absorption lines near the blue-edge may introduce a sizable uncertainty in the measurement of

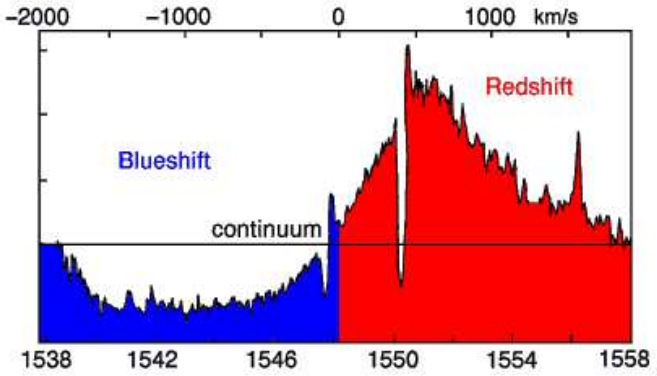

Figure 1.4: P Cygni line profile of the triply ionized carbon doublet at $\lambda\lambda$ 1548.2 Å - 1550.77 Å. Material that is moving toward (away from) the observer causes a blue-shift (red-shift) in the wavelength. The absorption is due to material in front of the stellar disk. The emission is symetric around the rest wavelength(s) of the doublet line. These type of profiles are characteristic for a radial outflow of gas. The sharp absorption lines are produced by the interstellar medium and mark the rest wavelengths of the triply ionized carbon doublet. Courtesy of the International Ultraviolet Explorer (IUE).

the terminal velocity, perhaps reaching 30 percent for specific types of stars. Typical values for the wind terminal velocity, v_∞ that have been deduced from these line profiles range between 400 km/s and 3300 km/s for stars hotter than 21 000 K and in between a 100 km/s and 1500 km/s for stars in the temperature range between 10 000 K and 21 000 K (Kudritzki & Puls 2000 based on Prinja et al. 1990; Howarth et al. 1997; Prinja & Massa 1998).

Deriving mass-loss rates for massive stars is a more complicated task. As mentioned above, there are several techniques that can be used depending on the strength of the stellar winds. In Figure 1.5, the logarithm of the empirically derived modified wind momentum – the product of the square root of the star's radius divided by the solar radius ($R_\star/R_\odot$), the terminal wind velocity and the mass-loss rate – $D_{\rm mom} = \sqrt{R_\star/R_\odot} \times \dot{M} v_\infty$, is plotted against the logarithm of the luminosity of the star. $D_{\rm mom}$ is for all practical purposes a measure of the mass-loss rate since v_∞ varies only within a factor 3 and $\sqrt{R_\star/R_\odot}$ within a factor 2 for the range of stars investigated in this figure. Considering $D_{\rm mom}$ rather than $\dot{M}$ has the advantage that it is (almost) independent of stellar mass and that also central stars of Planetary Nebulae and A supergiants, that also lose mass through the same mechanism, can be included in the comparison. The black dots are mass-loss rates determined from fitting the Hα line profile and the grey dots correspond to mass-loss rate estimates that strongly rely on ultraviolet resonance lines. One notes that there is a steep jump – of about a factor 100 – in the mass-loss rate at $10^{5.2}$ times the solar luminosity, illustrated by the red

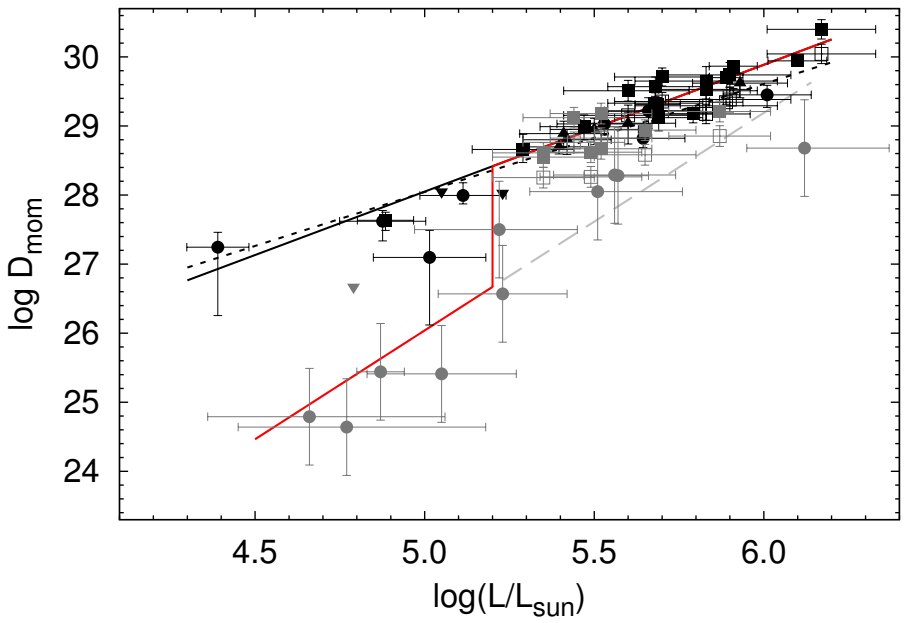

Figure 1.5: The modified wind momentum $\sqrt{R_\star/R_\odot}\dot{M}v_\infty$ as a function of stellar luminosity for galactic stars using the data of Mokiem et al. (2007) and references there in. Black symbols refer to mass-loss estimates based on the fitting of the Hα-profile; grey symbols are mass-loss estimates from ultraviolet resonance lines. Note that the Hα estimates at $L < 10^{5.2} L_\odot$ are upper limits. A steep jump – of about 2 dex – can be seen at a luminosity of $10^{5.2}\,L_\odot$. The black line corresponds to the empirical wind-momentum luminosity relation with rates not corrected for clumping, the black dashed line corresponds to the one corrected for clumping and the grey dotted line is obtained by fitting to the modified wind momentum obtained from ultraviolet resonance lines. The red lines, to guide the eye, overplot the black line in the high luminosity regime ($\log L/L_\odot > 5.2$) and the grey line in the low luminosity regime. The plot is based on a figure from Mokiem et al. (2007).

line. For stars to the left of this point the Hα line profile becomes too weak to use as a reliable mass-loss diagnostics and therefore the ultraviolet resonance lines have to be used.

For stars more luminous than $10^{5.2} L_{\odot}$, the theoretical predictions as done by Vink et al. (2000) and the empirical mass-loss rates (Mokiem et al. 2007) seem to be in (reasonably) good agreement. We will come back to this point later. However, for objects less bright than $10^{5.2} L_{\odot}$ there is a serious discrepancy between the predictions and observations, which is referred to in literature as the weak-wind problem (Martins et al. 2005b; Puls et al. 2008; Marcolino et al. 2009). What could be the cause of this discrepancy? On the observational side, at this luminosity the mass-loss diagnostic changes: for mass-loss rates above $10^{-7}\, M_{\odot}\mathrm{yr}^{-1}$ the Hα line diagnostic method is sensitive enough to provide mass-loss rates, whilst below this value one has to resort to the ultraviolet spectral range. Here the P Cygni-line diagnostics is more sensitive, but potentially also less reliable because of the uncertainties in ionization fraction (see e.g. Lamers & Leitherer 1993). On the theoretical side, the predictions have been derived subject to a set of assumptions. Some of the most stringent assumptions are: the stellar wind is a homogeneous medium, it is spherically symmetric, and time independent. Here, we want to discuss the assumption that a stellar wind is a homogeneous outflow.

There are several reasons that indicate that a stellar wind is not a continuous flow of gas but consists of an ensemble of fluid parcels of different densities and velocities. On the observational side: moving subpeaks in emission line profiles have been detected (see e.g. Eversberg et al. 1998), structure can be seen on large scales (see e.g. Kaper et al. 1996), and the linear polarization of the light from a wind can be variable (see e.g. Davies et al. 2007). From theory, it is predicted that the winds should be clumpy. The force accelerating the gas away from the stellar surface is unstable and therefore perturbations are expected (Lucy & Solomon 1970; Owocki et al. 1988).

These inhomogeneities are important since the mass-loss rates derived from Hα-profiles are affected by them, i.e. these mass-loss rates should be reduced if one accounts for clumping (Hillier 1991; Moffat & Robert 1994). In general clumping affects stellar wind diagnostics that are sensitive to the density squared, e.g. the Hα-profile, but not diagnostics that depend linearly on the density, e.g. P Cygni lines. We previously mentioned that there is a small discrepancy between the empirical mass-loss rates and the theoretical predictions for stars more luminous than $10^{5.2} L_{\odot}$: the empirical rates are higher. If one corrects only these empirical mass-loss rates for clumping, theory and observations agree already for only a modest clumpiness (Repolust et al. 2004; Mokiem et al. 2007).

However, relaxing on the assumption that the wind is a homogeneous outflow may also have an impact on the theoretical predictions of the mass-loss rate. In chapter 2 of this thesis, we account for effects caused by inhomogeneities in the flow. We

investigate whether observations and theory can still be reconciled after correcting the predictions for the stars with a luminosity larger than $10^{5.2} L_{\odot}$ for clumping, and whether clumping can be a solution for the weak-wind problem.

1.4 Theory of line-driven stellar winds

The atmospheres of most hot massive stars are not in hydrodynamic equilibrium. Gravity is overcome by radiation and gas pressure forces. As a consequence gas streams outward (Lucy & Solomon 1970). The processes between the gas and the photons, causing the radiation forces, can be divided in two categories: "continuum" processes and "line interactions". The gas in the atmosphere of the star is highly ionized and consists mostly of free electrons, fully ionized hydrogen, ionized helium, and multiply ionized species of more complex atoms. The continuum processes are interactions between photons and free electrons or ions of the following types: a photon interacts with a free electron, or an ion. In the latter case it can even further ionize it if it has sufficient energy. The strength of the continuum radiation force depends on the density of the gas and the number of photons. The contribution of this type of interactions to the total radiation force can be important deep in the wind, but it does not play a very important role once the strong acceleration due to line interaction has started in layers further out.

In case of a line interaction, a photon is absorbed in an atomic transition. A photon can be absorbed in such a transition only if its energy is equal to the energy needed to bring a bound electron to a higher energy level. The new state of the ion has a very short life time. The electron falls back to its original energy level, and a photon is re-emitted. In this process, energy and momentum are transferred from the radiation field to the absorping ion or vice versa. These absorbing ions share the momentum and energy gained in this manner with the other gas particles, dragging them along.[1]

The number of photons with the proper energy for the transition is limited in a medium with constant velocity. If the gas is accelerating, the ions are able to absorb photons that are Doppler shifted with respect to the photons absorbed in the layers below. This means that while the gas is moving out, it remains able to intercept an unattenuated flux at the right Doppler-shifted frequency, causing it to be accelerated even more. So, interestingly, an accelerating flow boosts a further acceleration. The radiation force associated with this process is called line force. It is the main force that drives the kind of stellar winds investigated here, the so called line-driven winds.

The important variables that determine the strength of this force are the stellar flux of photons at each frequency, the abundance of the various atoms, their excitation and ionization state, and the number of transitions the configurations have. Some ions

[1] In some cases this mechanism is not very effective but we do not consider this here.

are more efficient in absorbing photons than others. This efficiency is *grosso modo* determined by the product of the atom abundance, the ionization fraction, and the number of different transitions. Although hydrogen and helium are the most abundant species by far, they do not dominate the line force. Hydrogen is almost fully ionized. The fraction of neutral hydrogen times its abundance is almost equal to the number abundance of more complex atoms in their dominant ionization stage. So, these roughly cancel out. Therefore, the number of transitions is important. A complex ion can have many thousands of transitions in the region of the flux maximum of the star, many more than hydrogen which only has several tens. Therefore, the complex ions are the main contributors to the line force.

In order for a hot massive star to power a line-driven wind the radiation force – that will be described below – must overcome gravity. Whether or not this can be achieved, as well as the manner in which the flow is accelerated and the rate of mass loss in which this results, depend on the star's physical properties. The main goal of theoretical research into stellar winds is to understand the physics of this problem.

In this thesis different methods for predicting wind properties are applied. In chapter 2 a Monte Carlo method contrived by Abbott & Lucy (1985) and advanced and refined by de Koter et al. (1997) is used. Interestingly, it does not rely on a solution of the equation of motion of the stellar wind – often referred to as the wind equation. The detailed information on microscopic physics available in these simulations are the core element of two improved treatments of the wind problem presented in chapter 3. One of these, termed best-β method, follows the work of Müller & Vink (2008), the other, termed hydrodynamical method, is new. The latter method provides a consistent solution of the wind equation. The results presented in chapters 4 and 5 rely on the best-β method, which we show to provide solutions that agree well with those of the numerical method but is computationally faster.

The basis for the Monte Carlo method is that for the derivation of the mass-loss rate for a specific set of model parameters, one relies on an iteration procedure between the structure of the atmosphere and the radiation field (computed using the code ISA-WIND; de Koter et al. 1993), and the line force determined using a Monte Carlo simulation (computed using the code MC-WIND; de Koter et al. 1997; Vink et al. 1999). The structure of the atmosphere is determined using an input mass-loss rate. In the Monte Carlo code, it is derived how much mass per unit time can be accelerated by the radiation field of the ISA-WIND atmosphere out of the star's gravitational potential using global energy conservation. These two codes are iterated until the line force can drive the input mass-loss rate of the model atmosphere. In this case, the energy needed to accelerate the wind out of the star's gravitational field up to the terminal flow velocity of the wind equals the energy the gas absorbed from the photons, allowing for global energy conservation and not for local dynamical consistency. So indeed, the equation of motion remains unsolved.

1.4.1 The wind equation

The outflow of a line-driven stellar wind is governed by the forces at play. Assuming spherical symmetry this can be described by the following equation:

$$v\frac{dv}{dr} = -\frac{GM}{r^2} + g_{\rm rad} - \frac{1}{\rho}\frac{dp}{dr}, \tag{1.1}$$

where r is the distance from the center of the star, $v(r)$ is the velocity, $g_{\rm rad}(r)$ the radiation force per unit mass, $p(r)$ the pressure, $\rho(r)$ the density, G is Newton's gravitational constant, and M the stellar mass. Using mass continuity, $\dot{M} = 4\pi r^2 v\rho$, and the equation of state of the gas, we can rewrite the pressure term as:

$$\frac{1}{\rho}\frac{dp}{dr} = -\frac{a^2}{v}\frac{dv}{dr} - \frac{2a^2}{r} + \frac{k}{m}\frac{dT}{dr}, \tag{1.2}$$

where $T(r)$ is the temperature at radius r, k is Boltzmann's constant, m the mean particle mass and $a(r)$ the local sound speed, given by:

$$a = \sqrt{\frac{kT}{m}}. \tag{1.3}$$

The radiation force consist of a continuum radiation force $g_{\rm con}$, and a line force $g_{\rm line}$. If we take the continuum radiation force to be equal to the electron scattering force only, and assume the flow to be isothermal, we may write the wind equation in a fairly simple form:

$$a_\circ\left(\frac{v}{a_\circ} - \frac{a_\circ}{v}\right)\frac{dv}{dr} = -\frac{R_\star v_{\rm esc}^2}{2r^2} + \frac{2a_\circ^2}{r} + g_{\rm line}, \tag{1.4}$$

where $a_\circ$ is the isothermal sound speed at the effective temperature of the star and $v_{\rm esc}$ is the effective escape velocity, i.e.:

$$v_{\rm esc} = \sqrt{\frac{2GM(1-\Gamma_{\rm e})}{R_\star}}, \tag{1.5}$$

where $\Gamma_{\rm e}$ is the electron scattering force divided by the gravitational force. Equation (1.4) is a critical point equation. We discuss this aspect later and for now focus on the line force. The fairly simple form of the wind equation is deceitful due to the nature of this force. As already alluded to, it is a function of the acceleration (in this case we mean dv/dr and not, as commonly used, dv/dt), the number density of the ions and the flux at each frequency. It also depends on the specific characteristics of each atomic transition. The problem faced can be expressed in a simple way: the force driving and determining the structure of the flow *itself* depends in a complex way on this structure.

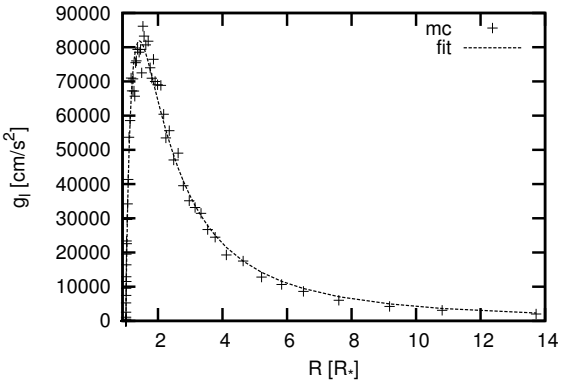

Figure 1.6: The line force (black cross) as simulated using the Monte Carlo method. A fit (black dotted line) using Eq. (1.7) to represent the line force is overplotted. Note the scatter on the Monte Carlo results due to noise.

The Monte Carlo method to study the line force relies on a model atmospheric structure to determine the amount of momentum and energy transferred from the radiation field to the gas, enabling the determination of the radiation forces. Given the structure of the wind, we can determine the probability of photons of all frequencies to be absorbed by the gas. We use this to determine the point of interaction and the nature of this interaction for photons emitted with a random frequency in a random direction at the inner boundary of the model, having a random probability to be absorbed at a specific location. The location where the photon is absorbed, is determined based on the physical properties of the medium the photon travels through, i.e. it is based on the distance a photon of the given frequency can travel on average before it is absorbed.

At the point of interaction the photons are re-emitted and the amounts of energy and momentum transferred are calculated. They are followed until they either back scatter through the inner boundary or escape through the outer boundary. Knowing the nature of each interaction, i.e which particle was involved and the amounts of energy and momentum transferred, we have a very powerful tool to study the radiation force. It equals (Abbott & Lucy 1985):

$$g_{\rm rad} = -\frac{1}{\dot{M}}\frac{dL}{dr}, \tag{1.6}$$

where dL is the amount of energy lost by the radiation field in a layer of thickness dr.

We want to use this radiation force to solve the wind equation. In Figure 1.6, the black plus-symbols show a typical output line force from a Monte Carlo simulation

as a function of the distance r from the center of the star. One notes that the line force shows a considerable amount of scatter as it has been determined in a statistical manner. Therefore, it is not very suitable to use as an input to solve the wind equation. We opt to formulate a fit function that describes the line force as a function of radial distance and captures the general behavior of the output Monte Carlo force following Müller & Vink (2008). This approach is distinct from the theory by Castor, Abbott and Klein (Castor et al. 1975, CAK), where $g_{\rm line}$ is a function of the velocity gradient and radial distance. To be clear, in our representation dv/dr also plays an important role, though this is not explicit in $g_{\rm line}$. Our $g_{\rm line}$ function should fulfill several requirements; *i)* $g_{\rm line}$ must be approximately zero at the stellar surface; *ii)* $g_{\rm line}$ should always be positive or zero as the flux of radiation from the photosphere is streaming outwards; *iii)* $g_{\rm line}$ is required to decrease as $1/r^2$ for large radial distance from the central star, and *iv)* $g_{\rm line}$ has an absolute maximum somewhere in the range between the stellar surface and the outer edge of the wind. The last requirement follows from properties *i-iii* above. The following function fulfills these requirements:

$$g_{\rm line} = \begin{cases} 0 & \text{if} \quad r < r_\circ \\ g_\circ \, (1 - r_\circ/r)^\gamma / r^2 & \text{if} \quad r \geq r_\circ, \end{cases} \tag{1.7}$$

where $g_\circ$, $r_\circ$, and γ are fit parameters to the Monte Carlo line force. Figure 1.6 displays a comparison of the fit function and the Monte Carlo line force. We used this function to solve the wind equation numerically. The solutions produce trans-sonic velocity laws that pass through the critical point. The critical point is defined as the location where both sides of equation (1.4) are zero. Using the above parametrization of the force this coincides with the sonic point, the location where the flow reaches the local sound speed.

The sonic point is an important point in the outflow. It is the point where gravity is almost exactly equal to the radiation force. Since the main force driving the flow depends on the acceleration, it is critical to initiate the flow. The more complex an ion, the more efficient the mechanism of line acceleration will work for small values of the velocity. The ensemble of transitions provided by iron-group elements, is more effective in driving the flow at the base of the wind.

If the metal content of the star is very low, or it does not produce a sufficient amount of photons, the radiation and pressure forces alone may be not strong enough to start a wind.

This principle is applied throughout this thesis. In chapter 3, we present the method developed to solve the wind equation and we apply it to galactic stars. In chapter 4, we investigate the mass-loss behavior of very luminous and very massive stars up to 300 times the mass of the Sun. In chapter 5, we apply this method to investigate the mass-loss behavior of carbon-nitrogen-oxygen enriched metal-poor stars.

1.5 Summary: a guide to this thesis

To conclude we give a brief overview of the main conclusions of the scientific chapters in this thesis:

In chapter 2 we investigate the effect of inhomogeneities on the wind properties of massive stars. The wind is envisioned to consist of clumps in which the density is high. The inter-clump medium is assumed to be void. On the one hand, due to the high clump density relative to the density under the assumption of a smooth medium, the excitation and ionization state of the gas are affected; the gas tends to recombine. On the other hand, photons emitted by the star have a probability to escape relatively easily 'in-between the clumps' or to become trapped in optically thick clumps. This behavior is called porosity. The processes mentioned compete in their effect on the mass-loss rate and terminal wind velocity. We adopt several prescriptions for the behavior of clumping as a function of distance and for the length-scale of the clumps. We show that in the case of small geometric clumps and small clumping factors, the energy transferred from the radiation field to the gas is barely affected, allowing to easily reconcile the empirical mass-loss rates of very luminous stars with the theoretical ones accounting for only a small amount of clumping. In the case of geometrically large clumps and large clumping factors, the wind energy can drop by as much as a factor 100. In these cases the mass-loss rates become too small to reconcile the empirical mass-loss rates with theoretical ones. In principle, such low mass-loss rates might provide a solution to the weak-wind problem – discussed in Sect. 1.3. This is however not likely, unless a mechanism can be identified that causes extreme structure to develop in the winds of stars with $L < 10^{5.2} L_\odot$ that have $\dot{M} \lesssim 10^{-7} M_\odot \mathrm{yr}^{-1}$ (weak winds) that is not active in denser winds.

In chapter 3 we present two methods to solve for the mass-loss rate and velocity profile of hot massive stars, and we apply this to dwarf, giant and supergiant O-type stars. An important finding is that we can not drive stellar winds for dwarf stars that are less luminous than $10^{5.2}\ L_\odot$. This coincides with the luminosity at which the weak-wind problem – discussed in Sect. 1.3 – occurs. We propose that in this regime the line force is too weak to accelerate the wind through the sonic point. As such relatively low luminosity stars do have (weak) winds, there must be an extra force that plays a role in driving the wind. For stars more luminous than $10^{5.2}\ L_\odot$ we find mass-loss rates that are in good agreement with previous estimates, notably the mass-loss recipe of Vink et al. (2000). Our derived terminal velocities are about 35 % to 45% higher than the mean of the observed values. This may be related to the presence of clumping in the outer wind and/or other physical processes not taken into account in our simulation.

The wind properties of stars in the range of 40–300 $M_\odot$ that approach their Eddington limit are investigated in chapter 4. We find a very well behaved relation between mass loss and the basic parameters mass and electron scattering Eddington factor Γ_e. The latter is a measure of the proximity of stars to their Eddington limit. We find an upturn in the mass loss versus Γ_e-dependence, exactly at the point where the model winds become optically thick. This is also the point where the wind efficiency numbers surpass the single-scattering limit (of $\eta = \dot{M}v_\infty c/L = 1$), reaching $\eta \simeq 2.5$ close to the Eddington limit. This suggests a natural transition from common O-type stars to Wolf-Rayet characteristics where the wind becomes optically thick. This 'transitional behavior' is also found in terms of the parameter describing the rate of acceleration of the flow (so-called β), which increases from the canonical value of 0.9 in normal O stars to values as high as 1.5, as well as in the spectral morphology of the characteristic He II line at 4686 Å.

In chapter 5 the winds of metal-poor stars that have their surfaces enriched by primary CNO are studied. So far, mass-loss estimates for such stars have been based on the assumption that the metal content implied by carbon, nitrogen and oxygen $Z_{\rm CNO}$ can be substituted for the metallicity, Z, as intended in mass-loss rate recipes using a mixture of elements that is scaled to the solar composition. We find that CNO driven winds feature much lower mass-loss rates than scaled solar metallicity winds if $Z_{\rm CNO} = Z$. The reason is that carbon, nitrogen and oxygen have simpler atomic structures than iron; consequently, iron has many more atomic transitions and drives the wind more efficiently near the sonic point. We find that driving CNO winds for stars hotter than 50 000 K is not possible, as the lines of the ions that are dominant at these temperatures do not provide sufficient driving. The mass-loss behavior of cooler stars is very complex, but can be summarized quite homogeneously by normalizing to rates implied by the mass-loss prescription of Vink et al. (2001). The latter is frequently used in stellar evolution codes. We further conclude that the winds of massive very metal-poor stars ($Z \lesssim 10^{-4}$), whether they are primary CNO enriched or not, are so weak that they do not significantly impact the total mass and/or angular momentum loss during their evolution. If other mass-loss mechanisms, such as η-Carinae type mass eruptions, do not occur for such objects, their supernova explosions are expected to be responsible for the major part of the early cosmological nucleosynthetic chemical enrichment, and may have left black holes with masses of $\sim 10^2\ M_\odot$.

2 Predictions of the effect of clumping on the wind properties of O-type stars

L.E. Muijres, A. de Koter, J.S. Vink, J. Krtička, J. Kubát and N. Langer

accepted by Astronomy & Astrophysics

Abstract

Both empirical evidence and theoretical findings indicate that the stellar winds of massive early-type stars are inhomogeneous, i.e. porous and clumpy. For relatively dense winds, empirically derived mass-loss rates might be reconciled with predictions if these empirical rates are corrected for the presence of clumping. The predictions, however, do not account for structure in the wind. To allow for a consistent comparison we investigate and quantify the effect of clumpiness and porosity of the outflow on the predicted wind energy and the maximal effect on the mass-loss rate of O-type stars.

Combining non-LTE model atmospheres and a Monte Carlo method to compute the transfer of momentum from the photons to the gas, the effect of clumping and porosity on the energy transferred from the radiation field to the wind is computed in outflows in which the clumping and porosity stratification is parameterized by heuristic prescriptions.

The impact of structure in the outflow on the wind energy is complex and is a function of stellar temperature, the density of gas in the clumps and the physical scale of the clumps. If the medium is already clumped in the photosphere the emergent radiation field will be softer, slightly increasing the wind energy of relatively cool O stars (30 000 K) but slightly decreasing it for relatively hot O stars (40 000 K). More important is that as a result of recombination of the gas in a clumped wind the line force increases. However, due to porosity the line force decreases, simply because

photons may travel in between the clumps, avoiding interactions with the gas. If the changes in the wind energy only affect the mass-loss rate and not the terminal velocity of the flow, we find that the combined effect of clumpiness and porosity is a small reduction in the mass-loss rate if the clumps are smaller than 1/100th the local density scale height H_ρ. For this case empirical mass-loss determinations based on Hα fitting and theory match for stars with dense winds ($\dot{M} \gtrsim 10^{-7} M_\odot \mathrm{yr}^{-1}$) if the over-density of gas in the clumps, relative to the case of a smooth wind, is modest. For clumps larger than 1/10th H_ρ the predicted mass-loss rates show about the same dependence on clumpiness as do empirical rates. We show that this implies that empirical and predicted mass-loss rates can no longer be matched. Very large overdensities of gas in clumps of such large size may cause the predicted $\dot{M}$ to decrease by a factor 10 to 100. This type of structure is likely not the cause for the "weak wind problem" in early-type stars, unless a mechanism can be identified that causes extreme structure to develop in winds that have $\dot{M} \lesssim 10^{-7} M_\odot \mathrm{yr}^{-1}$ (weak winds) that is not active in denser winds.

2.1 Introduction

In the last decade studies of the mass-loss rate of early type massive stars have focussed, for an important part, on the role of structure or inhomogeneities in the stellar outflow (for a review, see e.g. Puls et al. 2008). One reason is that recombination-based processes are very sensitive to the presence of structure in the wind and that therefore key mass-loss diagnostics, such as Hα and He II λ4686 line radiation and infrared and radio continuum radiation, being sensitive to the square of the density, are affected. As a result, analyses based on these diagnostics assuming a smooth outflow will lead to an overestimate of the mass-loss rate if in reality the wind has a clumpy structure. One can show that if the typical clumping factor, expressing the ratio of the actual density in clumps relative to the mean density, is given by $C_\mathrm{c} > 1$, the empirical mass-loss rate $\dot{M}$ needs to be scaled down by a factor $1/\sqrt{C_\mathrm{c}}$ (see section 2.2.2 for more details).

Attempts to empirically quantify the clumping factor in O stars, Luminous Blue Variables and Wolf-Rayet stars yield a rather broad spectrum of C_c values, from a factor of a few up to 100 (see e.g. Figer et al. 2002; Crowther et al. 2002; Hillier et al. 2003; Bouret et al. 2003; Repolust et al. 2004; Markova et al. 2004; Bouret et al. 2005; Fullerton et al. 2006). This implies that empirical mass-loss rates may have to be scaled down by factors 2–10. To give one explicit example, intended to serve as a frame of reference, empirical mass loss rates of O-type stars brighter than 175 000 $L_\odot$ based on the analysis of Hα and assuming smooth flows are brought into agreement with predictions (Vink et al. 2001) if clumping is modest ($C_\mathrm{c} \sim 3-4$; Mokiem et al. 2007; de Koter et al. 2008). Notice that recent stellar evolution calculations adopt

these predictions, therefore, if these predictions are correct, they implicitly account for a modest amount of clumping.

A second reason for the attention to this topic is that empirical studies of the radial stratification of the clumping factor throughout the wind sketch a picture that is discrepant from what is expected. Hydrodynamical modeling of the time-dependent structure of line-driven winds (for a review, see e.g. Owocki 1994; Feldmeier 1999) reveals the wind to be quite stable in the inner parts, but predicts that extensive structure – both in terms of density and velocity – develops further out (at $r \gtrsim 1.3$ times the stellar radius $R_\star$ or $v \gtrsim 0.4$ times the terminal velocity) and can survive out to very large distances ($r \gtrsim 1000R_\star$; see Runacres & Owocki 2005). Empirical studies, however, show that O stars develop clumping already close to the stellar surface (Markova et al. 2004; Repolust et al. 2004; Puls et al. 2006). Apparently, the line-driven instability – first proposed by Lucy & Solomon (1970) – is not the only mechanism at work and other effects, acting in different parts of the wind, may also cause structure.

In this paper we address the following question: does the presence of structure impact the rate at which massive stars lose mass? If, on the one hand, structure would cause the mass loss to increase, only modest clumping would be required to bring the above mentioned Hα based and predicted mass-loss rates into agreement. If, on the other hand, structure would cause a strong decrease in $\dot{M}$, strong clumping may be required to bring this agreement or no agreement may be reached at all.

The hydrodynamic models of line-driven winds (see again Owocki 1994) predict that the time-averaged terminal flow velocity and time-averaged mass-loss rate agree well with those following from a stationary approach, i.e. there is no significant impact of clumping on $\dot{M}$ or the terminal flow velocity v_∞. These predictions, however, are based on one-dimensional calculations (but see Dessart & Owocki 2003, 2005, for first results on two-dimensional flows), i.e. neglecting a possible porous structure of the wind. Also, the impact of the density and velocity perturbations on the excitation and ionization state of the gas, therefore on the local line force, is not treated.

In studying aspects of this problem we will take a heuristic approach. We feel this is justified given the discrepancies between the empirical clumping stratification and that predicted by the line-driven instability and the complex nature of the problem. We focus on effects of clumping and porosity on changes in the state of the gas and the continuum radiation field, and on the impact of these changes on the line force. These effects are computed self-consistently. The clumping and porosity is, however, described by simple empirical laws. In section 2.2 the method is described in detail. The results are presented in section 2.3 and discussed in section 2.4. We end with conclusions.

2.2 Method

2.2.1 NLTE hydrodynamic wind models

To determine the momentum transfer from the radiation field to the wind in O-stars, we employ the model atmospheres of de Koter et al. (1993) in combination with a Monte Carlo code for determining the line force as described by de Koter et al. (1997). The Monte-Carlo approach, though extensively modified, is essentially based on that developed by Abbott & Lucy (1985). This methodology of determining the properties of stellar winds has been used extensively to predict the mass-loss behavior of massive early-type stars, including O and B stars (Vink et al. 1999, 2000, 2001), Luminous Blue Variables (Vink & de Koter 2002) (LBVs) and selected Wolf-Rayet stars (de Koter et al. 1997; Vink & de Koter 2005). For details on the method we refer the reader to the above references. Here, we only give a very brief overview of essential aspects.

The atmospheric model extends from the base of the photosphere (at a Rosseland optical depth of about 25) to 20 stellar radii, and assumes that the outflow is homogeneous, spherically symmetric and stationary. To calculate the radiative transfer in spectral lines, the Sobolev method is used. The occupation numbers of (excited) levels and the ionization conditions are solved assuming statistical equilibrium. Model atoms for hydrogen, helium, carbon, nitrogen, oxygen and silicon are explicitly treated. Other atoms are accounted for using a modified nebular approximation.

It is important to realize that in our method the equation of motion for gas streaming out from the star is not solved explicitly (but see Müller & Vink 2008 and Muijres et al. in preparation). Instead, we adopt a β-type velocity law. For this velocity structure we compute, by means of Monte Carlo, the total radial momentum that is transferred from photons to the gas on their way from the photosphere to the interstellar medium. The cumulative effect of this process also yields the total rate at which the wind extracts energy from the radiation field. By requiring that this energy is used to accelerate the wind and to let the gas escape from the stellar potential well (so assuming no non-radiative forces are at work) we can iteratively derive a mass-loss rate, given by:

$$\Delta \mathrm{L} = \frac{1}{2}\dot{\mathrm{M}}\left(v_{\infty}^2 + v_{\mathrm{esc}}^2\right), \tag{2.1}$$

where ΔL is the energy extracted from the radiation field, v_{∞} is the terminal wind velocity and v_{esc} the escape velocity from the stellar surface.

The advantages of this method are that mass-loss rates can be derived with a modest computational effort, therefore relatively large fractions of parameter space can be explored. From a physical point the strong point of the method is that effects of multiple photon scattering (that are already important for O stars) are self-consistently accounted for and that changes in the line force due to excitation/ionization processes

are included. What is actually predicted in our method is the gain in total kinetic energy of the outflow due to transfer of momentum in the radiation field to the gas. This technique requires a pre-specified velocity law $v(r)$. Therefore, we do not predict the velocity stratification (nor for that matter the terminal flow velocity) but assume an empirically motivated $v(r)$. This allows to extract the predicted mass-loss rate. In this study we investigate the effects of clumping and porosity on the transferred energy ΔL, therefore on the wind energy. As our velocity stratisfication is pre-specified, we cannot investigate the effects of structure on v_∞. Therefore, if one contributes the full effect of clumping and porosity to a change in the mass-loss rate, one obtains the maximal effect of such processes on $\dot{M}$.

2.2.2 The implementation of clumping

A self-consistent treatment of clumping in a stellar outflow would in any case require a hydrodynamical simulation of the line-driven instability (see e.g. Owocki & Puls 1999, and references therein) subject to a non-local thermodynamic (NLTE) treatment of the gas. From a computation point this is extremely challenging. It is, moreover, currently unclear whether or not the line-driven instability is the only process causing inhomogeneities in the outflow (see Sect. 2.2.2). For these reasons we argue that a more heuristic approach to this problem is justified.

In our model we prescribe the radial behavior of clumping assuming: *i)* all the gas is concentrated in clumps, i.e. the space in between the clumps is void; *ii)* each clump is homogeneous, *iii)* clumps are distributed randomly on small spatial scales and follow a prescribed radial behavior on large spacial scales, and *iv)* the velocity law (of the clumpy medium) is a smooth function of radius.

The radial behavior of the clumping is prescribed in terms of the clumping factor, specifying the over-density in the clump relative to a smooth medium, and the porosity length, essentially specifying a physical scale of the clumps. We will first introduce these two concepts in more detail.

Clumping factor

Following e.g. Owocki & Cohen (2006), we introduce the clumping factor as

$$C_\mathrm{c}(r) = \langle \rho(r)^2 \rangle \,/\, \langle \rho(r) \rangle^2, \tag{2.2}$$

where the angle brackets denote volume averaging. Empirical arguments have motivated this definition. The strength of both the free-free continuum and of spectral lines formed through the process of recombination depend on the square of the density, while other processes, for instance that of electron scattering, show a linear dependence (see e.g. Hillier 1991).

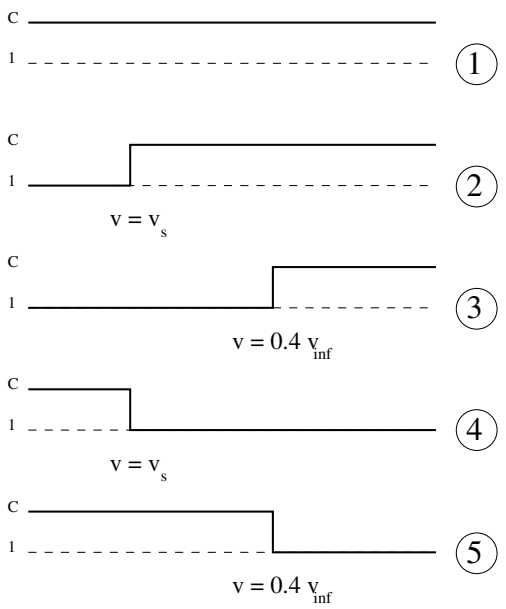

Figure 2.1: Schematic representation of the different clumping stratifications investigated in this study. Each stratification has been given an index number (at the right side of the figure) which is used in Figure 2.4. They represent: (1) constant clumping; (2) clumping starting at the sonic point; (3) clumping starting at $0.4v_\infty$; (4) clumping up to the sonic point, and (5) clumping up to $0.4v_\infty$.

In case of an interclump medium that is void (see above) the density in the clump is given by

$$\rho_{\rm c}(r) = C_{\rm c}(r)\,\langle\,\rho(r)\,\rangle. \tag{2.3}$$

The simplest possible assumption on the behavior of clumping is that it is constant throughout the photosphere and wind and equal to $C_{\rm c} > 1$. A clumping factor $C_{\rm c} = 1$ implies a smooth wind. To investigate a radial dependence in the clumping we introduce additional clumping prescriptions. A schematic representation of all clumping stratifications adopted in this study is given in Fig. 2.1. The top drawing (labeled 1) depicts the case of a constant clumping factor.

Clumping in the outer wind. In this prescription we assume that the onset of clumping occurs at some prescribed radius $r_{\rm p}$, i.e.

$$C_{\rm c}(r) = \begin{cases} 1.0 & \text{for} \quad r < r_{\rm p} \\ C_{\rm c} & \text{for} \quad r \geq r_{\rm p}. \end{cases} \tag{2.4}$$

The onset and development of stochastic structure in the acceleration zone of the outflow is a natural consequence of a line-driven wind. It is the result of a positive feedback in which a small increase in velocity of a fluid parcel exposes the parcel to a more intense (read: unattenuated) radiation from the star and causes it to be further accelerated (Owocki et al. 1988; Feldmeier 1995; Owocki & Puls 1996, 1999). Simulations of this *self-excited* wind instability show that the compression of gas in clumps typically starts at about 0.3–0.4 v_∞ and that it may extend to very large radii (Runacres & Owocki 2002). These simulations, however, do not account for (transonic) velocity curvature terms. In stars with relatively weak winds it has been shown that these terms may lead to gradient terms in the source function and modifications of the line acceleration (Puls et al. 1998b) causing a highly structured wind in the lower parts of the outflow (Owocki & Puls 1999). The theory of line driven winds dictates that the mass-loss rate is set by conditions at or below a critical point that is very roughly at $0.2v_\infty$.

Based on the above arguments for structure formation in line-driven winds we define two new clumping prescriptions, where we opt to initiate the clumping: 2) at the sonic velocity (about 15 km/s for the models of 30 kK and about 18 km/s for the models of 40 kK), and 3) at $0.4v_\infty$ (see Table 2.1 for values of v_∞). The former clumping stratification explores a potential effect of clumping on the mass-loss rate because clumping sets in before the mass-loss rate is formaly fixed. The latter prescription focusses on the effect of clumping on v_∞ (see again Fig. 2.1). The density in the clumps produced by the line-driven instability relative to the ambient medium can reach one to two orders of magnitude (Owocki & Puls 1999). We will adopt clumping factors C_c of unity through 100, in steps of 0.5 dex.

Clumping in the inner wind. In this prescription we assume that clumping occurs in the inner wind and that the outer wind is smooth, i.e.

$$C_\mathrm{c}(r) = \begin{cases} C_\mathrm{c} & \text{for} \quad r < r_\mathrm{p} \\ 1.0 & \text{for} \quad r \geq r_\mathrm{p}, \end{cases} \tag{2.5}$$

where r_p again refers to the prescribed radius defining the boundary between the two regimes. This clumping prescription is "opposite" to the one described in the previous paragraph and which was motivated by theoretical expectations. The clumping prescription of Eq. 2.5 is motivated by observational arguments. Puls et al. (2006) present empirical evidence for a radial dependence of clumping in hot star winds. These authors use Hα, infrared and radio diagnostics to investigate the clumping behavior of the inner wind (inside about two stellar radii) relative to the clumping in the outer wind (beyond tens of stellar radii) of a large sample of giant and supergiant stars. They find a qualitative difference in the radial behavior of clumping in stars with strong winds compared to stars with weak winds. In the case of dense winds

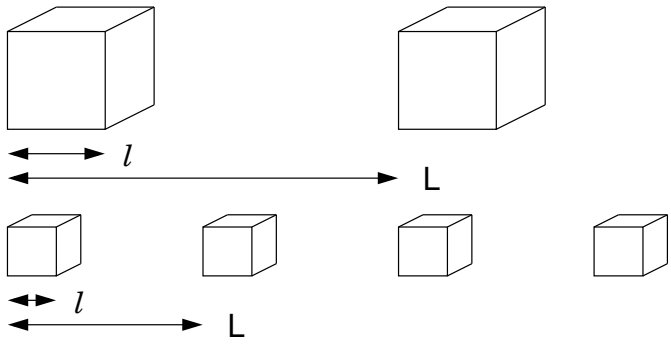

Figure 2.2: Schematic explanation of the difference between the filling fraction f, c.q. clumping factor $C_c = 1/f$, which is the same for the top and bottom case, and the separation of the clumps L, which is larger in the top case.

the inner wind is *more strongly* clumped than the outer wind, whereas in the case of thin winds the inner and outer region have similar clumping properties. Puls et al. speculate that the cause for this difference between strong and weak winds may be connected to photospheric instabilities and/or pulsations as their strong wind stars are usually supergiants with low gravity. Interestingly, Cantiello et al. (2009) show that the stars in the sample of Puls et al. that show stronger clumping in the inner wind compared to the outer wind have sub-surface convective layers due to iron opacity peaks. They suggest that this convection may (indirectly) trigger stochastic velocities and clumping in the photosphere and lower part of the wind.

Based on these arguments we define again two clumping stratifications: 4) clumping up to the sonic point, and 5) clumping up to $0.4v_\infty$ (see also Fig. 2.1).

Porosity length

If the physical scale of a clump is given by ℓ and the separation of clumps by L (see Fig. 2.2 for a visualization of the definition of L) a fraction $f = \ell^3/L^3$ of the medium will be filled with gas, again assuming that the inter-clumped medium is void. This filling fraction f relates to the clumping factor as $C_c = 1/f$. In Fig. 2.2 two possible configurations of regularly stacked cubic clumps having identical filling fractions f (and clumping factors C_c) are shown. The way in which these configurations differ is in the physical size and separation of the clumps. If in both configurations the individual clumps are optically thin for radiation the effects of clumping will be the same and will only occur through an adjustment of the excitation and ionization properties of the gas. If, however, the physical size of the large clumps is such that the individual clumps become optically thick, they will suffer from local self-shielding.

In that case the medium becomes *porous*, i.e. radiation will be able to travel more efficiently through inter-clump channels. The bigger the scale length L the more efficient this mechanism will be (imagine for instance that all material in the outflow is concentrated in a single clump). Porosity in stellar winds, sometimes referred to as macro-clumping, is discussed by (Feldmeier et al. 2003; Owocki et al. 2004; Owocki & Cohen 2006; Oskinova et al. 2007).

The effective opacity of a clump is given by

$$\kappa_{\rm eff} = \kappa_{\rm c}(\rho_{\rm c}) \, \frac{1 - \exp(\tau_{\rm c})}{\tau_{\rm c}}, \tag{2.6}$$

where $\kappa_{\rm eff}$ is the effective mass absorption coefficient (e.g. in $\mathrm{cm}^2\,\mathrm{gr}^{-1}$) considering an ensemble of clumps. The mass absorption coefficient of material in the clumps, $\kappa_{\rm c}$, is thus reduced because of the porous nature of the medium. The clump optical thickness $\tau_{\rm c} = \kappa_{\rm c}\,\rho_{\rm c}\,\ell = \kappa_{\rm c}\,C_{\rm c}\langle\rho\rangle\,\ell = \kappa_{\rm c}\,\langle\rho\rangle\,\ell/f$.

We introduce a radial dependence of the scale of the clumps, i.e.

$$L(r) = \begin{cases} \text{negligible} & \text{for} \quad r < r_p \\ H_\rho / D & \text{for} \quad r \geq r_p, \end{cases} \tag{2.7}$$

where H_ρ is the local density scale height and D is a constant, which we choose to be 10, 100 and 1000. The fact that L is negligible below r_s implies that we do not account for porosity in the subsonic part of the outflow. The increase of the physical scale $\ell = L\,C_{\rm c}^{-1/3}$ with radial distance reflects the likely case that the clumps expand and possibly merge while receding from the star.

To provide a quantitative feeling for the number of clumps we compute the number of clumps N passing a radial shell at r in a typical flow time $\tau = R_\star/v_\infty$. We define this as the total volume associated with one wind flow time divided by the volume in which there is one clump. One finds

$$N = 4\pi r^2 \left(\frac{D}{H_\rho}\right)^3 \frac{R_\star}{v_\infty}\, v(r). \tag{2.8}$$

In our dwarf model of 30 000 K the scale height has increased to about half a stellar radius at $r = 2\,R_\star$. At this point the flow velocity is $1100\,\mathrm{km\,s^{-1}}$. For N we obtain $\sim 200 D^3$. Notice that the number of clumps is not conserved, but decreases with distance. For instance, in the same model $H_\rho \sim 0.1 R_\star$ at $r = 1.1\,R_\star$, therefore the number of clumps passing this point in one flow time is about 3.5 times as large as that at $r = 2R_\star$. Physically, this implies that in our description clumps merge as they move away from the surface.

Vorosity

The velocity law of the structured medium is treated as a monotonic function of radius. We therefore do not assume that on a local scale (where the flow speed is about

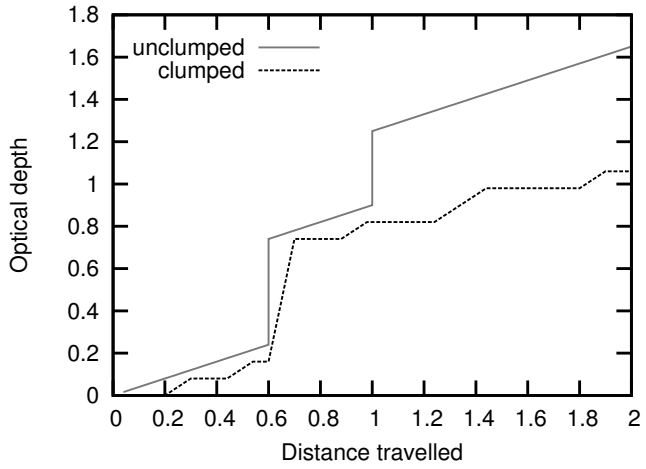

Figure 2.3: Schematic representation of the increase of the optical depth with distance. The latter is given in arbitrary units. The slope of the lines thus represent the linear extinction coefficient $\kappa\rho$. The solid line depicts the case of a smooth medium; the dashed line that of a clumpy medium. In the smooth flow, the slanted regions represent continuum extinction, while at the points where the line becomes vertical a line interaction occurs. The line interaction region is assumed to be infinitely narrow. In the case of a clumpy flow, the flat parts of the curve reflect the inter-clump medium. Within a clump the continuum extinction is relatively large, therefore the slope is relatively steep. For reasons explained in the text, we have assumed the line interaction region to have a finite width, determined by the Sobolev length. The line that can interact at about distance 1 is missed as it is associated with the inter-clump medium. Notice that in a clumpy medium the photon needs to travel a larger geometrical depth to cross a given optical depth.

constant) an ensemble of clumps may be distributed over a range in velocities, nor do we account for shape changes of individual clumps caused by internal velocity gradients. The overlaps and/or gaps in velocity space that may be the result of such motions are termed "vorosity" (which is short for velocity porosity). A general treatment of vorosity is beyond the scope of this study. We do point out that the intrinsic instability of the line-driving mechanism is expected to lead to velocity structure. Assuming the internal velocity dispersion in a clump is small, and that clump velocities sample the smooth outflow (matter being concentrated in the clumps), Owocki (2008) using one-dimensional dynamical simulations of the wind instability finds a reduction in the over-all line absorption of about 10-20%. In our simulations the velocity change inside a single clump is essentially treated in a similar way as in Owocki. It is assumed to be monotonic and amounts to $\delta v \sim (dv/ds) \times \ell$, where s is geometrical distance in the arbitrary direction s and v is the smooth flow velocity. The value of δv is typically small.

Radiation hydrodynamical simulations (in 2D) show, however, a large velocity

dispersion in the clumps (Sundqvist et al. 2010). Interestingly, Sundqvist et al. point out that this structure prevents a desaturation of lines (of intermediate strength) also implying only a modest reduction in the line absorption.

2.2.3 Inclusion of clumps in the Monte Carlo Code

The mass-loss prediction consists of two parts. First, an ISA-WIND non-LTE spherically symmetric model atmosphere with prescribed outflow properties is computed. The atomic models and non-LTE treatment are identical to Vink et al. (2000). The density, *casu quo* velocity stratification, in the photosphere and the onset region of the wind is computed accounting for the force due to the gradient in gas pressure and continuum radiation pressure. Near the sonic point the velocity stratification is smoothly connected to a β-law. For details, see also Vink et al. (2000). The treatment of clumping in the model atmosphere is through implementation of the clumping factor $C_c(r)$ in the description of the density, Eq. 2.3. In the description of optical depth, the clumping is treated in the effective opacity, Eq. 2.6, and the scale length L, Eq. 2.7.

By neglecting the porosity correction in describing the opacity (in both ISA-WIND and MC-WIND), we can single out the effect of clumping on the excitation and ionization structure. We will study the impact of clumping on the state of the gas in Sect. 2.3.1.

Second, the Monte Carlo simulation program MC-WIND is used to trace the momentum transfer of photons to the gas, from which a mass-loss rate can be derived following the method of Abbott & Lucy (1985). In order to study the full effect of clumping the porous nature of the medium needs to be accounted for. In a homogeneous medium without spectral lines a photon traveling an optical depth $\Delta\tau_\nu$ will cross a geometrical distance $s = \Delta\tau_\nu/\kappa_\nu\rho$. In a spherically symmetric stellar wind with a monotonically increasing wind velocity in which both continuum and line absorption may occur, the photon will experience a local barrier in optical depth at regions where its frequency matches that of a spectral line. If we map the distance in optical depth to a distance in physical space one may get a behavior as is schematically shown in Fig. 2.3. The figure depicts the situation in a spherical shell in which the density is assumed constant. The optical depth increases linearly with distance due to free-free processes, bound-free processes and Thomson scattering. These are the slanted parts of the line. In a rapidly expanding spherical outflow, a photon that is emitted at a wavelength that is slightly blue relative to the wavelengths at which a spectral line may absorb, may interact with the spectral line once it encounters particles that move with the proper relative Doppler (red)shift. Assuming the typical width of the line is given by the Doppler width, $v_D = \sqrt{kT/m}$, where T is the temperature, k the Boltzmann constant and m the mass of the particle, the geometrical length of a line absorption region is $L_{Sob} = v_D/(dv/dz)$, where z is measuring the di-

rection in which the photon is propagating. This length is referred to as the Sobolev length (Sobolev 1960). If the direction measured by z is at an angle θ with the radial direction, such that $\hat{z}/\hat{r} = \cos\theta = \mu$, then

$$\frac{dv}{dz} = \left(1-\mu^2\right)\frac{v}{r} + \mu^2\frac{dv}{dr}. \tag{2.9}$$

In computing the radiation field in spectral lines the Sobolev approximation is adopted in ISA-WIND, i.e. it is assumed that the velocity gradient is so large that the properties of the medium do not change within a length interval $L_{\rm Sob}$. In MC-WIND models without clumping we assume that line interactions take place at line center, i.e. the Sobolev absorption region is assumed to be infinitely narrow. The vertical solid lines in Fig. 2.3 reflect such line interactions, and represent an optical depth $\tau_{lu} = \kappa_{lu}\,\rho\,\lambda_{lu}\,L_{\rm Sob}/v_{\rm D}$. In this equation the mass abortion coefficient of the transition at wavelength λ_{lu} between lower level l and upper level u is given by

$$\kappa_{lu} = \frac{\pi e^2}{m_{\rm e}c} f_{lu}\frac{n_l}{\rho}\left(1-\frac{n_u}{n_l}\frac{g_l}{g_u}\right), \tag{2.10}$$

where e and $m_{\rm e}$ are the charge and mass of the electron, c the speed of light, f_{lu} is the oscillator strength, n_l and n_u the number density of the lower and upper level and g_l and g_u the statistical weight of the lower and upper level. In the Monte Carlo simulation the optical depth at which the photon should interact is randomly drawn and given by $\tau_\nu = -\ln p$, where $p \in \langle 0, 1]$ is a random number.

In a clumpy wind, with a clumping factor $C_{\rm c}$ and porosity length L, photons will travel alternatively through clumps or vacuum. If we assume the Sobolev length $L_{\rm Sob}$ to be infinitely small, photons would "miss" spectral lines for which the interaction point is in a void region. If the interaction region would be the actual Sobolev length, a fraction of these ineffective lines could still contribute to the opacity as part of the interaction region may coincide with the location of one or more nearby clumps. Accounting for the extent of the Sobolev interaction region yields a more representative sampling of the spectral lines contributing to the line force. For this reason we account for the actual $L_{\rm Sob}$ by introducing a mean line opacity in the line interaction region

$$\chi_{lu} = \frac{\tau_{lu}}{L_{\rm Sob}}. \tag{2.11}$$

This implies that we assume the line profile function to be a box function. The situation of a clumpy medium is depicted in Fig. 2.3 using a dashed line. If the dashed line runs flat, the photon is not encountering any material. If the randomly selected optical depth the photon will travel is within the Sobolev region of one (or more) lines, a random selection, using the opacities of the contributing extinction processes at the point of interaction as a weighing factor, will determine the type of interaction.

The outcome of this random process can be a free-free or bound-free interaction, an electron scattering, or a line interaction.

The clumps themselves are assumed to be cubes, of which the length of the edge is $\ell = L/C_c^{1/3}$. As explained, each volume L^3 contains a clump. The probability that a photon traveling this volume encounters a clump is given by the cross section of the clump relative to the cross section of the volume, i.e. $\ell^2/L^2 = C_c^{-2/3}$. The clumps are randomly placed along the path of the photon using this probability.

On average, due to the effect of porosity and because part of the lines become ineffective (i.e. those lines that have their line interaction region completely or partially in the inter-clump medium), photons need to travel a larger geometrical distance in a clumpy medium before being absorbed. Therefore, the dashed line in Fig. 2.3 is drawn such that it falls below the solid line. If a packet of photons interacts with material in a clump it will be re-emitted in a random direction. For this new direction we account for the fact that the photon packet starts in a clump.

2.2.4 Model grid

In order to study the effects of clumping and porosity we have set up a small grid of main sequence stars and supergiants. The input parameters are listed in Table 2.1. To facilitate a comparison with the results of Vink et al. (2000) we have adopted their solar abundance pattern, which follows Anders & Grevesse (1989). We note that applying the solar abundances by Asplund et al. (2005) would result in a typical reduction of the mass loss rate by 0.1 dex (see Krtička & Kubát 2007). Though the mass-loss rate is calculated, the velocity stratification is prescribed (see Sect. 2.2.1). We adopt a terminal velocity v_∞ that is 2.6 times the effective surface escape velocity, where 'effective' implies that the surface gravity is corrected for radiation pressure on free electrons. The parameter β describing the rate of acceleration of the flow is set to unity. Again this is similar to Vink et al. (2000). Theoretical support for this choice is given by Müller & Vink (2008).

For our five different clumping stratifications the predicted mass-loss rates are given, each time for five different clumping factors. These results will be discussed in the next section.

2.3 Results

2.3.1 The effect of clumping on $\dot{M}$ through its impact on the photospheric radiation field and ionization of the gas

In Fig. 2.4 we show predicted wind energies $E_{\rm kin} = 1/2\,\dot{M}\,v_\infty^2$ as a function of clumping prescription and clumping factor for two typical main sequence stars (top panels) and two typical supergiants (bottom panels). $E_{\rm kin}$ therefore has a dimension of energy

Table 2.1: Adopted model parameters together with predicted mass loss rates for all clumping assumptions. Porosity is not included in these predictions, i.e. the clumps are assumed to be optically thin. We stress that the mass-loss rates given here have been calculated assuming that all of the change in wind energy benefits $\dot{M}$. However, for instance for the case in which clumping sets in at $0.4v_\infty$ this is unlikely and most of the effect will benefit v_∞.

$T_{\rm eff}$	R	$\log L$	M	v_∞	$\log C_{\rm c}$	$\log \dot{M}$ [$M_\odot$yr^{-1}]				
[K]	[$R_\odot$]	[$L_\odot$]	[$M_\odot$]	[km/sec]		$C_{\rm c}$ constant	$C_{\rm c}$ from v_s	$C_{\rm c}$ from $0.4v_\infty$	$C_{\rm c}$ up to v_s	$C_{\rm c}$ up to $0.4v_\infty$
Dwarfs										
30 000	6.6	4.50	12.9	2176	0.0	-7.67	-7.67	-7.67	-7.67	-7.67
					0.5	-7.60	-7.64	-7.64	-7.63	-7.62
					1.0	-7.53	-7.56	-7.57	-7.63	-7.62
					1.5	-7.24	-7.32	-7.36	-7.56	-7.55
					2.0	-6.93	-7.01	-7.05	-7.58	-7.53
40 000	10.7	5.42	34.6	2585	0.0	-6.13	-6.13	-6.13	-6.13	-6.13
					0.5	-6.11	-6.00	-6.00	-6.21	-6.21
					1.0	-6.04	-5.93	-5.92	-6.23	-6.23
					1.5	-5.99	-5.86	-5.82	-6.24	-6.22
					2.0	-5.84	-5.78	-5.72	-6.27	-6.23

Table 2.1: Continued . . .

$T_{\rm eff}$ [K]	R [$R_\odot$]	$\log L$ [$L_\odot$]	M [$M_\odot$]	v_∞ [km/sec]	$\log C_{\rm c}$	$\log \dot{M}$ [$M_\odot$yr^{-1}]				
						$C_{\rm c}$ constant	$C_{\rm c}$ from v_s	$C_{\rm c}$ from $0.4v_\infty$	$C_{\rm c}$ up to v_s	$C_{\rm c}$ up to $0.4v_\infty$
Supergiants										
30 000	22.4	5.56	28.8	1506	0.0	-5.90	-5.90	-5.90	-5.90	-5.90
					0.5	-5.73	-5.80	-5.78	-5.93	-5.91
					1.0	-5.33	-5.54	-5.57	-5.87	-5.80
					1.5	-5.14	-5.23	-5.30	-5.88	-5.72
					2.0	-4.94	-4.99	-5.03	-5.85	-5.56
40 000	19.1	5.93	58.1	2212	0.0	-5.22	-5.22	-5.22	-5.22	-5.22
					0.5	-5.21	-5.12	-5.11	-5.31	-5.29
					1.0	-5.20	-5.05	-5.00	-5.36	-5.36
					1.5	-5.19	-5.08	-4.90	-5.42	-5.43
					2.0	-5.10	-5.04	-4.84	-5.42	-5.46

per unit time. The reason why we discuss the results in terms of $E_{\rm kin}$ and not in terms of $\dot{M}$ is that our Monte Carlo calculation essentially predicts the change in kinetic energy (see Sect. 2.2.1), but does not predict the effect on the velocity structure. If in presenting the results we assume that the terminal velocity is not affected[1], the effect of clumping can be expressed in a (change in) mass loss rate. This most certainly is not appropriate for the case in which clumping starts at $0.4v_\infty$. It is to be expected that only for those cases where clumping has developed near the sonic point the above assumption has merit. So; though we cannot disentangle the effects on $\dot{M}$ and v_∞, we still opt to present changes in $\dot{M}$ only in all clumping prescription in Table 2.1 (and also in Table 2.2). However, in the discussion Sect. 2.4 we will concentrate on the physically most relevant cases.

As explained in section 2.2.4, the first four columns of Table 2.1 list stellar parameters and the fifth the adopted terminal velocity. In column six the clumping factor is given that is used in five different clumping prescriptions: constant clumping (column 7; filled red circles in the plot); clumping starting at the sonic point (column 8; green crosses) and at $0.4v_\infty$ (column 9; blue plusses), and clumping in the photosphere and lower part of the wind up to the sonic point (column 10; purple crosses) and up to $0.4v_\infty$ (column 11; black triangles). The fact that in these predictions porosity is not included implies that we assume the clumps to be optically thin.

Clumping introduces two effects that impact the mass loss of the star. First, if clumping occurs in the stellar photosphere the increased continuum opacity will shift the layer of continuum formation to lower temperatures, i.e. softening the radiation field. As a result, the Lyman and He I continuum flux decrease, while the Balmer continuum flux increases. For a 30 000 K star the wind driving relies strongly on the contribution of Fe IV, with Fe III supplying a non-negligible part. As the lines of these ions tend to cluster in the Balmer continuum, clumping in the photosphere will result in an increase of the mass-loss rate. For a 40 000 K star the wind driving relies on Fe V and Fe IV lines (as well as on lines of carbon, nitrogen and oxygen), preferentially located in the Lyman and He I continuum. Therefore in this case clumping in the photosphere will slightly lower the mass-loss rate. Second, clumping in the stellar wind will push the ionization balance of the wind driving ions towards a lower ionization stage. As has been shown by Vink et al. (1999) a dramatic increase in the mass loss rate is to be expected when iron recombines from Fe IV to Fe III near the sonic point. This occurs at $\sim 25\,000$ K in a smooth wind and is referred to as the bi-stability jump. Though Fe III does not become dominant in even the most clumped winds (i.e. $C_{\rm c} = 100$) of our 30 000 K star, the Fe III contribution does increase very substantially for large clumping factors causing a higher mass-loss. For the 40 000 K

[1]Notice that this neglects the possibility of feedback, i.e. a fully consistent hydrodynamical treatment of clumping might in principle result in a complex reaction that does not obey $\Delta\dot{M} \propto \Delta v_\infty^{-2}$ for a given ΔL.

star the increased importance of Fe IV relative to Fe V (and e.g. C III and C IV relative to C V) in a clumped outflow also has a positive effect on $\dot{M}$, though not as pronounced as in the 30 000 K star.

These considerations allow to interpret the results in Fig. 2.4. In the 30 000 K stars both the effect of clumping on the photospheric radiation field and the ionization balance work in the direction of an increase in the mass-loss rate (see also Gräfener & Hamann 2008). The small effect on $\dot{M}$ in clumping prescriptions 4 and 5, which both have clumping in the photosphere but not in the outer wind, shows that for this model the impact of clumping on the photospheric radiation field is negligible. The other three clumping prescriptions, 1, 2 and 3, show the importance of clumping in the outer wind. The situation of omnipresent clumping (prescription 1) is most extreme. Here the mass loss may increase by up to a factor 3 for $C_c = 10$ and 7 for $C_c = 100$. Notice that if clumping is only modest ($C_c \lesssim 3$) only small changes in the mass-loss are expected.

The situation for the 40 000 K stars is slightly different. Here the two effects of clumping – the softening of the radiation field and the recombination of the gas – work in opposite directions. In clumping prescriptions 4 and 5 the impact of clumping on the photospheric spectrum causes a modest decrease in the mass loss (less than a factor of two for even the most extreme clumping). Clumping in the outer wind has the reverse effect, which is now most prominent in clumping prescriptions 2 and 3 that have no clumping in the photosphere. As prescription 1 has clumping everywhere this model now falls in between 2 and 3 and 4 and 5. For the strongest clumping the most extreme effect is found for prescription 2 though here the increase in mass loss is only about a factor of two. Notice that modest clumping ($C_c \lesssim 3$) has about a 30% effect on $\dot{M}$.

2.3.2 The effect of porosity on $\dot{M}$

So far, the results that we have presented assume the clumps are optically thin. Now, we will account for the actual optical depth of the clumps. This may cause the medium to become porous. To do so, we have to introduce the physical scale of the separation of the clumps L, as introduced in Sect. 2.2.2. The results for this case are given in Table 2.2. In Fig. 2.5 we show the effect of porosity for the case that clumping sets in at the sonic point (i.e. model 2 in Fig. 2.4) and at 0.4 v_∞ (model 3). The separation between the clumps is either 1/10, 1/100 or 1/1000 of the local scale-height, i.e. $D = 10, 100$ or 1000. Though it seems reasonable to assume that such separations may develop in the wind, these rather large separations (small values of D) are very unlikely to occur in the stellar photosphere. For this reason we focus on models 2 and 3.

In interpreting the results it is important to realize that one should compare these to the predicted mass-loss rates shown in Fig. 2.4 for the relevant clumping factor, and

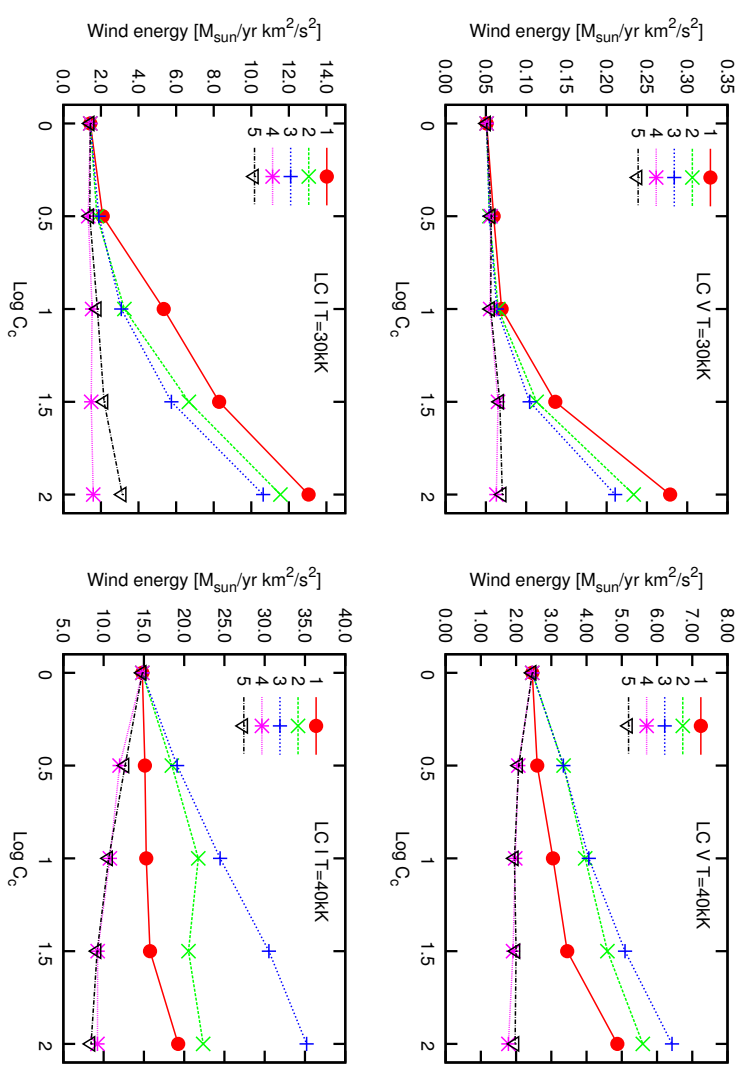

Figure 2.4: Wind energy predictions for different clumping stratifications of selected O-type stars. The smooth wind models have $C_c = 1$. The numbers refer to those used in Fig. 2.1 to identify the clumping behavior. Clumping in the outer winds (stratifications 1 through 3) results in an increase of E_{kin} because of an increased number of effective driving lines. The effect of clumping on the photospheric spectrum (which occurs in stratifications 1, 4 and 5) is temperature dependent; for the 30 000 K (40 000 K) model it leads to an increase (decrease) of $\dot{M}$. See Sect. 2.3.1 for a discussion.

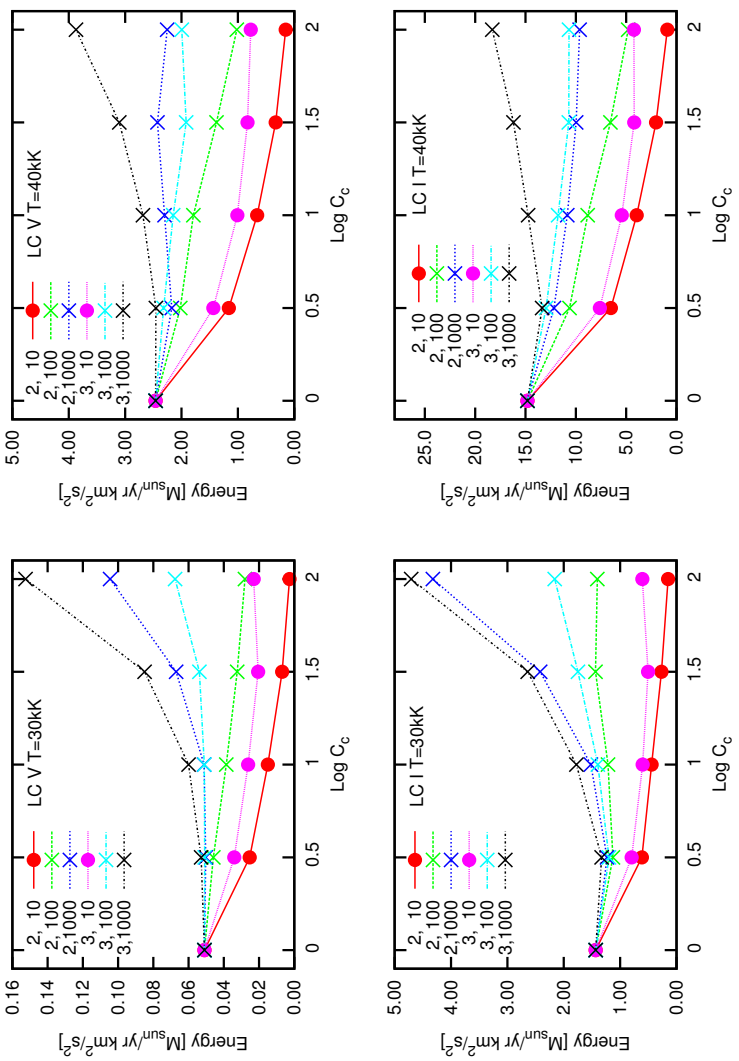

Figure 2.5: Wind energy predictions accounting for both clumping *and* porosity for the clumping stratification in which clumping sets in at the sonic velocity (models labeled 2) and at $0.4\upsilon_\infty$ (models labeled 3). The scale of the clumps is given by H_ρ/D, where D = 10, 100, 1000. These results should be compared to the corresponding models in Fig. 2.4 that account for clumping but not for porosity. The addition of porosity always causes a decrease in $E_{\rm kin}$. See Sect. 2.3.2 for a discussion.

not to the model that has a homogeneous outflow. Only through such a comparison one will single out the effect of porosity on $\dot{M}$. It is clear that if the separation between the clumps is large (D is small) the effect of porosity will be strongest. Photons may travel relatively undisturbed through the interclump medium, avoiding interactions with the gas. For the extreme case $D = 10$ the drop in $\dot{M}$ due to the geometrical effect of porosity may be as large as one to two orders of magnitude. For $D = 1000$ the drop is at most a factor of three. The impact of porosity is less severe if clumping sets in farther out in the wind, as expected.

As an example of the quantitative behavior let us concentrate on the model where clumping sets in at the sonic point and $C_c = 100$. The drop in mass-loss (relative to the results discussed in the previous section) is 0.9 dex for the 30 000 K models and 0.7 dex for the 40 000 K models. For the 30 000 K supergiant model the increase in mass-loss due to the clumping effects discussed in Sect. 2.3.1 is essentially cancelled when porosity is also accounted for. In all other cases of this particular clumping stratification and clumping factor, the inclusion of porosity overcompensates for the effects of clumping on the photospheric radiation field and ionization of the gas and causes a decrease in the mass loss relative to a smooth outflow. Notice that for the smallest clump separation ($D = 1000$) the increase in $\dot{M}$ due to clumping effects alone is typically not fully compensated by the porous nature of the medium. The mass-loss rate may go up, though not more than a factor of three.

Notice that for modest clumping ($C_c \leq 3$) the combined effects of clumping and porosity has a negligible effect for the case $D = 1000$; leads to about a 20% decrease in $\dot{M}$ for $D = 100$, while the mass-loss may drop by about a factor of two in case $D = 10$.

2.4 Discussion

In order to facilitate a quantitative discussion of the effects of clumping and porosity on predicted values of the mass-loss rates of O-type stars and to be able to assess what the actual clumping factors should be in order to bring agreement between empirical and predicted mass-loss rates, we approximate the clumping and porosity effects on the predicted total kinetic energy $E_{\rm kin}$ by a power-law. We thus assume that

$$E_{\rm kin}^{\rm pred}(C_c) = C^{\alpha} \times E_{\rm kin}^{\rm pred}(C_c = 1), \tag{2.12}$$

where the superscript "pred" stands for prediction and $E_{\rm kin}(C_c = 1)$ implies a homogeneous outflow. The typical uncertainty in this relation is 10 to 20 percent for the 30 000 K stars and less than 10 percent for the 40 000 K stars. Values for the power-law index α are given in Table 2.3 in case clumping starts at the sonic point (model 2) and at $0.4v_\infty$ (model 3) for different values of the porosity length, prescribed by the parameter D (see Eq. 2.7).

Table 2.2: Adopted model parameters together with predicted mass loss rates for two clumping stratifications and porosity descriptions. The scale of the clumps is given by H_ρ/D. The clumping laws are: clumping starts at the sonic point (i.e. C_c from v_s) and clumping starts at $0.4v_\infty$ (i.e. C_c up to v_s). We again stress that the mass-loss rates given here have been calculated assuming that all of the change in wind energy benefits $\dot{M}$. However, for instance for the case in which clumping and porosity set in at $0.4v_\infty$ this is highly unlikely; most of the effect will benefit v_∞.

$T_{\rm eff}$	R	$\log L$	M	v_∞	$\log C_c$	$\log \dot{M}$ [$M_\odot$yr^{-1}]					
[K]	[$R_\odot$]	[$L_\odot$]	[$M_\odot$]	[km/sec]		C_c from v_s			C_c from $0.4v_\infty$		
						D = 10	D = 100	D = 1000	D = 10	D = 100	D = 1000
Dwarfs											
30 000	6.6	4.50	12.9	2176	0.0	-7.67	-7.67	-7.67	-7.67	-7.67	-7.67
					0.5	-7.97	-7.71	-7.67	-7.84	-7.67	-7.65
					1.0	-8.20	-7.79	-7.67	-7.96	-7.67	-7.60
					1.5	-8.54	-7.86	-7.55	-8.06	-7.64	-7.45
					2.0	-8.95	-7.93	-7.36	-8.01	-7.54	-7.19
40 000	10.7	5.42	34.6	2585	0.0	-6.13	-6.13	-6.13	-6.13	-6.13	-6.13
					0.5	-6.46	-6.22	-6.19	-6.37	-6.16	-6.13
					1.0	-6.71	-6.27	-6.16	-6.52	-6.19	-6.10
					1.5	-7.01	-6.38	-6.14	-6.61	-6.24	-6.03
					2.0	-7.34	-6.52	-6.17	-6.64	-6.22	-5.94

Table 2.2: Continued ...

$T_{\rm eff}$	R	$\log L$	M	v_∞	$\log C_{\rm c}$	$\log \dot{M}$ [$M_\odot$yr^{-1}]					
[K]	[$R_\odot$]	[$L_\odot$]	[$M_\odot$]	[km/sec]		$C_{\rm c}$ from v_s			$C_{\rm c}$ from $0.4v_\infty$		
						$D = 10$	$D = 100$	$D = 1000$	$D = 10$	$D = 100$	$D = 1000$
Supergiants											
30 000	22.4	5.56	28.8	1506	0.0	-5.90	-5.90	-5.90	-5.90	-5.90	-5.90
					0.5	-6.26	-6.00	-5.96	-6.15	-5.98	-5.93
					1.0	-6.41	-5.97	-5.87	-6.28	-5.91	-5.81
					1.5	-6.63	-5.90	-5.67	-6.35	-5.81	-5.63
					2.0	-6.88	-5.91	-5.42	-6.27	-5.72	-5.38
40 000	19.1	5.93	58.1	2212	0.0	-5.22	-5.22	-5.22	-5.22	-5.22	-5.22
					0.5	-5.57	-5.36	-5.30	-5.51	-5.28	-5.26
					1.0	-5.79	-5.44	-5.35	-5.64	-5.32	-5.22
					1.5	-6.08	-5.57	-5.39	-5.77	-5.36	-5.18
					2.0	-6.43	-5.71	-5.41	-5.76	-5.36	-5.13

Empirical mass-loss rates derived using the Hα line or the radio continuum may suffer from the presence of clumping as these diagnostics scale with the square of the density. Fits to these data assuming a homogeneous outflow should thus be corrected for clumping according to the relation

$$\dot{M}^{\rm emp}(C_{\rm c}) = C_{\rm c}^{-1/2} \times \dot{M}^{\rm emp}(C_{\rm c} = 1), \tag{2.13}$$

where the superscript "emp" stands for empirical. To facilitate a further comparison we assume that for the models where clumping develops near the sonic point the effect of clumping dominantly impacts the mass-loss rate. If clumping sets in further out in the wind (at, say, $0.4v_\infty$), the dominant impact is on the terminal flow velocity and not on $\dot{M}$ (see Krtička et al. 2008). We therefore focus our discussion on the results that have been obtained for models in which clumping sets in at the sonic point. In doing so, we replace the term $E_{\rm kin}^{\rm pred}$ in Eq. 2.12 by $\dot{M}^{\rm pred}$. In order to match empirical and predicted mass-loss rates for a wind that suffers from clumping and porosity it should thus hold that

$$\log\left(\frac{\dot{M}^{\rm emp}(C_{\rm c} = 1)}{\dot{M}^{\rm pred}(C_{\rm c} = 1)}\right) = (\alpha + 0.5) \log C_{\rm c}. \tag{2.14}$$

2.4.1 Accounting for clumping in both empirical estimates and predictions of mass-loss rates

In a comparison of empirical and predicted mass-loss rates of O-type stars brighter than $175\,000\,L_\odot$, having strong winds ($\dot{M} \gtrsim 1 - 2 \times 10^{-7} M_\odot {\rm yr}^{-1}$), Mokiem et al. (2007) found that the empirical rates are consistently higher than the predicted rates. This implies that in principle a clumping factor (for given porosity length) can be found such that $\dot{M}^{\rm emp}(C_{\rm c})$ and $\dot{M}^{\rm pred}(C_{\rm c})$ match *if* $\alpha > -0.5$. For smaller values of α the drop in predicted mass-loss rate due to the effect of clumping and porosity is so severe that it can never be matched by the correction of the empirical mass-loss rate for the effect of clumping. Our predictions show that this situation will occur if clumping develops relatively close to the surface (near the sonic point) for large clump separations $L(r) \gtrsim 0.1 H_\rho$ (or $D \lesssim 10$).

The offset between empirical and predicted mass-loss rates assuming homogeneous outflows as determined by Mokiem et al. (2007) is +0.27 dex for Galactic stars (see the left panel of their figure 4). This value is derived by comparing the empirical and predicted modified wind momentum (MWM) relation at a luminosity $\log(L/L_\odot) = 5.75$, which is typical for the stars investigated by these authors. As the slopes of these MWM relations show tiny differences, the choice of luminosity may in principle have a small effect on the derived offset. The offset of +0.27 dex in the mass-loss rate implies that a clumping $C_{\rm c} \simeq 3.5$ is sufficient to bring agreement

between $\dot{M}^{\rm emp}$ and $\dot{M}^{\rm pred}$ *assuming clumping has no effect on the predicted mass-loss rates*. If one does account for clumping and porosity effects in the theoretical values, the clumping that is required may increase up to $C_{\rm c} \sim 10$ for the case $D \sim 100$, but may be slightly lower ($C_{\rm c} \sim 2.5 - 3.5$) if $D \sim 1000$ as, on average, the derived α values are positive. For porosity lengths corresponding to $D \lesssim 100$ the required clumping factor will increase steeply.

2.4.2 Observational constraints on the number of clumps

In section 2.2.2, we estimated that the number of clumps per wind flow-time that we assumed in our models is $\sim 200\, D^3$. The question is whether there are any empirical constraints either in support of, or contradicting the assumed clump sizes and numbers in our models. Currently, only rather rough order-of-magnitude estimates can be made.

Lépine & Moffat (1999) monitored a number of Wolf-Rayet stars spectroscopically discovering line-profile variations (LPVs) which were interpreted as a large number (more than 10^4) of randomly distributed, radially propagating, discrete wind emission elements, or DWEEs, in order to account for the LPVs. Another way to derive the number and spatial scales of clumps is via the use of linear polarimetry that provides information on the geometry of the innermost portions of the stellar wind. Davies et al. (2007) showed that in order to reproduce the observed level of polarization variability of the LBVs P Cygni and AG Car the winds should consist of $\sim 10^3$ clumps per wind flow-time.

Quantitative estimates of the typical number of clumps in O-type stars have not yet been made, though line-profile variations do point to the presence of structure in their winds as well (see e.g. Eversberg et al. 1998; Lépine & Moffat 2008). The origin of the clumps likely controls their number. Cantiello et al. (2009) recently suggested that wind clumping might be induced by sub-surface convection induced by the iron opacity peak in massive stars, where the density scale height in the iron opacity zone is approximately a factor 10^2 larger in LBV than in O star models. If wind clumping in LBVs and O stars were indeed induced by this iron opacity peak, one would then expect a factor 10^2 more clumps per wind flow-time in O star than in LBV winds, which would bring us in the range of 10^5 clumps per wind flow-time for O stars. This appears to be consistent with values of D on the lower end ($D \sim 10$) of the range studied in our paper. As pointed out in section 2.4.1, such a relatively modest number of clumps would lead to lower expected mass-loss rates making it hard to reconcile empirical and predicted mass-loss rates for stars with dense winds.

Table 2.3: Fitted behavior of the effects of clumping and porosity for the case that clumping sets in at the sonic point (model 2) and at $0.4v_\infty$ (model 3). The total kinetic energy is fitted to the function $E_{\rm kin} = E_{\rm kin}(C_{\rm c} = 1) \times C_{\rm c}^{\alpha}$, for each type of star and clump separation $L(r) = H_\rho(r)/D$. For given values of D the table lists the values of α. $D = \infty$ implies non-porous models.

D	30 000 V	40 000 V	30 000 I	40 000 I
clumping sets in at the sonic point (model 2)				
10	-0.61	-0.59	-0.50	-0.60
100	-0.13	-0.18	-0.02	-0.24
1000	+0.11	-0.02	+0.17	-0.11
∞	+0.26	+0.19	+0.43	+0.10
clumping sets in at $0.4v_\infty$ (model 3)				
10	-0.22	-0.30	-0.26	-0.33
100	+0.04	-0.06	+0.06	-0.08
1000	+0.19	+0.08	+0.20	+0.03
∞	+0.24	+0.21	+0.40	+0.20

2.4.3 The weak wind problem

For luminosities below about 175 000 $L_\odot$, a comparison between empirical and predicted mass-loss rates shows a large discrepancy referred to as the "weak wind problem": empirical mass-loss rates appear to be up to two orders of magnitude lower than the predicted rates. At the moment, the nature of this weak wind problems eludes us; for a discussion see e.g. Martins et al. (2004, 2005b); de Koter (2006); Fullerton et al. (2006); Mokiem et al. (2007); Puls et al. (2008). In the context of the current study a possible explanation could be that the wind of relatively low luminosity O stars become extremely clumpy and porous. Estimating the magnitude of the weak wind problem for stars of 100 000 $L_\odot$ at about a factor of 30 (see for instance the right panel of figure 1 in Mokiem et al. 2007), a clumping factor $C_{\rm c} \approx 500$ and porosity length $D \approx 10$ could bring empirical and predicted estimates into agreement. It is however unclear why preferentially in low density stellar winds, typically at $\dot{M} \lesssim 1 - 2 \times 10^{-7} M_\odot {\rm yr}^{-1}$, such extreme inhomogeneities would develop.

2.5 Conclusions

We have investigated effects of clumping and porosity on predictions of the wind energy of O-type dwarf and supergiant stars using a method that is based on Monte Carlo radiative transfer. These results can be viewed as an addition to prescriptions provided by Vink et al. (2000, 2001). For five heuristic clumping stratifications we investigate the effects of a clumpy medium on the wind energy through induced changes in the (photospheric) radiation field and the excitation and ionization state of the gas throughout the wind. Also, we investigate the effect of porosity by introducing a prescription in which the clump size is expressed as a fraction of the local density scale height. Clumps of size H_ρ/D equal to 1/10th, 1/100th and 1/1000th of H_ρ are considered. The main conclusions are:

(I) The presence of optically thin clumps favors the recombination of the gas, which for the temperature range investigated (between 30 000 and 40 000 K) causes an increase in the line force, therefore an increase in the mass-loss rate. The larger the clumping factor C_c and the closer the star is to the bi-stability jump (at $\sim$ 25 000 K) the stronger is the effect.

(II) Accounting for porosity effects in the clumped medium and the (wavelength dependent) optical depth of the clumps, the mass-loss rate is found to decrease simply because photons may travel in between the clumps, avoiding interactions with the gas. For small clumps ($D \gtrsim 1000$) this effect is not very important, but for larger clumps ($D \lesssim 100$) the overall effect is a net decrease in $\dot{M}$.

(III) For clump sizes corresponding to $D \sim 100$ or larger the net effect on $\dot{M}$ is small. Assuming that the velocity structure is not affected by clumps the mass loss rate decreases by less than a factor of two, even for clumping factors $C_c \sim 100$. For large clumps, corresponding to $D \lesssim 10$, the effect is more dramatic. Already for modest clumping we find that $\dot{M} \propto C_c^\alpha$ with $\alpha \sim$ -0.5 to -0.6. For such a steep dependence empirical mass-loss rates based on Hα measurements, which are found to be about a factor of two higher than predictions assuming smooth outflows, can no longer be reconciled with theoretical $\dot{M}$ values by applying clumping corrections.

(IV) Though large clumps and very large clumping factors may dramatically reduce the mass-loss rate, the occurrence of this type of structure is likely not the explanation for the "weak wind problem" for stars with $L \lesssim 10^{5.2} L_\odot$, unless a

mechanism can be identified causing extreme structure to develop in winds of $\dot{M} \lesssim 1 - 2 \times 10^{-7}\ M_{\odot}\mathrm{yr}^{-1}$ that is not active in denser winds.

Acknowledgements We would like to thank Joachim Puls for suggestions on how to verify the implementation of clumping and constructive discussions. JK and JK kindly acknowledge support from grant GA ČR 205/08/0003.

3 Predictions for mass-loss rates and terminal wind velocities of massive O-type stars

L. Muijres, Jorick S. Vink, A. de Koter, P.E. Müller, and N. Langer

submitted to Astronomy & Astrophysics

Abstract

Mass loss from massive stars forms an important aspect of the evolution of massive stars, as well as for the enrichment of the surrounding interstellar medium.

Our goal is to predict accurate mass-loss rates and terminal wind velocities. These quantities can be compared to empirical values, thereby testing radiation-driven wind models. One specific topical issue is that of the so-called "weak-wind problem", where empirically derived mass-loss rates and (modified) wind momenta fall orders of magnitude short of predicted values.

We employ an established Monte Carlo model and a recently suggested new line acceleration formalism to solve the wind dynamics more consistently.

We provide a new grid of mass-loss rates and terminal wind velocities of O-type stars, and compare the values to empirical results. Our models fail to provide mass-loss rates for main-sequence stars below a luminosity of $\log(L/L_{\odot}) = 5.2$, where we appear to run into a fundamental limit. At luminosities below this critical value there is insufficient momentum transferred to the wind in the region below the sonic point in order to kick-start the acceleration of the flow. This problem occurs at almost the exact location of the onset of the weak-wind problem. For O dwarfs, the boundary between being able to start a wind, and failing to do so, is at spectral type O6/O6.5. The direct cause of this failure for O6.5 stars is a combination of the lower luminosity and a lack of Fe v lines at the base of the wind. This might indicate that – in addition to radiation pressure – another mechanism is required to provide the necessary

driving to initiate the wind acceleration.

For stars more luminous than $10^{5.2}\,L_{\odot}$, our new mass-loss rates are in excellent agreement with the mass-loss prescription by Vink et al. 2000 using our terminal wind velocities as input to this recipe. This implies that the main assumption entering the method of the Vink et al. prescriptions – i.e. that the momentum equation is not explicitly solved for – does not compromise the reliability of the Vink et al. results for this part of parameter space. Finally, our new models predict terminal velocities that are typically 35 and 45 percent larger than observed values. Such over-predictions are similar to those from (modified) CAK-theory.

3.1 Introduction

In this article, we present predictions for mass-loss rates and velocity structures for a grid of O-type stars, using two distinct methods for solving the wind dynamics.

Mass loss forms an integral aspect characterizing massive O-type stars. Because of their short lifetimes, massive stars are important tracers of star formation in galaxies. Furthermore, they enrich the interstellar medium with metals, both during their lives via stellar winds, as well as when they explode at the very end of their evolution. In order to build an evolutionary framework for massive stars, it is essential to map the mass-loss processes (whether continuous or in bursts) during the various evolutionary stages, as the exact rates of mass loss greatly influence the evolutionary tracks (e.g. Maeder 1981; Chiosi & Maeder 1986). The effects of mass loss on the evolutionary tracks are at least two-fold: first and foremost the stellar mass is reduced, and secondly, the rotational velocity is strongly affected, as the mass also carries away angular momentum (e.g. Langer 1998; Maeder & Meynet 2000).

For the continuous stellar winds from massive stars, the outflow is thought to be driven by the transfer of energy and momentum from the radiation field to the atmosphere through the absorption of photons in atomic transitions. The exact amount of momentum and energy transfer has been the subject of both theoretical and observational studies for many decades (Lucy & Solomon 1970; Castor et al. 1975; Pauldrach et al. 1986; Puls et al. 1996; de Koter et al. 1997; Vink et al. 1999; Krtička & Kubát 2004; Mokiem et al. 2007). For luminous O-type stars, with $\log(L/L_{\odot}) > 5.2$, the theoretical predictions of Vink et al. (2000) seem to be in reasonable agreement with empirical mass-loss rates provided that O-stars are only subject to modest amounts of wind clumping (with clump filling factors of only 5-10). However, for objects with luminosities $\log(L/L_{\odot})$ below approximately 5.2, a severe drop – by a factor of $\sim$100 – in the empirically determined modified wind momentum (basically a multiplication of the mass-loss rate and the terminal velocity) has been revealed. This problem has in literature been referred to as "the weak-wind problem" (Puls et al. 1996; Martins et al. 2005b; Puls et al. 2008; Marcolino et al. 2009).

It deserves proper investigation simply because of the enormity of the effect. It is particularly important to find out whether the problem is caused by the mass-loss diagnostics or the predictions, as both are also applied to more luminous stars, where agreement between diagnostics and predictions has seemingly been achieved. But how certain can we be that this agreement is not a coincidence if we are aware of severe problems at lower luminosity?

Furthermore, we note that the oft-used mass-loss predictions of Vink et al. (2000) are semi-empirical, in the sense that empirical values for the wind velocity structure and terminal velocity are used as input to the modelling. In order to trust our overall knowledge of the mass-loss rates from O-type stars – at *all* masses and luminosities – it is pivotal to further scrutinize the Vink et al. (2000) assumptions, most notably that of the adopted wind dynamics.

Recently, Müller & Vink (2008) suggested a new parametrization of the line acceleration, expressing it as a function of radius rather than of the velocity gradient, Castor et al. (1975; henceforth CAK) theory. The implementation of this new formalism allows for local dynamical consistency, as one can determine the energy and momentum transfer at each location in the wind through the use of Monte Carlo simulations. Although the formalism was applied with three independent starting conditions that showed convergence to the same wind parameters, it has thus far only been applied to one object, that of an O5 dwarf.

Interestingly, for the adopted line force parameterization Müller & Vink identify an exact solution in case the medium is isothermal. However, their iterative scheme designed to converge on the parameters describing the line force introduces some assumptions (see Sect. 3.2.5 for further details) in addition to that of a constant gas temperature. To study the importance of these assumptions – and to further improve on the physical treatment – we employ the new line acceleration parameterization but solve for the wind dynamics consistently by applying a numerical method.

The purpose of our study is threefold: *i)* to solve the wind dynamics numerically, and compare the results to those of Müller & Vink (2008), *ii)* to compute a larger grid of dynamically derived O-star mass-loss rates and wind terminal velocities, and determine the accuracy of the predictions made by Vink et al. (2000), and *iii)* to utilize the grid in order to investigate the weak-wind problem.

Our paper is organized as follows. In Sect. 3.2, we start off describing the core of our method and the different methods to treat the wind equation. The results are presented in Sect. 3.3 and discussed in the Sect. 3.4. We end with the conclusions (Sect. 3.5).

3.2 Method

The method of de Koter et al. (1997) and Vink et al. (1999), applied to derive the mass-loss rates of O and early-B type stars (Vink et al. 2000, 2001), Luminous Blue Variable stars (Vink & de Koter 2002) and Wolf-Rayet stars (Vink & de Koter 2005), is an extension of a treatment developed by Abbott & Lucy (1985). It is based on an iteration cycle between the stellar atmosphere model ISA-WIND (de Koter et al. 1993) and a Monte Carlo simulation, MC-WIND (de Koter et al. 1997), in which the energy per unit time ΔL that is extracted from the radiation field in interactions of photons with the gas, is computed. From this a mass-loss rate $\dot{M}$ is computed on the basis of which a new ISA-WIND model is constructed. The predicted mass loss is the one for which the input mass-loss rate of ISA-WIND equals the mass-loss rate computed by MC-WIND.

As is consistently pointed out in the papers referred to above, the method does not address the equation of motion but uses a prescribed trans-sonic velocity structure. This implies that though in a global sense the method fulfills the constraint of energy conservation, it need not hold that the actual local forces acting on the gas are consistent with the force implied by the adopted velocity law. Müller & Vink (2008) relax on this assumption and present an improved treatment of the problem introducing a new way to parametrize the line force. We first discuss one type of solution presented by these authors, which we refer to as "best-β" method. In a second step, we present solutions that numerically solve the wind dynamics.

We first briefly introduce ISA-WIND in Sect. 3.2.1, emphasizing the treatment of the heuristic velocity law, and MC-WIND in Sect. 3.2.2, focusing on the determination of the mass-loss rate using the global energy argument. In Sect. 3.2.3 we recapitulate the essentials of the parametrization of the line force by Müller & Vink and the principle of their best-β method. In the following subsection we introduce our hydrodynamical method. Finally, Sect. 3.2.6 is devoted to a discussion of the physical conditions at the sonic point.

3.2.1 The model atmosphere

The code ISA-WIND computes the structure, radiation field and ionization/excitation state of the gas of an outflowing stellar atmosphere in non local thermodynamic equilibrium (non-LTE), assuming radiative equilibrium. No artificial separation between the photosphere and wind is assumed. The temperature structure is treated somewhat simplified in that it results from initial LTE based Rosseland opacities (i.e. grey). The fact that the temperature structure is not affected by possible departures from the populations from their LTE state implies that the effect of line blanketing is not treated self-consistently, although non-LTE line blocking is taken into account. Radiation transfer in spectral lines is treated in the Sobolev approximation (Sobolev 1960).

The input stellar parameters are the luminosity L, the effective temperature $T_{\rm eff}$ (specifying the radius R), the mass M and chemical abundances. The wind is described by the mass-loss rate $\dot{M}$ and a velocity structure, which are connected through the equation of mass continuity

$$\dot{M} = 4\pi r^2 v(r)\rho(r), \tag{3.1}$$

where $\rho(r)$ is the mass density and $v(r)$ is the velocity at radius r. Outside the photosphere, the velocity structure is assumed to follow a β-law, i.e.

$$v(r) = v_\infty \left(1 - \frac{r'}{r}\right)^\beta . \tag{3.2}$$

The free parameter β is a measure of the velocity gradient. A low value of β implies that the velocity approaches the terminal flow velocity v_∞ relatively close to the star; for a large value this happens only further out in the wind. The β-law does not hold in the photosphere since the line force is not the dominant term in the equation of motion, but gravity and the acceleration due to the gas pressure gradient also contribute (very) significantly to the flow structure. The radius r' is a smoothing parameter that is used to connect the β-law to the (quasi) hydrostatic photosphere and must assure that $v(r)$ and its spatial derivative are continuous at the point where one couples the photospheric velocity law to the β-law. The velocity structure in the photosphere is determined by solving the non-isothermal equation of motion, neglecting line radiation pressure and assuming that continuum radiation pressure is the result from Thomson scattering only. An inner boundary velocity (or density) is chosen, which may be used to tune the total Rosseland optical depth of the photosphere and wind (see below).

The wind is assumed to be homogeneous, i.e. the outflowing gas is not clumped (but see Muijres et al. 2010a), and the terminal velocity is chosen to be 2.6 times the effective escape velocity from the stellar photosphere, which is in reasonable concordance with empirically determined terminal velocities of O-stars (Lamers et al. 1995; Kudritzki & Puls 2000). The base of the photosphere is positioned at a Rosseland optical depth of about 20-25 and the wind extends out to 20 $R_\star$.

3.2.2 The Monte Carlo method MC-WIND

The code MC-WIND uses the model atmosphere structure computed by ISA-WIND to determine the total amount of energy that is transferred from the radiation field to the wind – in interactions of photons with ions in the gas – by means of a Monte Carlo simulation of the trajectories of photon packets emitted at the base of the photosphere and escaping through the outer boundary of the model. Each photon can travel an optical depth weighted (random) distance to a point of interaction. This point is

determined by taking into account all the opacity the photon encounters on its path, so it includes contributions from both lines and continua. At the point of interaction the type of interaction is determined, using proper weighing functions (Vink et al. 1999). The possible interactions are thermal absorption and emission, electron scattering and line scattering. The interaction is assumed to be coherent in the co-moving frame of the ion. In the observers frame, however, energy can be exchanged from the radiation field to the gas (or vice versa). It is traced which ion is involved in the interaction, such that, for instance, the contributions to the radiative force can be dissected and identified. This provides us with a powerful tool to study the nature of the line force at each location in the wind.

The radiative force per unit mass equals (Abbott & Lucy 1985):

$$g_{\rm rad} = -\frac{1}{\dot{M}}\frac{dL}{dr}, \tag{3.3}$$

where dL is the amount of energy lost by the radiation field in a layer of thickness dr.

Once the total amount of energy transferred to the wind is known, the mass-loss rate that can be driven *for the density and velocity structure of the adopted* ISA-WIND *model* can be calculated. Neglecting enthalpy:

$$\Delta L = \frac{1}{2}\dot{M}\left(v_\infty^2 + v_{\rm esc,N}^2\right), \tag{3.4}$$

where ΔL is the total amount of energy lost by the radiation field and

$$v_{\rm esc,N} = \sqrt{\frac{2GM_*}{R_*}}, \tag{3.5}$$

is the Newtonian escape velocity from the stellar surface. G is the gravitational constant. A new ISA-WIND atmosphere, adopting the mass-loss rate as determined in MC-WIND, is computed followed by a new Monte Carlo simulation. This procedure is repeated until the input mass-loss rate of MC-WIND equals the output mass-loss rate. Though the mass-loss rate that is predicted in this way reflects that in a *global* sense the energy that is needed to drive the wind is indeed extracted from the radiation field, it does not mean that the input line force (implied by the velocity law) equals the output line force from the Monte Carlo simulation *locally*, i.e. the equation of motion of the wind is not solved.

Next we improve on this situation using two methods. Both methods A and B require a parametrization of the line force predicted by MC-WIND. We therefore first discuss this aspect.

3.2.3 Line force parametrization

Figure 3.1 shows the Monte-Carlo line force (black crosses) as is produced in the first iteration step of a typical O3 V star ($L = 10^{5.83}\,L_\odot$, $T_{\rm eff}$= 44,600 K and $M = 58\,M_\odot$).

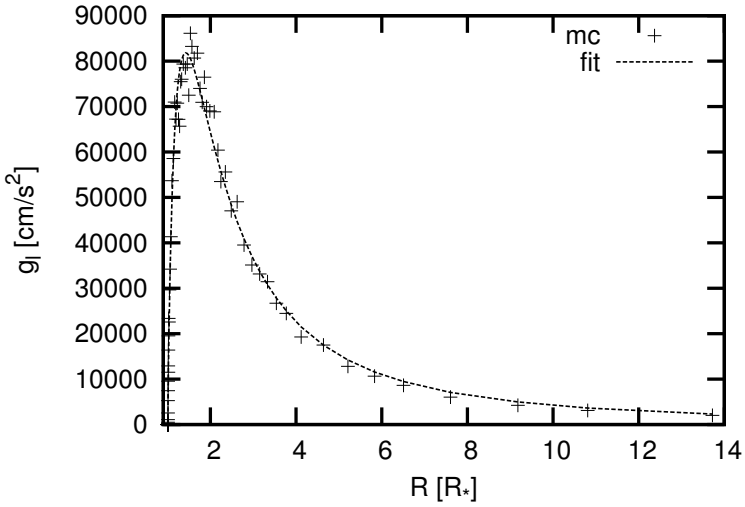

Figure 3.1: The line force (black crosses) as predicted by MC-WIND in the first iteration step. A fit (black dotted line) using Eq. 3.6 to represent the line force is overplotted. Note the modest scatter on the Monte Carlo results due to noise.

The Monte Carlo line force is determined in a statistical way and shows scatter. Given the delicate nature of the equation of motion it can not be used as such and must be represented by an appropriate analytical fit function. We adopt a parametrization of the line force as a function of radius, rather than of optical depth, as opted for by Castor et al. (1975). In Sect. 3.4.2 we show that this leads to a more accurate representation of the line force, at least for the type of stars studied here. In doing so we follow Müller & Vink (2008), who motivate

$$g_{\rm rad}^{\rm line} = \begin{cases} 0 & \text{if} \quad r < r_\circ \\ g_\circ \, (1 - r_\circ/r)^\gamma / r^2 & \text{if} \quad r \geq r_\circ, \end{cases} \tag{3.6}$$

where $g_\circ$, $r_\circ$, and γ are fit parameters to the Monte Carlo line force. Figure 3.1 shows a typical result for this fit (black dotted curve). The deviations are (as mentioned) due to scatter in the simulation.

3.2.4 Method A: Best-β solution

In this section, we use the line force representation Eq. 3.6 to determine – after making certain assumptions – an analytical solution of the velocity law in the outer part of the wind, following Müller & Vink (2008). This solution can be compared to the

β-law (Eq. 3.2) and used to derive v_∞ and the β value that is most representative. This is useful in comparing to the often applied β-law.

We aim to find a solution of the equation of motion

$$v\frac{dv}{dr} = -\frac{R_* v_{\rm esc}^2}{2r^2} + g_{\rm rad}^{\rm line} - \frac{1}{\rho}\frac{dp}{dr}, \tag{3.7}$$

where p is the gas pressure and

$$v_{\rm esc} = v_{\rm esc,N}\sqrt{1-\Gamma}, \tag{3.8}$$

is the effective surface escape velocity of the star. Γ is the continuum radiation pressure in units of the Newtonian gravitational acceleration. Sufficiently far from the photosphere this term is dominated by radiation pressure on free electrons, i.e. $\Gamma = \Gamma_{\rm e}$, where $\Gamma_{\rm e}$ is essentially constant for early-type stars. Close to or in the photosphere, the acceleration due to free-free and bound-free processes may compete with electron scattering and should, in principle, be considered in Eq. 3.8. For our best-β solution, however, we assume a constant continuum acceleration, which we set to $\Gamma_{\rm e}$. Substituting the equation of state for an ideal gas and using Eq. 3.1, the term $(1/\rho)\,dp/dr$ can be written as:

$$\frac{1}{\rho}\frac{dp}{dr} = -\frac{a^2}{v}\frac{dv}{dr} - \frac{2a^2}{r} + \frac{k}{m}\frac{dT}{dr}, \tag{3.9}$$

where k is Boltzmann's constant, m the mean particle mass and $a(r)$ is the local sound speed, given by:

$$a = \sqrt{\frac{kT}{m}}. \tag{3.10}$$

We assume the wind to be isothermal, such that the sound speed is constant. The equation of motion can now be rewritten as

$$a_\circ\left(\frac{v}{a_\circ} - \frac{a_\circ}{v}\right)\frac{dv}{dr} = -\frac{R_* v_{\rm esc}^2}{2r^2} + \frac{2a_\circ^2}{r} + g_{\rm rad}^{\rm line}, \tag{3.11}$$

where $a_\circ$ is the isothermal sound speed at the effective temperature of the star. Equation 3.11 is a critical point equation. For it to yield a physical (trans-sonic) solution the left- and right-hand side need to vanish at the point $v = a_\circ$, i.e. at the sonic point. Müller & Vink (2008) show that for the isothermal case and a line force as described by Eq. 3.6, an analytical expression for the solution of Eq. 3.11 can be constructed by means of the Lambert W function (see also Müller 2001). The shape of this function is very complex, however, a useful approximate solution for the velocity law can be constructed if the pressure related terms $2a^2/r$ and a/v can be neglected. We note, however, that at the sonic point the contribution of the two pressure terms is

non-negligible (Müller & Vink 2008). After some manipulation one finds that the approximate velocity law is given by:

$$v(r) = \sqrt{\frac{R_* v_{\rm esc}^2}{r} + \frac{2}{r_\circ}\frac{g_\circ}{(1+\gamma)}\left(1 - \frac{r_\circ}{r}\right)^{\gamma+1} + C}, \tag{3.12}$$

where C is an integration constant. From this equation, the terminal wind velocity can be derived if the integration constant C can be determined. This can be done assuming that at radius $r_\circ$ the velocity approaches zero. This yields

$$C = -\frac{R_* v_{\rm esc}^2}{r_\circ}. \tag{3.13}$$

In the limit $r \to \infty$ we find that:

$$v_\infty = \sqrt{\frac{2}{r_\circ}\frac{g_\circ}{(1+\gamma)} - \frac{R_* v_{\rm esc}^2}{2}}. \tag{3.14}$$

The terminal velocity v_∞ can also be determined from the equation of motion. At the critical point, the left-hand and right-hand side of Eq. 3.11 both equal zero. Introducing v_∞ in relation to $g_\circ$ as expressed in Eq. 3.14, we find

$$v_{\infty,\rm new} = \sqrt{\frac{2}{r_\circ}\left[\left(\frac{r_s}{r_s - r_\circ}\right)^{\gamma}\frac{r_s}{(1+\gamma)}\left(\frac{v_{\rm esc}}{2} - 2r_s\right) - v_{\rm esc}^2\right]}, \tag{3.15}$$

where r_s is the radius of the sonic (critical) point.

A direct comparison to the β-law can be made for the regime $v_\infty \gg v_{\rm esc}$ and results in

$$\beta = \frac{1+\gamma}{2}. \tag{3.16}$$

Given the assumptions made in this derivation, this result is only approximately correct.

The procedure that is followed to obtain the best-β solution is that in each Monte Carlo simulation the values of $g_\circ$, $r_\circ$, and γ are determined by fitting the output line force. Using these values and the current value of the sonic point radius, Eqs. 3.14, 3.15 and 3.16 are used to determine v_∞ and β. v_∞ derived from Eq. 3.15, the mass loss predicted in MC-WIND, and the expression derived for β serve as input for a new ISA-WIND model. The two codes are iterated until convergence is achieved.

Following Müller & Vink (2008), we assume that convergence is achieved when all fitparameters and the values for $\dot{M}$ and the sonic point radius are stable to within five to ten percent, *and* the values for v_∞ derived from Eqs. 3.14 and 3.15 agree within 10 percent. This implies that our predicted terminal velocities have at least this uncertainty.

3.2.5 Method B: Hydrodynamic solution

The accuracy of the best-β solution hinges on several important assumptions: *i)* the wind is assumed to be isothermal; *ii)* $\Gamma = \Gamma_e$; *iii)* the gas pressure terms are neglected in the derivation of the terminal velocity Eq. 3.14, *iv)* $v_\infty/v_{\rm esc} \gg 1$. Regarding the latter assumption, empirical determinations of the ratio $v_\infty/v_{\rm esc}$ (Lamers et al. 1995; Kudritzki & Puls 2000) result in values of about 2–3 for O-type stars, 1–2 for B-type supergiants and < 1 for A-type supergiants. It may be expected that the above assumptions have an impact on the velocity structure near the sonic point, which is where the mass-loss rate is set. To assess this impact and to improve on the physical treatment, we devise a numerical solution of the equation of motion (Eq. 3.11) throughout the entire photosphere and wind, referred to as the hydrodynamic solution.

To this end we start our solution at the critical point $v = a$ and proceed both down-stream and up-stream using a $4^{\rm th}$ order Runge Kutta method with adaptive stepsize control (Press et al. 1992). Applying l'Hôpital's rule (see e.g. Lamers & Cassinelli 1999) an expression can be devised to determine dv/dr at $v(r_s) = a$. In order to determine the location of the sonic point r_s we require

$$-\frac{R_* v_{\rm esc}^2}{2r_s^2} + \frac{2a^2}{r_s} + g_{\rm rad}^{\rm line} = 0. \tag{3.17}$$

The above equation is solved numerically.

So far, the hydrodynamic solution assumes an iso-thermal medium. At the sonic point the temperature gradient is very small, therefore the location of r_s can be reliably determined using Eq. 3.17, even if dT/dr would be taken into account. The neglect of the temperature gradient in the hydrodynamic solution in the region below the sonic point has a significant impact on the structure – for instance on the total (Rosseland) optical depth from the inner boundary to the sonic point. To solve this problem, we account for the temperature structure inward of the critical point. This requires an iterative procedure between the solution of the non-isothermal equation of motion

$$a\left(\frac{v}{a} - \frac{a}{v}\right)\frac{dv}{dr} = -\frac{R_* v_{\rm esc}^2}{2r^2} + \frac{2a^2}{r} + g_{\rm rad}^{\rm line} - \frac{k}{m}\frac{dT}{dr}, \tag{3.18}$$

and the temperature structure (see Sect. 3.2.1). After starting numerical integration of the velocity structure at the sonic point r_s (now determined by applying Eq. 3.17, but using the local value of the temperature at the sonic point) in the down-stream direction, we include the dT/dr term in Eq. 3.18. This implies that the location of the sonic point is not affected. In the up-stream direction the temperature gradient is negligible, and is ignored.

Figure 3.2 compares method A and B for an O3 main sequence star. It shows that the best-β solution behaves very similar to the numerical velocity law. However, if

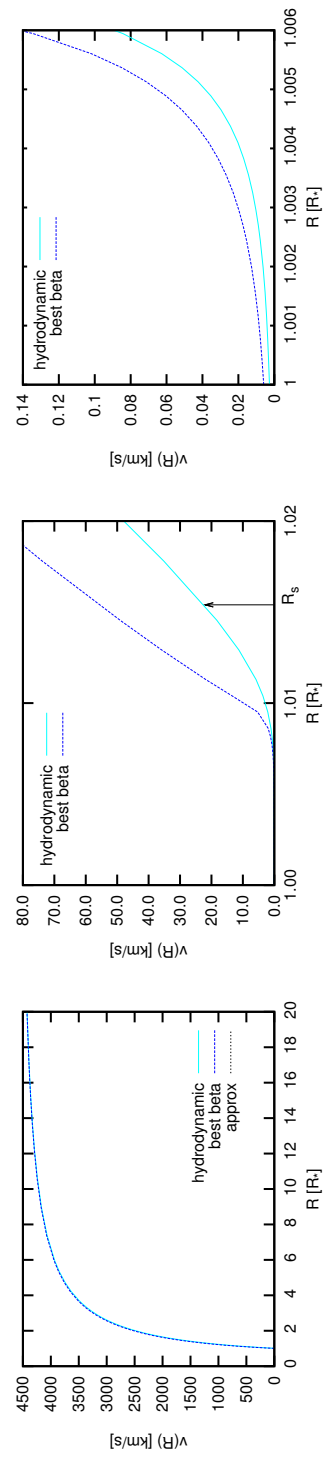

Figure 3.2: A comparison between the velocity laws for an O3 V star based on the best-β (method A) and hydrodynamic solution (method B). Here, the best-β solution is the one determined by using the fitparameters of the hydrodynamic solution. The label 'approx' in the left panel refers to the approximate velocity law, as given by Eq. 3.12. Three different radial regimes are plotted: full radial range (left panel); the region around the sonic point (middle panel) in which the location of the sonic point in the hydrodynamic solution is indicated with an arrow, and the photospheric region (right panel). Note that at high velocities both methods, as well as the approximate velocity law, yield very similar velocity stratifications. Near the sonic point the best-β solution differs significantly from the hydrodynamic velocity law in that it is much steeper near the onset of the wind. Its sonic point is therefore closer to the star. The higher velocity of this best-β solution extends into the photosphere, where hydrostatic equilibrium determines the shape of the velocity profile.

one zooms in on the location of the sonic point, one sees that in the best-β method r_s is positioned slightly more inward, or, alternatively, that the velocity law is steeper in the lower part of the wind. In the best-β method, the absolute scaling of the velocity structure in the photosphere is based on the adopted velocity at the inner boundary of the model (see Sect. 3.2.1), therefore, only the position of r_s as predicted by the hydrodynamical method is physically meaningful.

Once this iterative procedure has converged, and the non-LTE state of the gas is computed throughout the atmosphere, we iterate between ISA-WIND and MC-WIND in the same manner as described in Sect. 3.2.4. Again, save for v_∞, the fit parameters converge on an accuracy of better than ten percent in a few iteration cycles. For v_∞ we are forced to adopt an accuracy of 20 percent. Our predicted terminal velocities have at least this uncertainty.

Remaining assumptions and uncertainties

In the hydrodynamic solution the contribution of bound-free and free-free opacity to the continuum radiation pressure is ignored (see Sect. 3.2.1). In the photosphere, the contribution of these processes to Γ is not negligible and may in fact be of the order of Γ_e.

We use the Sobolev approximation for line radiation transfer. The Sobolev approximation becomes ill-founded for small velocity gradients dv/dr or velocities lower than the sound speed. Pauldrach et al. (1986) showed that in the photosphere (where the velocity is very small) the line force is underestimated in the Sobolev approximation. Further out, in the region of the sonic point, the line optical depth is overestimated compared to comoving frame values, implying an overestimate of the line force in this region and therefore an overestimate of the mass-loss rate.

In addition to the above two sources of uncertainty to the balance of forces at and below the sonic point is the quality of the fitting function Eq. 3.6 in this part of the wind, that may be uncertain by up to a factor of two. This is not expected to be a big problem deep in the photosphere, as both the fit function as well as the simulated Monte Carlo line force are small compared to the radiative force on free electrons, but at the sonic point it might play a role.

3.2.6 The line force at the sonic point: a test for the validity of the best-β method

The critical point of the equation of motion is the sonic point. A dissimilarity between the sonic point and the critical point may occur when the line force is represented by an explicit function of dv/dr, such as in CAK and modified-CAK theory (Pauldrach et al. 1986). Though these descriptions provide extremely valuable insights, they do make assumptions regarding the behavior of $g_{\rm rad}^{\rm line}$ (See Sect. 3.4.2). The same applies

for our method. Here we want to point out that Eq. 3.17 implies that – whatever the description of the line force – at the sonic point $g_{\rm rad}^{\rm line} \simeq g_{\rm eff}$, as the pressure gradient term $2a^2/r$ is small compared to the line force. Here $g_{\rm eff} = GM_*(1-\Gamma)/r^2 = R_* v_{\rm esc}^2/2r^2$. This implies that for the velocity structure to be a physical solution it must be that at the sonic point $g_{\rm rad}^{\rm line}/g_{\rm eff} \simeq 1$, as pointed out by e.g. Castor et al. (1975). We require from our best-β solutions, that this criterion is fulfilled. If $g_{\rm rad}^{\rm line}/g_{\rm eff}$ is not approximately equal to 1 at the sonic point, we interpret this as a failure of the wind to become trans-sonic due to a lack of line force at the location in the wind where it is essential. Dynamical effects might occur, such as fall back, that are beyond the topic of this paper. In any case, we interpret such solutions as cases in which the wind cannot be initiated by line driving alone. For the hydrodynamical solution a failure to fulfill the above requirement implies that we do not find a solution at all.

3.3 Results

3.3.1 Grid

In order to study our predictions of the wind properties of O-type stars in a systematic manner, we define a grid of main sequence, giant and supergiant stars using the spectral calibration of Martins et al. (2005a) adopting theoretical effective temperature scales. This calibration is based on non-LTE models that take into account line blanketing effects and an outflowing stellar wind. We have applied solar abundances as derived by Anders & Grevesse (1989), consistent with the predictions of Vink et al. (2000). For all stars in the grid, we have derived the mass-loss rate, terminal velocity and β-parameter. The hydrodynamic solution does not feature a β, rather γ is the parameter that describes the slope of the velocity law. To better facilitate a comparison between the different methods we have applied Eq. 3.16 to convert γ into a β-value, referred to as β_γ. The calculated grid is given in Table 3.1. The final column lists the mass-loss rate as predicted using the fitting formula of Vink et al. (2000) that assume a fixed value of $\beta = 1$, but for an input variable value of $v_\infty = 2.6\, v_{\rm esc}$.

Figures 3.3, 3.4 and 3.5 show wind properties as a function of effective temperature, for dwarfs, giants and supergiants respectively.

We present all the results of the best beta method, i.e. prior to applying the requirement defined in Sect. 3.2.6 that at the sonic point the acceleration due to the line force should approach the effective gravity. Having pointed this out, we first draw attention to the striking behavior in our best-β predictions of dwarfs. In the direction of decreasing temperature, the terminal flow velocity drastically increases for spectral types O6.5 or later. For giants the O7 star shows a similar behavior. We argue below that this behavior reflects the failure of the wind to become supersonic, therefore we interpret these solutions to be non-physical.

3.3.2 Early O-stars (spectral types O3 through O6)

Let us, however, first focus on stars of spectral type earlier than O6.5. The two methods give quite comparable results. The best-β method predicts $\dot{M}$ values that are higher by up to ~0.1 to 0.3 dex in all cases, i.e. dwarfs, giants and supergiants. The best-β terminal flow velocities are ~10 to 20 percent lower compared to the hydrodynamic solutions. These differences can be understood by focusing on the velocity structures near the sonic point. In the best-β solution the velocity law is steeper in the region near the sonic point, therefore the sonic point is closer to the photosphere. This leads to a higher mass-loss rate and lower terminal velocity. The absolute value of the terminal velocity and the ratio of v_∞ to the effective escape velocity as a function of temperature will be compared to observations in Sect. 3.4. Typical error bars on the v_∞ determination are 10 percent for the best-β solutions (see Sect. 3.2.4) and 20 percent for the exact solutions (see Sect. 3.2.5) due to Monte Carlo noise on the line force (see also Fig. 3.1).

The slope of the velocity law in the best-β solution increases slightly with luminosity class, from typically 0.85 in dwarfs, to 0.95 in giants, to 1.0 in supergiants. In the hydrodynamic models (method B) the β_γ value is typically 0.05-0.10 lower than the corresponding best-β solution.

3.3.3 Late O-stars (spectral types O6.5 through O9.5)

Figures 3.3 and 3.4 show that for spectral type O6.5 the terminal velocity of dwarfs and giants suddenly peaks, relative to spectral type O6. We investigate this behavior in more detail in Fig. 3.6 in which the line force from the Monte Carlo simulation is plotted in the region around the sonic point for the best-β solutions of the dwarf O6 and O6.5 star. For the O6 star, the line force at the base of the wind (below the sonic point) rises steeply. *At first the dominant contributors are iron lines, notably from Fe* v. The ensemble of transitions mainly occur between exited states, though some are from meta-stable states that are relatively strongly populated. Further out, the iron contribution levels out (at ~ 30%) and other elements start to contribute to the force, such as carbon, nitrogen, sulpher, argon and nickel. The contribution of resonance lines of carbon and nitrogen at the sonic point amounts to ~ 20%. Note that at the sonic point the $g_{\rm rad}^{\rm line}/g_{\rm eff} \sim 1$ -condition is nicely fulfilled for the O6 V.

For the O6.5 star this is not the case. Here the line force at the base of the wind (below the sonic point) rises only gradually. The difference with the O6 V star is that in this region iron is mainly in the form of Fe IV, which for this particular spectral flux distribution is less efficient in absorbing stellar flux than are Fe V lines[1]. Therefore the velocity structure will be shallower, limiting the potential of other elements in

[1]We note that a similar situation occurs at spectral type B1, where the relatively inefficient Fe IV lines are replaced by the more effective Fe III lines (Vink et al. 1999).

Table 3.1: Model parameters, following Martins et al. (2005a), and predicted wind properties for dwarfs, giants and supergiants. The label "spec" indicates that spectroscopic masses are adopted from Martins et al. Predictions give the mass-loss rate, terminal velocities and β parameters for both method A (best-β solution) and B (hydrodynamic solution). The 11th column states whether or not the best-β solution fulfills the requirement that at the sonic point $g_{\rm rad}^{\rm line}/g_{\rm eff} \simeq 1$ (see Sect. 3.2.6). For the hydrodynamic solutions a failure of this requirement implies that we do not find a solution at all. The last column provides the $\dot{M}$ by Vink et al. (2001) when we use $v_\infty = 2.6\,v_{\rm esc}$ in their mass-loss recipe. The hydrodynamic solution does not provide a β value, but rather the fit parameter γ. As to facilitate a comparison, we applied Eq. 3.16 to convert this γ into a β.

Model Parameters							Method A			Method B				Vink et al.
ST	$T_{\rm eff}$	$\log g_{\rm spec}$	$\log L$	R	$M_{\rm spec}$	$v_{\rm esc}$	$\log \dot{M}$	v_∞	β	$\Gamma \simeq 1$	$\log \dot{M}$	v_∞	β_γ	$\log \dot{M}$
	K	cm s^{-2}	$L_\odot$	$R_\odot$	$M_\odot$	km/sec	log $M_\odot$/yr	km/sec		at v_s	$M_\odot$/yr	km/sec		$M_\odot$/yr
Dwarfs														
3	44616	3.92	5.83	13.84	58.34	1054	-5.641	3794	0.92	yes	-5.972	4530	0.87	-5.375
4	43419	3.92	5.68	12.31	46.16	1016	-5.836	3599	0.90	yes	-5.929	3973	0.83	-5.571
5	41540	3.92	5.51	11.08	37.28	992	-5.969	2838	0.84	yes	-6.118	3394	0.79	-5.829
5.5	40062	3.92	5.41	10.61	34.17	990	-6.152	2762	0.84	yes	-6.265	3260	0.77	-6.011
6	38151	3.92	5.30	10.23	31.73	994	-6.386	2697	0.81	yes	-6.493	3277	0.77	-6.234
6.5	36826	3.92	5.20	9.79	29.02	983	[-7.243]	[6395]	[1.87]	no	-6.918	5244	0.95	-6.427
7	35531	3.92	5.10	9.37	26.52	972	[-7.340]	[7325]	[2.65]	no	–	–	–	-6.624
7.5	34419	3.92	5.00	8.94	24.15	959	[-7.745]	[12028]	[1.81]	no	–	–	–	-6.820
8	33383	3.92	4.90	8.52	21.95	944	[-7.781]	[10650]	[1.57]	no	–	–	–	-7.019
8.5	32522	3.92	4.82	8.11	19.82	923	[-7.802]	[9427]	[1.40]	no	–	–	–	-7.167
9	31524	3.92	4.72	7.73	18.03	908	[-7.818]	[8283]	[1.21]	no	–	–	–	-7.374
9.5	30488	3.92	4.62	7.39	16.46	892	[-7.793]	[6704]	[1.10]	no	–	–	–	-7.590

Table 3.1: Continued ...

Model Parameters						Method A			Method B				Vink et al.	
ST	$T_{\rm eff}$	$\log g_{\rm spec}$	$\log L$	R	$M_{\rm spec}$	$v_{\rm esc}$	$\log \dot{M}$	v_∞	β	$\Gamma \simeq 1$	$\log \dot{M}$	v_∞	β_γ	$\log \dot{M}$
	K	cm s^{-2}	$L_\odot$	$R_\odot$	$M_\odot$	km/sec	log $M_\odot$/yr	km/sec		at v_s	$M_\odot$/yr	km/sec		$M_\odot$/yr
Giants														
3	42942	3.77	5.92	16.57	58.62	915	-5.445	3275	0.90	yes	-5.551	3756	0.87	-5.182
4	41486	3.73	5.82	15.83	48.80	866	-5.540	2945	0.90	yes	-5.641	3272	0.84	-5.303
5	39507	3.69	5.70	15.26	41.48	837	-5.630	2460	0.90	yes	-5.810	3053	0.83	-5.491
5.5	38003	3.67	5.63	15.13	38.92	833	-5.867	2852	0.96	yes	-5.946	3160	0.83	-5.629
6	36673	3.65	5.56	14.97	36.38	825	-6.100	3165	0.98	yes	-6.108	3200	0.84	-5.769
6.5	35644	3.63	5.49	14.74	33.68	810	-6.278	3534	1.07	yes	-6.320	3743	0.91	-5.902
7	34638	3.61	5.43	14.51	31.17	798	[-6.804]	[7140]	[3.46]	no	–	–	–	-6.016
7.5	33487	3.59	5.36	14.34	29.06	785	-6.606	4408	1.20	yes	–	–	–	-6.166
8	32573	3.57	5.30	14.11	26.89	768	-6.655	3668	1.05	yes	-6.692	3857	0.93	-6.286
8.5	31689	3.55	5.24	13.88	24.84	749	-6.557	2266	0.80	yes	-6.770	3490	0.91	-6.409
9	30737	3.53	5.17	13.69	23.07	733	-6.812	2960	0.90	yes	–	–	–	-6.564
9.5	30231	3.51	5.12	13.37	21.04	709	-6.848	2594	0.89	yes	-6.923	3002	0.85	-6.646

Table 3.1: Continued ...

Model Parameters							Method A			Method B				Vink et al.
ST	$T_{\rm eff}$	$\log g_{\rm spec}$	$\log L$	R	$M_{\rm spec}$	$v_{\rm esc}$	$\log \dot{M}$	v_∞	β	$\Gamma \simeq 1$	$\log \dot{M}$	v_∞	β_γ	$\log \dot{M}$
	K	cm s^{-2}	$L_\odot$	$R_\odot$	$M_\odot$	km/sec	$\log M_\odot$/yr	km/sec		at v_s	$M_\odot$/yr	km/sec		$M_\odot$/yr
Supergiants														
3	42551	3.73	6.00	18.47	66.89	912	-5.347	3346	0.92	yes	-5.445	3719	0.86	-5.083
4	40702	3.65	5.94	18.91	58.03	837	-5.387	2877	0.92	yes	-5.497	3299	0.86	-5.144
5	38520	3.57	5.87	19.48	50.87	779	-5.561	2974	0.95	yes	-5.554	3030	0.86	-5.247
5.5	37070	3.52	5.82	19.92	48.29	764	-5.611	2938	1.04	yes	-5.664	3153	0.87	-5.352
6	35747	3.48	5.78	20.33	45.78	747	-5.751	3000	1.05	yes	-5.814	3270	0.90	-5.438
6.5	34654	3.44	5.74	20.68	43.10	732	-5.945	3531	1.16	yes	-5.920	3328	0.93	-5.520
7	33326	3.40	5.69	21.14	40.91	715	-5.995	3230	1.09	yes	-6.059	3606	0.96	-5.642
7.5	31913	3.36	5.64	21.69	39.17	702	-6.036	2702	1.03	yes	-6.116	3043	0.90	-5.781
8	31009	3.32	5.60	22.03	36.77	678	-6.058	2366	1.06	yes	-6.181	2756	0.88	-5.873
8.5	30504	3.28	5.58	22.20	33.90	644	-6.143	2498	1.08	yes	-6.189	2572	0.90	-5.895
9	29569	3.23	5.54	22.60	31.95	629	-6.385	2988	1.05	yes	-6.319	2640	0.91	-5.998
9.5	28430	3.19	5.49	23.11	30.41	613	-6.487	2921	1.08	yes	-6.449	2642	0.93	-6.148

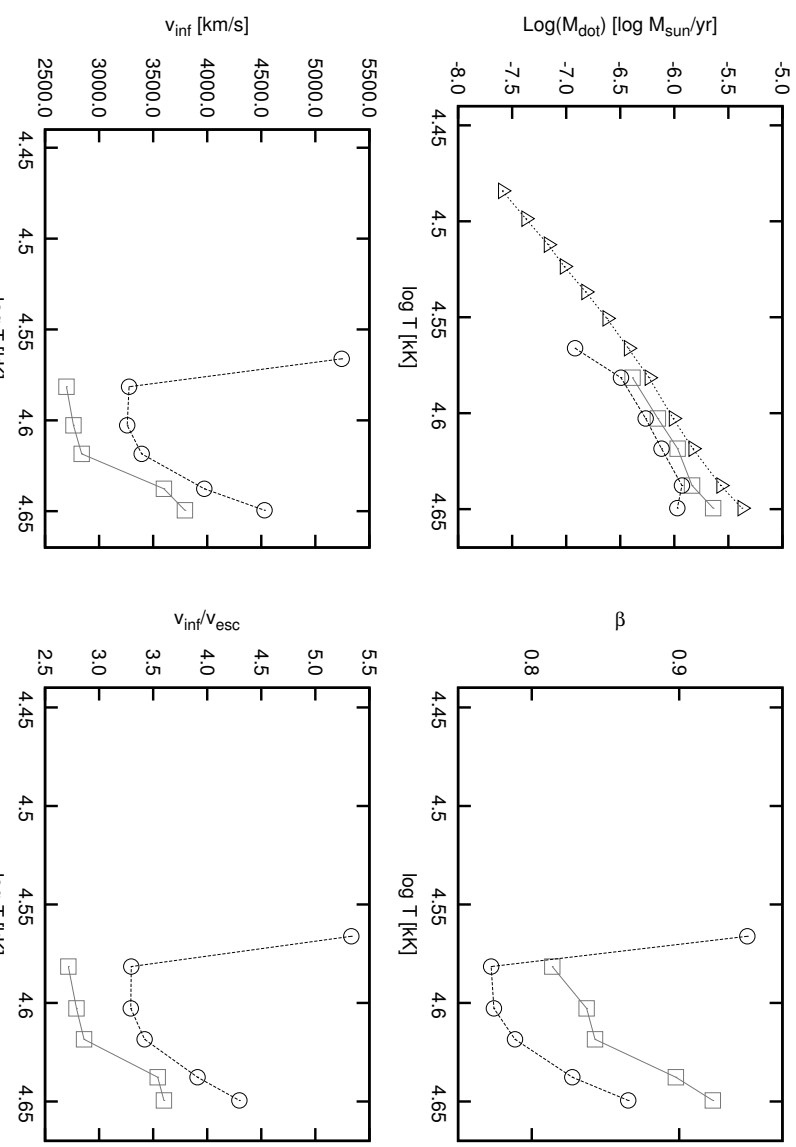

Figure 3.3: Predicted $\dot{M}$, v_∞ and β for the main sequence stars. Best-β solutions are given in grey squares and hydrodynamic solutions in black circles. For comparison, theoretical results by Vink et al. (2001) are provided in black triangles.

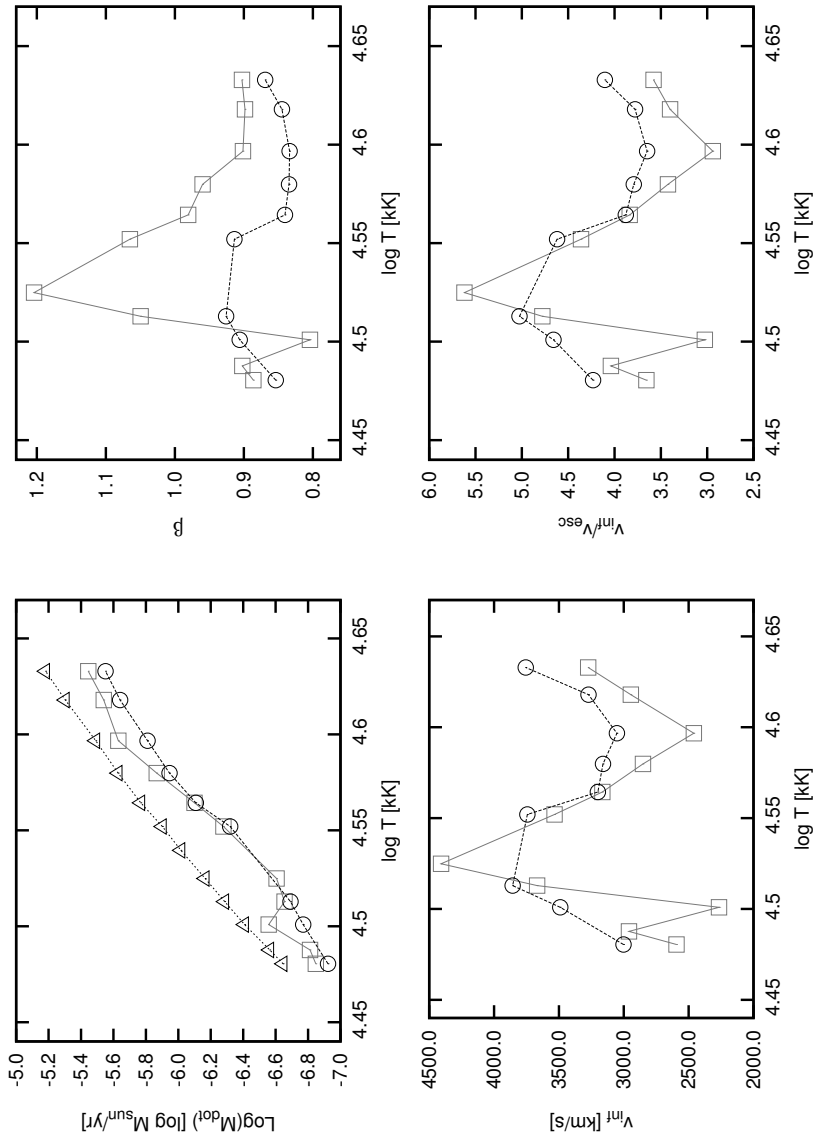

Figure 3.4: Predicted $\dot{M}$, v_∞ and β for giants. Symbols have the same meaning as in Fig. 3.3.

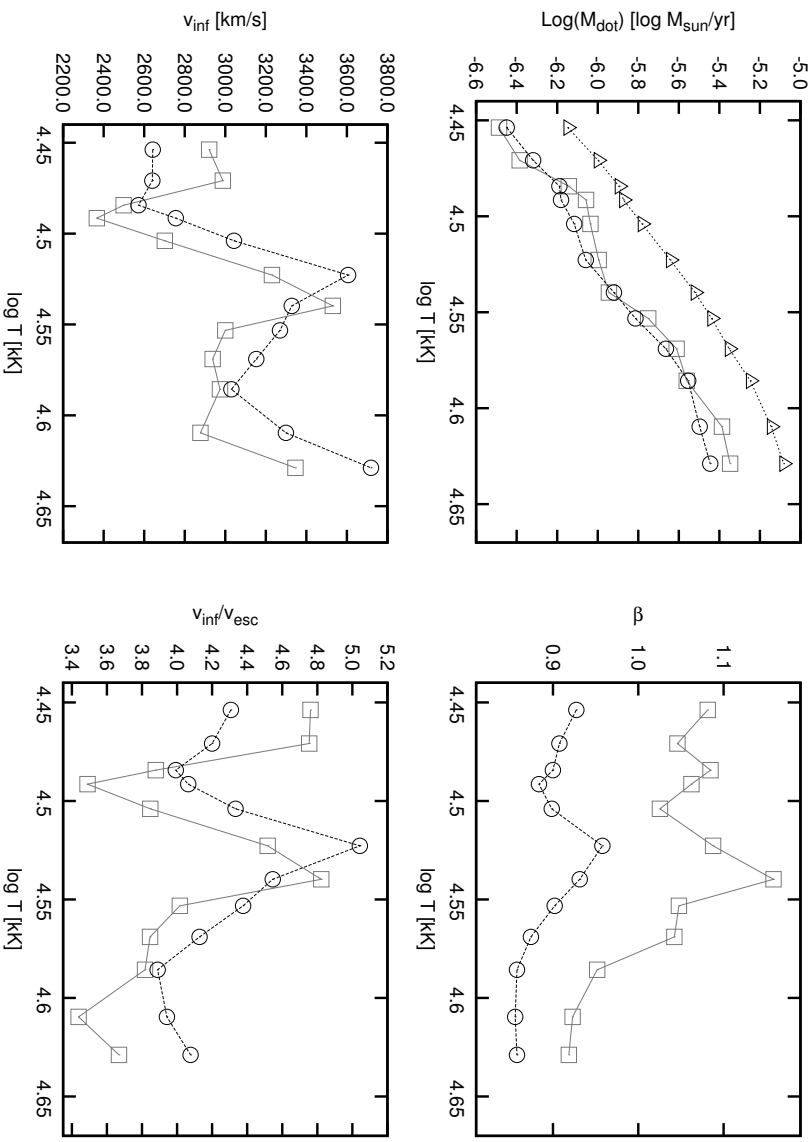

Figure 3.5: Predicted $\dot{M}$, v_∞ and β for supergiants. Symbols have the same meaning as in Fig. 3.3.

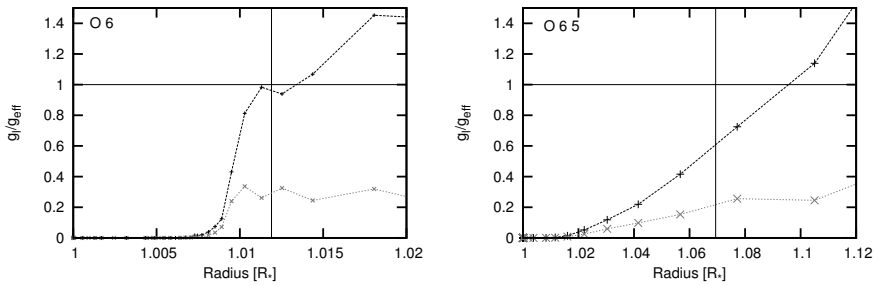

Figure 3.6: The Monte Carlo line force as a fraction of the effective gravity in the region around the sonic point for the best-β solution of the O6 V (left panel) and O6.5 V (right panel) stars. The contribution of iron is shown separately (grey dotted line). Note that in the case of the O6.5 star the line acceleration does not balance the effective gravity at the sonic point. This is interpreted as a failure to support a line driven wind.

contributing to the force. As a result the sonic point starts to shift out to larger radii, and we find that at the sonic point the cumulative line acceleration is some 40% less than the effective gravity. We therefore interpret this outcome as a failure of the wind to become supersonic at r_s and do not consider it to be a physical solution.

The best-β solutions where we clearly encounter this problem have brackets placed around the predicted wind properties as listed in Table 3.1. These include all the dwarf stars of spectral type O6.5 or later. They are to be considered non-physical.

The supergiants do not suffer from this problem. In all cases the $g_{\rm rad}^{\rm line}/g_{\rm eff} \sim 1$ was reached at the sonic point and we consider them physical solutions. The terminal velocities for the O6.5 I to O9.5 I scatter by about 20%, with a small hint that here also the O6.5 star has a higher v_∞. The latter occurs because elements such as silicon, iron and sulfur add to the line force in the outer wind along with the normal contribution of carbon, nitrogen and oxygen.

The value of β for the late spectral types increases to 1.05 from 1.0 for earlier spectral types. The β_γ values associated to the hydrodynamic solutions increase marginally compared to that in early-O stars.

3.4 Discussion

In discussing our results we first compare with previous theoretical predictions for mass-loss rates and terminal velocities in sections 3.4.1 and 3.4.2. We compare to observations in section 3.4.3.

3.4.1 Comparison to Vink et al. mass-loss recipe

The Monte Carlo method by de Koter et al. (1997) as summarized in Sect. 3.2 has been used by Vink et al. (2000, 2001) to compute a grid of mass-loss rates for O-type stars from which a fitting formula has been derived that provides $\dot{M}$ as a function of luminosity, effective temperature, mass and the ratio of the terminal velocity over the effective escape velocity, i.e. $v_\infty/v_{\rm esc}$. This mass loss prescription is widely used in stellar evolution predictions (see e.g Meynet & Maeder 2003; Palacios et al. 2005; Limongi & Chieffi 2006; Eldridge & Vink 2006; Brott et al. 2009; Vink et al. 2010a). The method presented in this paper builds on the de Koter et al. (1997) method and tests the Vink et al. prescription (see Sect. 3.2).

For the spectral range that is investigated here the canonical value, based on empirical findings, for the ratio of terminal velocity over escape velocity is 2.6. To compare to the Vink et al. (2000) results, we calculated the mass-loss rate of our grid of stars using their prescription, that assumes $\beta = 1$. The results are given in the last column of Table 3.1. Figure 3.7 shows the total energy that is extracted from the radiation field and that is transferred to the stellar wind for all three methods: best-β, hydrodynamic and Vink et al. prescription. All three methods yield similar, but not identical, results in the regime where the best-β and hydrodynamical method provide physical solutions. In terms of mass loss rates, we find that the predictions with the best-β and hydrodynamical method are on average about 0.2 to 0.3 dex lower than Vink et al., again with the clear exception of the stars for which we fail to drive a stellar wind. As suggested by the similar wind energies the terminal velocities predicted by our best-β and hydrodynamical method turn out to be higher than adopted by Vink et al.. We discuss these v_∞ in more detail in Sect. 3.4.3 as well as the reason why Vink et al. are able to predict $\dot{M}$ values for late O-type dwarfs and giants, where we fail.

We emphasize that if the Vink et al. prescription is used assuming the terminal velocities predicted by our best-β or hydrodynamical method, wherever these yield physical solutions, the mass loss rates agree to within ∼0.1 dex.

3.4.2 Comparison to (Modified)CAK-theory

Since Lucy & Solomon (1970) it is generally accepted that the winds of massive stars are driven by the transfer of momentum (and energy) from the radiation field to the atmospheric gas, and that atomic transitions play a pivotal role in this process. Castor et al. (1975) describe the force associated to atomic transitions by introducing a force multiplier

$$M(t) = \frac{g_{\rm rad}^{\rm line}(t)}{g_{\rm e}(t)} = k\, t^{-\alpha}, \tag{3.19}$$

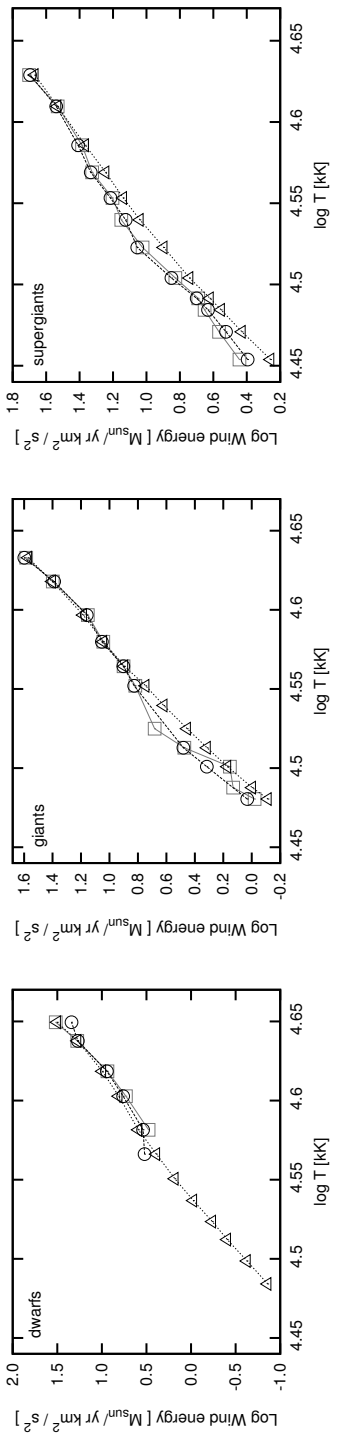

Figure 3.7: The wind energy as a function of the effective temperature for dwarfs (left panel), giants (middle panel) and supergiants (right panel). The best-β method is given by the grey squares, the hydrodynamic method by the black circles and the Vink et al.-recipe by the black triangles. Note that the kinetic energy in the wind is almost equal for all three methods. The mass-loss rate and terminal velocity for the three methods vary.

where k and α are fitting parameters and t is an optical depth like parameter given by:

$$t = \sigma_e \rho v_{th} \left(\frac{dv}{dr} \right)^{-1} . \tag{3.20}$$

Here ρ is the density, v_{th} the thermal velocity of carbon ions at the effective temperature of the star (Pauldrach et al. 1986) and σ_e the mass scattering coefficient of the free electrons. This parametrization of the line force is based on the expression of the force multiplier for a single spectral line,

$$M_{line}(t) = \frac{\Delta\nu_D F_\nu}{F} \frac{1}{t} \left[1 - \exp(\eta t) \right], \tag{3.21}$$

where $\Delta\nu_D$ is the Doppler shift of the frequency of the spectral line due to the thermal velocity of the particles in the wind, F_ν is the flux at frequency ν, F the total flux and η is the ratio of line opacity to electron scattering opacity. Note that for optically thin lines $M_{line}(t)$ becomes independent of t, whilst for optically thick lines $M_{line}(t) \propto t$. The cumulative effect of an ensemble of lines of various strengths is then expressed by Eq. 3.19. The constant α in this expression is a measure of the ratio of line acceleration from optically thick lines only to the total line acceleration and k is related to the overall (line)strength of the ensemble of lines. See Puls et al. (2000) for a more in depth discussion on the CAK line force. It is assumed that α and k are constants throughout the wind (but see Kudritzki 2002). The effects of changes in the ionization structure of the wind are modeled by multiplying expression 3.19 by the term $(n_e/W)^\delta$, introduced by Abbott (1982). n_e is the electron number density, W the dilution factor and δ is a constant.

The parametrization of the line force as given by Eq. 3.19 leads to an analytical expression for $\dot{M}$ and v_∞ as a function of the fitting parameters k and α and the stellar parameters. These expressions are given by Castor et al. (1975). Pauldrach et al. (1986) extend these expressions to account for the finite size of the stellar disk.

To allow for a comparison with Abbott's results for the behavior of the force multiplier as a function of t, we ignore the effect of n_e/W. We calculated the force multiplier of the simulated line force, i.e. Eq. 3.6, at all our radius grid points and determined the corresponding value t. Typically, the optical depth like parameter ranges from $t = 10^{-5}$ to large t. At large t the line force can be neglected compared to the continuum radiation force. Following Abbott (1982), we do not consider these large t points in this discussion but we focus on the range $t < 10^{-0.5}$.

Figure 3.8 compares the behavior of the force multiplier for our best-β solution of the O3 V star. *Note that our Monte Carlo solution shows that $M(t)$ can not be fully described by a strict power law, as assumed in (modified) CAK*, or equivalently, α is not independent of t. Two causes can be pointed out (see e.g. Puls 1987; Schaerer & de Koter 1997): *i)* the presence of a diffuse field due to multiple scatterings; *ii)* a

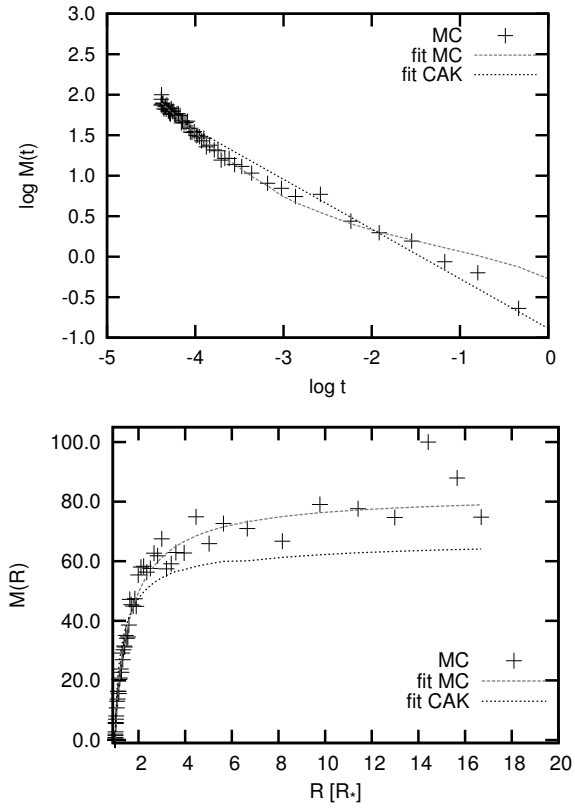

Figure 3.8: *Top panel:* The logarithm of the force multiplier $M(t)$ for the hydrodynamic solution of our O3 V model (black plusses) as a function of the optical depth like parameter t; our fit function Eq. 3.6 to this data (grey line) and the CAK fit function Eq. 3.19 to this data (black line). *Bottom panel:* The force multiplier as a function of radius r for the same star. Note that the CAK force multiplier is smaller than ours for large radii, resulting in a lower predicted v_∞.

complex behavior of radial stratification of the excitation and ionization, specifically near the sonic point. Here the wind accelerates rapidly, which causes a sudden steep drop in the electron density. As a result, elements which happen to have two dominant ionization stages (near r_s) may temporarily re-ionize.

The introduction of a δ-dependence of the CAK force multiplier in Eq. 3.19, by adding the term $(n_e/W)^\delta$, does not improve the fit to the Monte Carlo line force. This extended CAK description describes a plane through the three dimensional space spanned by the logarithms of t, n_e/W and $M(t)$, while the Monte Carlo line force follows a curved line through this space and is thus not confined to that plane.

Our fitting function, Eq. 3.6, better captures the behavior of the line force in the supersonic part of the flow.[2] Using the force multipliers k and α as derived from the Monte Carlo line force we can compute the CAK mass loss and terminal velocity (Castor et al. 1975). The $\dot{M}_{\rm CAK}$ values derived from these k and α are typically 0.0 to 0.3 dex higher than our best-β results and our hydrodynamic solutions. A comparison of the terminal velocities is not meaningful since the slope in the supersonic part of the wind is not represented well by α. Therefore, the velocities derived with our k and α are on the order of the escape velocity. If we compare to the modified CAK terminal velocities, following (Pauldrach et al. 1986), we note that they are slightly lower than the velocities we derive (see also section 3.4.3).

3.4.3 Comparison with observations

In this section, we compare our results to observations. We first compare predicted and empirical terminal velocities. Given that we find that for stars more luminous than $10^{5.2}\,L_\odot$ our mass-loss rates agree well with the Vink et al. prescription – which has been extensively scrutinized (see e.g. Repolust et al. 2004) – we focus the comparison of empirical and predicted mass-loss rates on lower luminosity stars, for which a 'weak-wind problem' has been identified.

Terminal velocities

Several studies have been devoted to measuring the terminal velocities of early-type stars. Summarizing the work by Howarth & Prinja (1989); Prinja et al. (1990); Lamers et al. (1995); Howarth et al. (1997); Puls et al. (1996), and Kudritzki et al. (1999), Kudritzki & Puls (2000) derive that the average value of empirically determined terminal velocities for stars hotter than 21 000 K is $v_\infty = 2.65\,v_{\rm esc}$. The quoted accuracy of this mean value is roughly 20 percent. The v_∞ values are "measured" from the maximum blue-shifted absorption $v_{\rm max}$ in resonance lines of ions such as C IV, N V and Si IV, located in the ultraviolet part of the spectrum. These measurements are prone to systematic uncertainties, that have been extensive discussed in the literature (see for instance the above references). They may work in both directions. Effects that may cause the terminal velocity to be higher than $v_{\rm max}$ are measurements from lines that are not saturated in the outer wind (where for all practical purposes v_∞ is reached) or from ions that recombine in the outer wind. The former may be expected for stars with weak winds, the latter is more likely to occur in very dense winds. Effects that may cause v_∞ to be smaller than $v_{\rm max}$ may be the presence of turbu-

[2] We also compared our fitting formula to the output of the starting model of the iteration cycle of the O3 V star. This allows us to assess whether the iteration procedure perhaps *forces* the line force into the shape of Eq. 3.6. However, also the line force as results from the first iteration cycle is well represented by our description, indicating that it is quite generic.

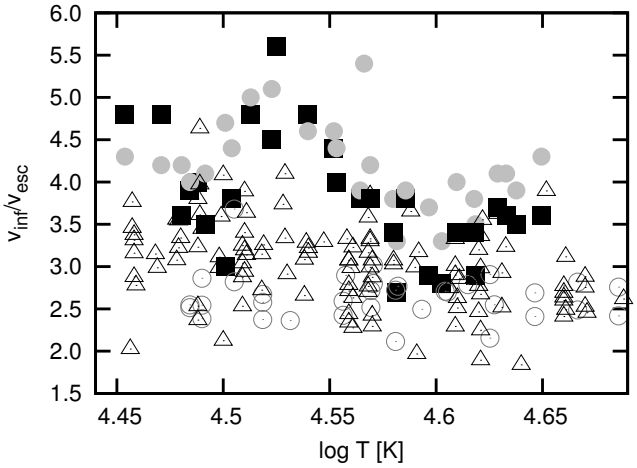

Figure 3.9: Predictions of the ratio of terminal velocity over effective escape velocity at the surface for both the best-β (with black filled squares) and hydrodynamic method (with grey filled circles) as a function of effective temperature. The grey open circles denote the data from Lamers et al. (1995) and the black triangles show the empirical values from Howarth & Prinja (1989) in which v_∞ is determined from the ultraviolet P-Cygni profiles.

lence in the outflow or the presence of strong atmospheric absorption at wavelengths slightly bluer than the wavelength corresponding to the terminal velocity, mistakenly contributed to absorption in the resonance line. Given the possible occurrence of these systematic effects, the uncertainty in the terminal velocity may be 10-15 percent for supergiants, and substantially larger than 20 percent for dwarfs. The error in the ratio $v_\infty/v_{\rm esc}$ also includes uncertainties in $v_{\rm esc}$. The largest contribution to this error comes from uncertainties in the stellar masses, that have been derived from a comparison to tracks of stellar evolution. It seems realistic to adopt a 30-40 percent uncertainty in the empirical values of $v_\infty/v_{\rm esc}$ rather than the 20 percent; quoted at the beginning of this section.

Though Kudritzki & Puls (2000) (and also Lamers et al. 1995) conclude that the ratio $v_\infty/v_{\rm esc}$ is constant for O-type stars, the results of Howarth & Prinja (1989) show this ratio to decrease with temperature, from about 3.5 at 31 500 K to about 2.4 at 43 500 K. A luminosity class dependence of $v_\infty/v_{\rm esc}$ has to our knowledge not yet been reported.

Figure 3.9 shows our predictions of $v_\infty/v_{\rm esc}$ plotted against temperature. Different symbol types denote best-β, hydrodynamic results and empirical values from Howarth & Prinja (1989) and Lamers et al. (1995). As discussed in Sections 3.2.4 and 3.2.5 our predictions of v_∞ have individual random error bars of 10 to 20 percent

In all cases, our predictions result in terminal velocities that are larger than ob-

served. For the main sequence O3-O6 stars the mean predicted ratio is 3.1 for the best-β method and 3.6 for the hydrodynamical method. This is 17% and 36% higher than the observed mean value of 2.65. For giants the discrepancies are respectively 30% and 44%. For the supergiants the largest discrepancies are found. Using all O stars, the best-β method over-predicts the ratio by 54%. The hydrodynamical method yields values that are on average 60% higher. The discrepancy between theory and observations thus seems to increase from dwarfs to giants to supergiants. Given the uncertainties, the over-prediction for the dwarfs may not be significant.

The predictions show a tentative trend of a decreasing $v_\infty/v_{\rm esc}$ with temperature. As pointed out, recent empirical studies do not recover this behavior. Interestingly, this type of trend appears to be visible in the study by Howarth & Prinja (1989). Their trend is plotted in Fig. 3.9, featuring a slope that is comparable to the slope of our predictions. However, given the uncertainties in the current empirical estimates of v_∞, we do not feel that this can be applied to (further) scrutinize the theory.

Larger predicted terminal velocities are also reported by Lamers et al. (1995). In their sample, dominated by supergiants, a comparison to CAK models yields over-predictions by about 33 percent, so slightly less compared to what we find. The reason for the over-predicted v_∞ values is unclear. Possible explanations (for part of the problem) include, *i)* overestimated corrections for the effect of turbulence (see above), *ii)* a clumped and porous outer wind, hampering the acceleration of the flow in this part of the outflow from reaching as high a terminal velocity as predicted here and in (modified) CAK (see Muijres et al. 2010a), or *iii)* a systematic over-estimate of stellar masses. A systematic discrepancy between masses of galactic stars derived from comparing their positions in the Hertzsprung-Russell diagram to evolutionary tracks and masses calculated from the spectroscopically determined gravity was reported by (Herrero et al. 1992). Later improvements in the model atmospheres and fitting procedure used for the latter method, have reduced, but not (yet) eliminated, the size of this discrepancy (Repolust et al. 2004; Mokiem et al. 2005).

Unfortunately, progress in resolving the differences in predicted and empirical $v_\infty/v_{\rm esc}$ ratios quite strongly depends on our knowledge of stellar masses. Hopefully, detailed studies of very large populations, such as the VLT-FLAMES Survey of massive stars (Evans et al. 2005) and the VLT-FLAMES Tarantula Survey (Evans et al. 2010) may help resolve this issue.

Mass loss rates: the weak-wind problem

Relatively recent, analysis of appreciable samples of galactic stars using sophisticated model atmospheres has revealed a mismatch, possibly as high as a factor of 100, between empirically derived mass-loss rates and theoretical predictions for stars less luminous than about $10^{5.2}$ $L_\odot$ (see e.g. Martins et al. 2005b; Mokiem et al. 2007; Marcolino et al. 2009, and Fig. 3.10). As mass loss scales with some power of the

luminosity, this problem occurs below a critical mass-flux and is termed the 'weak-wind' problem (for a recent review, see Puls et al. 2008). Proposed explanations address deficiencies in determining the empirical mass-loss rates as well as in mass-loss predictions. Regarding empirical $\dot{M}$ determinations it should be realized that only UV resonance lines can be used as a diagnostic in the weak-wind regime, whilst in the (lets call it the) strong wind regime Hα and, in the Galactic case, radio-fluxes may also be used. The ions that produce the UV resonance profiles, such as C IV, N V and Si IV, often represent minor ionization species. The ionization continua of these species border the soft X-ray regime and therefore wind material may be susceptible to (non-thermal) processes producing soft X-ray emission, such as shocks or magnetic mechanisms (Martins et al. 2005b).

From a theoretical viewpoint, potential causes of the weak-wind problem include the decoupling of the major driving ions (the metals) from the bulk of the plasma at low densities, when Coulomb coupling fails, and the subsequent ionic runaway (Springmann & Pauldrach 1992; Babel 1995, 1996; Krtička & Kubát 2000; Owocki & Puls 2002; Krtička et al. 2003); the shadowing of wind-driving lines by photospheric lines (Babel 1996), and the neglect of curvature terms in the velocity field (Puls et al. 1998a; Owocki & Puls 1999).

The results presented in this paper point to a cause related to the predictions of mass loss. This possible cause was quantitatively explored by Lucy (2010), who points out that the global dynamical constraint imposed by Vink et al. (2000) need not guarantee that the derived mass-loss rates are consistent with stationary transsonic flows. Here we have shown that though this assumption by Vink et al. (2000) is allowed for stars with luminosities above $10^{5.2}\,L_{\odot}$, it is not for lower luminosities. The boundary between these two regimes corresponds to the critical luminosity of the onset of weak winds to within about 0.1 dex. The physical cause of the different $\dot{M}$ regimes (weak and strong winds) is a lack of line acceleration at the base of the wind. In main sequence stars, a contribution of Fe V lines is present in O6 stars and is missing in the (lower luminosity and cooler) O6.5 stars, where Fe IV is more dominant (see Sect. 3.3.3). The importance of the Fe V/IV ionization balance has been pointed out by Lucy (2010) and is confirmed by our results.

In one fundamental aspect our results differ from that of Lucy (2010). For the sample of low luminosity stars (i.e. less than $10^{5.2}\,L_{\odot}$) investigated by Marcolino et al. (2009), Lucy (2010) predicts mass-loss rates that are about 1.4 dex lower than anticipated by Vink et al. (2000). The hydrodynamical method presented in this paper fails to drive a wind at all. As it is clear form the presence of the shape of UV resonance lines that these stars do have stellar winds (with average mass loss rates that are 0.8 dex lower than Lucy's predictions), our result implies that either some other mechanism is driving the wind or is supplementing the line acceleration at the base of the wind. Which force (or forces) counterbalances gravity remains to

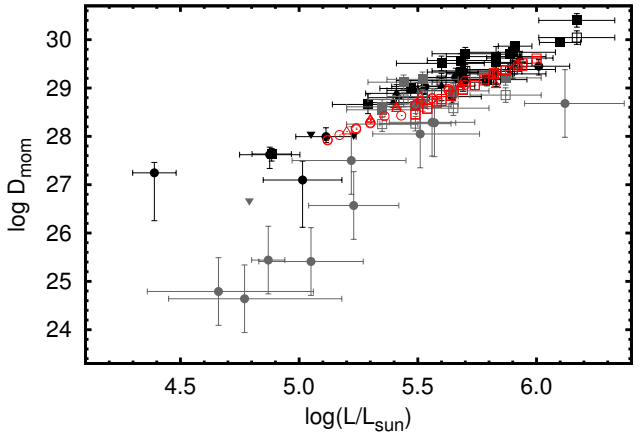

Figure 3.10: The modified wind momentum $D_{\rm mom} = \sqrt{R_\star/R_\odot}\dot{M}v_\infty$ as a function of stellar luminosity using the data of Mokiem et al. (2007). Black symbols refer to mass-loss estimates based on the fitting of the Hα-profile; grey symbols are mass-loss estimates that rely strongly on ultraviolet resonance lines. Note that the Hα estimates at $L < 10^{5.2}\,L_\odot$ are upper limits. A steep jump–of about 2 dex–can be seen at a luminosity of $10^{5.2}\,L_\odot$. The red dots are our predictions for $D_{\rm mom}$. The squares denote the supergiants, the circles the giants and the triangles the mainsequence stars. Below $10^{5.2}\,L_\odot$ we do not find wind solutions for dwarf stars. At higher luminosity our predictions are close to the observed values. We therefore interpret the origin of the weak-wind problem in dwarf stars to be connected to a lack of line driving for objects less bright than about $10^{5.2}\,L_\odot$.

be identified, but perhaps magnetic pressure, effects of turbulence, and/or pulsations may play a role.

We do point out that once material is accelerated, there is sufficient opacity available to further accelerate it to larger velocities. Interestingly, Martins et al. (2005b) report that for their sample of galactic weak-wind objects the average value of $v_\infty/v_{\rm esc}$ is rather close to unity, and not 2.65. Though they concede that given the low wind densities their v_∞ values may be lower limits, they point to a mechanism of X-ray heating proposed by Drew et al. (1994) that may perhaps explain these results. In the outer atmospheres of weak winds the cooling times can become quite long, such that heating of the material in for instance shocks may warm up the medium and strongly modify the ionization structure, in effect canceling the line force.

Modified CAK theory does not predict the weak-wind discontinuity. In this theory the adopted values for k and α are based on the input stellar spectrum, while the dilution and excitation/ionization changes throughout the wind are described by a fixed δ. Therefore, no self-consistent feedback between the wind properties and the line acceleration is accounted for. We note that in the predictions by Pauldrach et al.

(2001) a change of slope of the modified wind momentum luminosity relation can be seen at a luminosity of about $10^{5.2}\,L_\odot$. It is tentative to suggest that if Pauldrach et al. would have implemented the iterative procedure that we use, they might have identified a weak-wind regime on theoretical grounds.

3.5 Conclusions

We have presented new mass-loss rates and terminal wind velocities for a grid of massive O-type stars, improving the treatment of physics in the Monte Carlo method by Abbott & Lucy (1985) and de Koter et al. (1997) to predict wind properties of early-type stars. Two new types of solutions have been discussed. First, building on the work of Müller & Vink (2008), we present so-called best-β solutions in which one still assumes a β-type velocity law (see Eq. 3.2) in the wind, but in which the terminal velocity and β are no longer adopted but constrained by requiring that they best fit the line force (distribution). Second, we abandon the β-type velocity structure and introduce numerical solutions of the wind stratification. Our main conclusions are:

(I) For stars more luminous than $10^{5.2}\,L_\odot$ the best-β and hydrodynamical method yield β and v_∞ results in agreement with each other (within 5-20 percent), whilst the mass-loss rates agree within a factor of 2.

(II) Furthermore, both methods are in very good agreement with the mass-loss prescription by Vink et al. (2000) using our terminal velocities in their recipe. This implies that the main assumption entering the method on which the Vink et al. results are based – i.e. that the momentum equation is not solved explicitly – *is not compromising their predicted $\dot{M}$ in this luminosity range*. Terminal velocity is an input parameter to the Vink et al. recipe. If we apply the canonical value $v_\infty = 2.6 v_{\rm esc}$, the discrepancy between our mass-loss rates and their mass-loss rates is of the order of 0.2, though occasionally 0.6 dex.

(III) At luminosities $\lesssim 10^{5.2}\,L_\odot$ our hydrodynamical method fails to produce an outflow because of a lack of line driving at the base of the wind. This critical luminosity coincides with the onset of the 'weak-wind problem'.

(IV) For O dwarfs the above luminosity criterium translates to a boundary between starting and failing to start a wind at O6/O6.5. The direct cause of the failure to start a wind in O6.5 V stars is the lower luminosity and the lack of Fe v lines at the base of the wind compared to O6 V stars.

(V) The fact that our hydrodynamical method fails to drive a wind at $L \lesssim 10^{5.2}$ $L_\odot$ may imply that some other mechanism is driving the weak winds or is

supplementing the line acceleration at the base of the wind to help drive gas and initiate the wind.

(VI) For stars more luminous than $10^{5.2}\,L_{\odot}$ we predict, using the best-β and hydrodynamical method, terminal velocities that are typically 35 and 45 percent higher than observed. Such over-predictions are similar to what is seen in MCAK-theory (Lamers et al. 1995).

(VII) We predict beta values in the range 0.85 to 1.05, with a trend that supergiants have slightly higher β's than dwarfs. This range of β fits very well with empirical results by Massa et al. (2003).

4 Wind models for very massive stars up to 300 solar masses

J.S. Vink, L.E. Muijres, A. de Koter, B. Anthonisse, G. Gräfener, N. Langer

to be submitted to Astronomy & Astrophysics

Abstract

The upper limit of massive stars is highly uncertain. Some studies have claimed the existence of a universal stellar mass upper limit of ∼150 $M_\odot$, but the true initial masses of these objects may have been significantly higher, possibly superseding 200 $M_\odot$. We present mass-loss predictions from Monte Carlo radiative transfer models for very massive stars in the mass range 40-300 $M_\odot$, and with luminosities $6.0 \leq \log(L_\star/L_\odot) \leq 7.03$. Such objects have a high Eddington factor Γ.

Using a new dynamical approach, we find an upturn (or "kink") in the mass-loss versus Γ dependence, where the model winds become optically thick. This is also the point where our wind efficiency numbers surpass the single-scattering limit (of $\eta = 1$), reaching values up to $\eta \simeq 2.5$. Our modelling thus suggests a natural transition from common O-type stars to Wolf-Rayet characteristics when the wind becomes optically thick. This "transitional" behaviour is also found in terms of the wind acceleration parameter β, which naturally reaches values as high as 1.5-2, as well as in the spectral morphology of the Of and WN characteristic He II line at 4686Å.

When we express our mass-loss predictions as a function of the electron scattering Eddington factor $\Gamma_e \sim L_\star/M_\star$ only, we obtain an $\dot{M}$ vs. Γ_e dependence that is consistent with a previously reported power-law $\dot{M} \propto \Gamma_e^5$ (Vink 2006). However, when we express $\dot{M}$ in terms of both Γ_e and stellar mass, we find optically thin winds and $\dot{M} \propto M_\star^{0.68}\Gamma_e^{2.2}$ for the Γ_e range $0.4 \lesssim \Gamma_e \lesssim 0.7$, and mass-loss rates that are in agreement with the standard Vink et al. (2000) recipe for normal O stars. For higher Γ_e values the winds are optically thick and, as pointed out, the dependence is much steeper, $\dot{M} \propto M_\star^{0.78}\Gamma_e^{4.77}$.

4.1 Introduction

The prime aim of this paper is to investigate the mass-loss behavior of stars with masses up to 300 $M_\odot$ that are approaching the Eddington limit.

Mass loss from massive stars is driven by radiative forces on spectral lines (Lucy & Solomon 1970; Castor, Abbott & Klein 1975; CAK). CAK developed the so-called 'force multiplier formalism' to treat all relevant ionic transitions. This enabled them to simultaneously predict the wind mass-loss rate, $\dot{M}$, and terminal velocity, v_∞, of O-type stars. Although these predictions provided reasonable agreement with observations, they could not account for the large wind efficiencies $\eta = \dot{M}\, v_\infty \,/\, L/c$ of the denser Of stars, with their strong He II 4686Å lines, nor that of the even more extreme Wolf-Rayet (WR) stars. This discrepancy had been proposed to be due to the neglect of multi-line scattering (Lamers & Leitherer 1993, Puls et al. 1996). Using a "global energy" Monte Carlo approach (Abbott & Lucy 1985, de Koter et al. 1997) in which the velocity law was adopted aided by empirical constraints, Abbott & Lucy (1985) and Vink et al. (2000) provided mass-loss predictions for galactic O stars including multi-line scattering. This appeared to solve the wind momentum problem for the denser O-star winds. Mass-loss rates were obtained that were a factor ∼3 higher than for cases in which single scattering was strictly enforced.

Historically, the situation for the WR stars was even more extreme. Here η values of ∼10 had been reported (e.g. Barlow et al. 1981). With the identification of major wind-clumping effects on the empirical mass-loss rates (Hillier 1991; Moffat et al. 1994; Hamann & Koesterke 1998) these numbers should probably be down-revised to values of $\eta \simeq 3$. Although it was argued that WR winds were also driven by radiation pressure (Lucy & Abbott 1993, Springmann 1994, Gayley et al. 1995, Nugis & Lamers 2002, Gräfener & Hamann 2005) the prevailing notion is still that these optically thick outflows of WR stars, where the sonic point of the accelerating flow lies within the (pseudo or false) photosphere, are fundamentally different from the transparent CAK-type O-star winds (e.g. Gräfener & Hamann 2008).

Müller & Vink (2008) have recently suggested a new parametrization of the line acceleration, expressing the line acceleration as a function of radius rather than of the velocity gradient (as in CAK theory). The implementation of this new formalism improves the local dynamical consistency of our models that initially adapted a velocity law. Not only do we find fairly good agreement with observed terminal velocities (see also Muijres et al. 2010b), but as our method naturally accounts for multi-line scattering it is also applicable to denser winds, such as those of WR stars.

Still adopting a velocity stratification, Vink & de Koter (2002) and Smith et al. (2004) predicted mass-loss rates for Luminous Blue Variables (LBVs), and showed that for these objects $\dot{M}$ is a strong function of the Eddington factor Γ_e. They also showed that despite their extremely large radii, even LBV winds may develop pseudo-

photospheres under special circumstances: when they find themselves in close proximity to both the bi-stability and Eddington limit – at a transition value for Γ_e of approximately 0.7.

In this paper, our aim is to study the mass-loss behaviour of stars as they approach the Eddington limit, in a systematic way targeting very massive stars in the range 40-300 $M_\odot$. A pilot study was performed by Vink (2006) who found a steep dependence of $\dot{M}$ on Γ_e, finding $\dot{M} \propto \Gamma_e^5$, but this was obtained using the earlier Vink et al. (2000) global energy approach (in which the velocity stratification was adopted) rather than the improved dynamically consistent approach applied here.

The upper limit of massive stars is highly controversial. On purely statistical grounds some studies have claimed the existence of a universal stellar mass upper limit of ~150 $M_\odot$ (e.g. Weidner & Kroupa 2004, Oey & Clarke 2005, Figer 2005). However as a result of strong mass loss, the true *initial* masses of these objects may have been significantly higher, likely super-seeding 150-200 $M_\odot$ (e.g. Figer et al. 1998, Crowther et al. 2010). This illustrates that the issue of the highest mass star is highly uncertain because of the limited quantitative knowledge of mass-loss rates of stars close to their Eddington limit. Our aim is thus to model the mass-loss rates of stars with masses up to 300 $M_\odot$. Very massive stars have been proposed to lead to the production of intermediate mass (of order 100$M_\odot$) black holes that have been suggested to be at the heart of ultra-luminous X-ray sources (Belkus et al. 2007 and Yungelson et al. 2008). Clearly, the success of such theories depends critically on the applied mass-loss rates. The present study may help advance these theories.

Our paper is organized as follows. In Sect. 4.2 we briefly describe the Monte Carlo mass-loss models, before presenting the parameter space considered in this study (Sect. 4.3). The mass-loss predictions (Sect. 4.4) are followed by a description of the spectral morphology of the Of-WN transition in terms of the characteristic He II 4686Å line in Sect. 4.5. Subsequently, we compare our new mass-loss predictions against empirical values determined by Martins et al. (2008) for the most massive stars in the Arches cluster in Sect. 4.6, before ending with a discussion and summary in Sects. 4.7 and 4.8.

4.2 Monte Carlo models

Mass-loss rates are calculated with a Monte Carlo method that follows the fate of a large number of photon packets from below the stellar photosphere throughout the wind. The core of our approach is related to the total loss of radiative energy that is coupled to the momentum gain of the outflowing material. Since the absorptions and scatterings of photons in the wind depend on the density in the wind and hence on the mass-loss rate, one can find a consistent model where the momentum of the wind material equals the transferred radiative momentum. We have recently improved our

dynamical approach (Müller & Vink 2008, Muijres et al. 2010b) and we are now able to predict $\dot{M}$ simultaneously with v_∞ and the wind structure parameter β. The essential ingredients and assumptions of our approach have more extensively been discussed in Abbott & Lucy (1985), de Koter et al. (1997) and Vink et al. (1999). Here we provide a brief summary.

The Monte Carlo code MC-WIND uses the density and temperature stratification from a prior model atmosphere calculation performed with ISA-WIND (de Koter et al. 1993, 1997). These model atmospheres account for a continuity between the photosphere and the stellar wind, and describes the radiative transfer in spectral lines adopting an improved Sobolev treatment. The chemical species that are explicitly calculated (in non-LTE) are H, He, C, N, O, S, and Si. The iron-group elements, which are crucial for the radiative driving and the $\dot{M}$ calculations, are treated in a generalized version of the "modified nebular approximation" (e.g. Schmutz 1991). However, we performed a number of test calculations in which we treated Fe explicitly in non-LTE. These tests showed that differences with respect to the assumption of the modified nebular approximation for Fe were small. Therefore, we decided to treat Fe in the approximate way, as was done in our previous studies.

The line list used for the MC calculations consists of over 10^5 of the strongest transitions of the elements H - Zn extracted from the line list constructed by Kurucz & Bell (1995). The wind was divided into 90 concentric shells, with many narrow shells in the subsonic region, and wider shells in supersonic layers. For each set of model parameters a certain number of photon packets was followed, typically 2 10^6.

Other assumptions in our modelling involve wind stationarity and spherical geometry. The latter seems to be a good approximation, as the vast majority of O-type stars show little evidence of significant amounts of linear polarization (Harries et al. 2002, Vink et al. 2009). Nevertheless, asphericity has been found in roughly half the population of Luminous Blue Variables (Davies et al. 2005, 2007), although those polarimetry results have been interpreted as the result of small-scale structure or "clumping" of the wind, rather than of significant wind asymmetry.

With respect to wind clumping, it has been well-established that small-scale clumping of the outflowing gas has a pronounced effect on the ionization structure of both O-star and Wolf-Rayet atmospheres (e.g. Hillier 1991). This has lead to a downward adjustment of *empirical* mass-loss rates, by factors of up to three (e.g. Moffat et al. 1994, Hamann & Koesterke 1998, Mokiem et al. 2007, Puls et al. 2008), and possibly even more (Bouret et al. 2003; Fullerton et al. 2006). In addition, clumping may have a direct effect on the radiative driving, therefore on *predicted* mass-loss rates. This was recently investigated by Muijres et al. (2010a) for O dwarfs and supergiants. Whilst it was found that the impact on $\dot{M}$ can be large for certain clumping prescriptions, the overall conclusion was that for moderate clumping factors and porosity, clumping does not affect the wind properties dramatically. Stars approaching the Ed-

dington limit, however, may be much more susceptible to – even modest – clumping (Shaviv 1998, 2000; van Marle et al. 2008). In the present set of computations we do not account for the effects of clumping.

4.3 Parameter space and model applicability

Stars aproach the Eddington limit when gravity is counterbalanced by the radiative forces, i.e. $\Gamma = g_{\rm rad}/g_{\rm Newton} = 1$. Photons can exert radiative pressure through bound-free, free-free, electron scattering and bound-bound interactions. In early type stars hydrogen, the dominant supplier of free electrons, is fully ionized. Therefore $\Gamma_{\rm e} = g_{\rm e}/g_{\rm Newton}$ is essentially independent of distance and a fixed number for each model. Because of this useful property, that provides a well-defined and simple quantitative handle, we opt to discuss our results in terms of $\Gamma_{\rm e}$. We discuss this choice in more detail in Sect. 4.3.1

The dependence of the mass-loss rate $\dot{M}$ on $\Gamma_{\rm e}$ represents a non-trivial matter as $\dot{M}$ depends on both the mass M and the stellar luminosity L. In order to properly investigate the effect of high $\Gamma_{\rm e}$ on mass-loss predictions, we first need to establish the relevant part of parameter space in terms of M, L, and $\Gamma_{\rm e}$. We express $\Gamma_{\rm e}$ as:

$$\Gamma_{\rm e} \equiv \frac{g_{\rm e}}{g_{\rm Newton}} = \frac{L_\star \sigma_{\rm e}}{4\pi c G M_\star} = 7.6610^{-5} \sigma_{\rm e} \left(\frac{L_\star}{L_\odot}\right)\left(\frac{M_\star}{M_\odot}\right)^{-1} . \tag{4.1}$$

In order to determine the electron scattering coefficient $\sigma_{\rm e}$ the prescription from Lamers & Leitherer (1993) is used, which includes a dependence on the helium abundance. The luminosities are chosen in such a way that in combination with the stellar mass M, the desired $\Gamma_{\rm e}$ value is obtained. The effective temperature sets the ionization stratification in the atmosphere and thus determines which lines are most active in driving the wind. As a result, $T_{\rm eff}$ affects the predicted mass-loss rate. For most parts of this paper, we investigate the influence of $\Gamma_{\rm e}$ for a fixed stellar temperature of 50 000 K. The $T_{\rm eff}$ dependence is studied separately in Sect. 4.4.4. All models are for a solar chemical composition, as derived by Anders & Grevesse (1989).

We divide our model stars in three different groups according to their characteristics. The first group comprises objects that have relatively common O-star masses in the range 40-70 $M_\odot$. They are approaching their Eddington limit as a result of prior mass loss. The second group of objects are rather high-mass stars within the "observable range" of 70-120 $M_\odot$. They might be close to the Eddington limit already early-on on the main sequence because of their intrinsically high luminosity. The third group involves very massive stars in the mass range 120-300 $M_\odot$. They are near the Eddington limit for the same reason as the second group. So far, there is a lack of compelling observational evidence for the actual existence of such stars in the

present-day universe. We note, however, that Crowther et al. (2010) have suggested a revision of the upper mass limit to ~300 $M_\odot$.

The bulk of the models in our grid have been chosen such that the behavior of mass loss as a function of M and L can be studied separately. The grid is presented in Table 4.1. We note that the (M, L) combinations are intentionally rather extreme to assure high Γ_e values. The reason is to specifically map that part of parameter space where physically the most extreme winds are expected to appear.

4.3.1 Model applicability regime

With respect to the potential limitations of our modelling approach, we make one rather stringent assumption in the manner the (sub-) photospheric density structure is set-up. In the deepest layers of the model atmosphere (with $v << 1$km/s) we assume that the run of density is provided by the equation of motion using $g_{\rm rad} = g_e$, hence we apply $\Gamma = \Gamma_e$. In reality $\Gamma > \Gamma_e$, as well as being depth-dependent, as a result of bound-bound, bound-free, and free-free processes. Notably, the opacities from millions of weak iron lines may contribute significantly, but they are largely neglected in the deep layers of our models.

Nugis & Lamers (2002) highlighted the importance of the iron peak opacities in deep photospheric layers for the initiation of Wolf-Rayet winds (see also Heger & Langer 1996). This approach was subsequently included in models by Gräfener & Hamann (2005, 2008) for WC and WNL stars. They found that the presence of these opacity bumps may locally cause Γ to approach unity, leading to the formation of optically thick winds. In our Monte Carlo approach we trace the radiative driving of the entire wind, and as most of the energy is transferred in the supersonic part of the outflow, we are less susceptible to the details of the (sub)photospheric region. However, this also means that we do not treat these deep regions self-consistently. This implies that we can (and we will) compute model atmospheres with values of Γ_e very close to one. In reality this may not be achieved for solar-metallicity stars, as this would result in super-critical Γ-values below the sonic point. However, our strategy has the advantage to allow us to explore the transition from transparent to dense stellar winds. As our models do capture the full physics in the layers around and above the sonic point, we argue that they correctly predict the qualitative behaviour of dense winds, but that Γ_e for one of our optically thick wind models would correspond to a model with smaller Γ_e if the ionic contributions were included in the deepest parts of the atmosphere. This "shift" in Γ_e is not fixed but would depend on the sonic point temperature and density. From the behaviour of the Rosseland mean opacity, we would expect the size of the shift to increase at higher Γ_e and higher temperatures.

If Γ exceeds unity at some depth in the sub-photospheric part of the atmosphere, a density inversion is expected to occur for the static case, i.e. for increasing radial distance from the center the density very near the domain where $\Gamma > 1$ is anticipated

to increase. This is encountered in studies of stellar structure and evolution, but it is unclear what really happens in nature. The potential effects may involve strange-mode pulsations (e.g. Glatzel & Kiriakidis 1993), sub-surface convection (Cantiello et al. 2009), or an inflation of the outer stellar envelope (e.g. Ishii et al. 1999). These processes tend to occur only when Γ is *very close* to unity, or above (see e.g. Petrovic et al. 2006). In assessing the outcome of our computations, we find that at $\Gamma_e > 0.95$ the results behave rather suspect. Though we show the wind results over the entire Γ_e range, we only quantify the mass-loss rates up to this value of Γ_e. This boundary is indicated with a vertical dashed line in all relevant figures.

4.4 Results

4.4.1 Mass-loss predictions at high Γ_e

Table 4.1 lists our mass-loss predictions for all three considered mass ranges. Most columns are self-explanatory, but we note that the effective escape velocity $v_{\rm esc}^{\rm eff}$ (6th column) is defined as $\sqrt{2GM_\star(1-\Gamma_e)/R}$. The predicted wind terminal velocities, mass-loss rates, wind efficiency numbers, and wind acceleration parameter β are given in columns (7), (8), (9), and (10) respectively. For comparison column (11) lists the mass-loss values from the standard mass-loss recipe of Vink et al. (2000) where β was held fixed at unity.

The predicted mass-loss rates (column 8) are shown in Fig. 4.1. Different symbols are used to identify the different mass ranges. We repeat that all models are computed at an effective temperature of $T_{\rm eff} = 50\,000$ K (but see Sect. 4.4.4).

The figure shows that $\dot{M}$ increases with Γ_e. This is in qualitative agreement with the luminosity dependence of the standard mass-loss recipe of Vink et al. (2000), derived from a set of models with $\Gamma_e \lesssim 0.4$. Analogous to the results from the standard Vink et al. (2000) recipe, Fig. 4.1 suggests that there exists an additional mass-loss dependence on mass, as for fixed Γ_e the higher mass stars have larger mass-loss rates. This finding confirms that mass-loss rates cannot solely be described by a dependence on luminosity or Eddington factor. This will be discussed in Sect. 4.4.2.

When comparing columns (8) and (11) from Table 4.1, it can be noted that our new high Γ_e mass-loss predictions tend to be larger than those determined using the standard Vink et al. (2000) recipe. In order to quantify these differences, we divide the new mass-loss rates over those determined using the Vink et al. (2000) recipe (with the derived terminal wind velocities as input), and show the results in Fig. 4.2. For the range $\Gamma_e \lesssim 0.7$, the differences are small. However, for values of Γ_e exceeding $\sim$0.7, the new and the old results diverge sharply. The maximum difference reaches a factor of five, which is similar in magnitude as reported previously for LBVs (Vink & de Koter 2002) and WR stars (Vink & de Koter 2005). We note that although these

Table 4.1: High Γ_e mass-loss predictions for all three mass-range grids. $T_{\rm eff}$ is kept constant at 50,000 K. The wind-efficiency number $\eta = \dot{M}v_\infty/L_\star c$ is given in the 10th column. The last column provides the mass-loss rates as computed using the formula by Vink et al. (2000) using the computed terminal wind velocity as input.

model #	$M_\star$ [$M_\odot$]	$\log L$ [$L_\odot$]	Γ_e	$R_\star$ [$R_\odot$]	$v_{\rm esc}$ [km s^{-1}]	$v_{\rm esc}^{\rm eff}$ [km s^{-1}]	v_∞ [km s^{-1}]	$\log \dot{M}$ [$M_\odot$yr^{-1}]	η	β	$\log \dot{M}_{\rm Vink2000}$ [$M_\odot$yr^{-1}]
Mass Range I:											
1	50	6.00	0.52	13.3	1197	829	4320	-5.33	0.96	1.10	-5.30
2	60	6.00	0.43	13.3	1311	990	5044	-5.47	0.82	1.07	-5.40
3	40	6.00	0.66	13.3	1070	625	3823	-5.20	1.16	1.20	-5.25
4	60	6.25	0.78	17.8	1133	529	3733	-4.81	1.33	1.27	-4.98
5	40	6.08	0.80	14.6	1021	457	3283	-4.92	1.47	1.34	-5.12
6	40	6.12	0.88	15.3	998	346	2995	-4.77	1.85	1.47	-5.09
7	60	6.31	0.90	19.0	1097	347	3147	-4.53	1.99	1.56	-4.92
8	50	6.25	0.94	17.8	1034	253	2622	-4.46	2.38	1.63	-4.96
9	60	6.345	0.984	19.9	1072	135	(1936)	(-4.13)	(3.02)	(1.90)	-4.76

Table 4.1: Continued ...

model #	$M_\star$ [$M_\odot$]	$\log L$ [$L_\odot$]	Γ_e	$R_\star$ [$R_\odot$]	v_{esc} [km s^{-1}]	v_{esc}^{eff} [km s^{-1}]	v_∞ [km s^{-1}]	$\log \dot{M}$ [$M_\odot$yr^{-1}]	η	β	$\log \dot{M}_{Vink2000}$ [$M_\odot$yr^{-1}]
Mass Range II:											
10	85	6.25	0.55	17.8	1349	905	5112	-5.12	1.03	1.14	-5.10
11	80	6.25	0.59	17.8	1308	838	4865	-5.08	1.04	1.15	-5.07
12	90	6.25	0.52	17.8	1388	961	5281	-5.16	0.96	1.13	-5.12
13	100	6.25	0.47	17.8	1463	1065	5926	-5.26	0.85	1.11	-5.18
14	85	6.39	0.77	20.9	1245	597	4138	-4.71	1.48	1.30	-4.86
15	100	6.50	0.84	23.7	1268	507	3977	-4.51	1.70	1.37	-4.76
16	85	6.43	0.84	21.9	1216	486	3778	-4.56	1.75	1.41	-4.81
17	100	6.52	0.88	24.2	1255	435	3735	-4.40	1.98	1.54	-4.74
18	100	6.53	0.90	24.5	1247	394	3638	-4.36	2.15	1.59	-4.73
19	100	6.54	0.92	24.8	1240	351	3595	-4.33	2.17	1.60	-4.74
20	90	6.50	0.93	23.7	1203	318	3613	-4.40	2.29	1.60	-4.81
21	100	6.57	0.982	25.7	1218	163	(1752)	(-3.81)	(2.78)	(2.10)	-4.46
22	85	6.50	0.987	23.7	1169	133	(1808)	(-3.89)	(3.11)	(2.09)	-4.57

Table 4.1: Continued ...

model #	$M_\star$ [$M_\odot$]	$\log L$ [$L_\odot$]	Γ_e	$R_\star$ [$R_\odot$]	v_{esc} [km s^{-1}]	v_{esc}^{eff} [km s^{-1}]	v_∞ [km s^{-1}]	$\log \dot{M}$ [$M_\odot$yr^{-1}]	η	β	$\log \dot{M}_{Vink2000}$ [$M_\odot$yr^{-1}]
Mass Range III:											
23	120	6.42	0.58	21.6	1455	945	5744	-5.00	1.03	1.17	-4.96
24	120	6.50	0.70	23.7	1389	761	5122	-4.78	1.29	1.22	-4.82
25	300	6.97	0.83	40.7	1676	700	5527	-4.20	1.74	1.34	-4.36
26	180	6.76	0.85	31.95	1465	568	4642	-4.31	1.76	1.37	-4.53
27	250	6.91	0.86	38.0	1583	593	4885	-4.16	1.87	1.37	-4.40
28	225	6.87	0.87	36.3	1537	554	4657	-4.17	2.03	1.43	-4.43
29	275	6.97	0.90	40.7	1604	508	4427	-4.01	2.13	1.46	-4.32
30	300	7.03	0.95	43.6	1619	362	(3728)	(-3.82)	(2.34)	(1.62)	-4.23
31	200	6.87	0.977	36.3	1449	219	(2500)	(-3.63)	(2.51)	(2.17)	-4.30
32	120	6.65	0.986	28.1	1276	151	(3136)	(-4.10)	(2.87)	(1.68)	-4.69
33	250	6.96	0.97	40.2	1539	267	(4085)	(-3.96)	(2.82)	(1.93)	-4.40
34	153	6.75	0.975	31.6	1359	215	(3409)	(-4.02)	(3.04)	(1.81)	-4.58

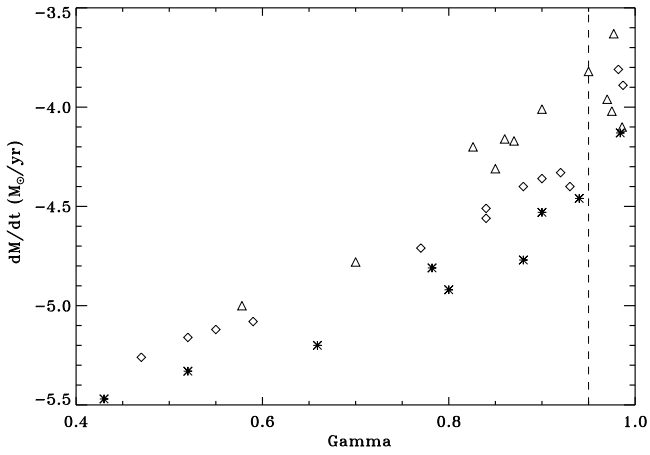

Figure 4.1: The predicted mass-loss rates versus Γ_e for models approaching the Eddington limit. Asterisks, diamonds, and triangles correspond to models of the respective mass ranges I, II, and III. Our model assumptions likely break down to the right of the vertical dashed line.

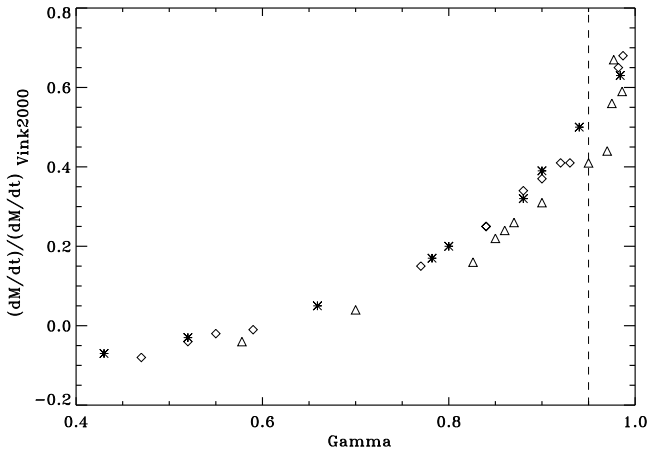

Figure 4.2: The logarithmic difference between the new Γ_e mass-loss predictions and the standard Vink et al. (2000) recipe for models approaching the Eddington limit. Symbols are the same as in Fig.4.1.

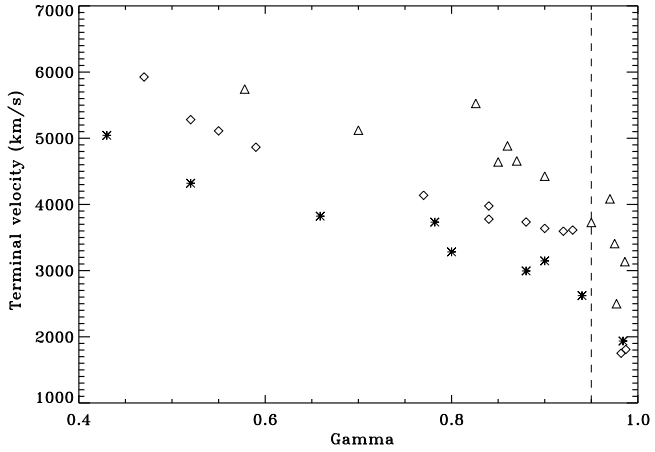

Figure 4.3: The predicted terminal wind velocities versus Γ_e for models approaching the Eddington limit. Symbols are the same as in Fig.4.1.

prior results were based on global energy consistency, where the velocity stratification was adopted, the reason for the differences revealed in Fig. 4.2 is that we probe an entirely different part of parameter space.

We now turn our attention to the wind velocity structure. We first inspect the associated terminal wind velocity predictions. Figure 4.3 shows the behaviour of terminal wind velocity versus Γ_e. The highest values are reached for the highest mass stars and exceed 5000 km/s. As expected: v_∞ drops with Γ_e. In the Γ_e range 0.4-0.95, the terminal wind velocity divided over the escape velocity is of the order 3-4, which is similar to the values for common O-type stars (Muijres et al. 2010b), where $T_{\rm eff}$ is in the range 30-40 kK, and the wind velocities are closer to 3000 km/s (see Sect. 4.4.4).

We next turn our attention to the other wind velocity structure parameter, β, which describes how rapidly the wind accelerates. The predicted values of β are depicted in Fig. 4.4. β does not show a significant dependence on stellar mass. For Γ_e up to 0.7, β values are of order unity, in accordance with the dynamical consistent models of Pauldrach et al. (1986), Müller & Vink (2008) and Muijres et al. (2010b). However, when Γ_e exceeds 0.7 and approaches unity, β steadily rises to values of about 1.7. These larger β values have been suggested to be more commensurate in Wolf-Rayet stars (see e.g. Ignace et al. 2003) and it is reassuring to find that our models naturally predict this transition, without the use of *any* free parameters. *In fact, our overall results suggest a natural extension from O-type mass loss to more extreme WR behaviour for increasing* Γ_e. *An upturn in the* $\dot{M}$ *behaviour is found at* $\Gamma_e \sim 0.7$.

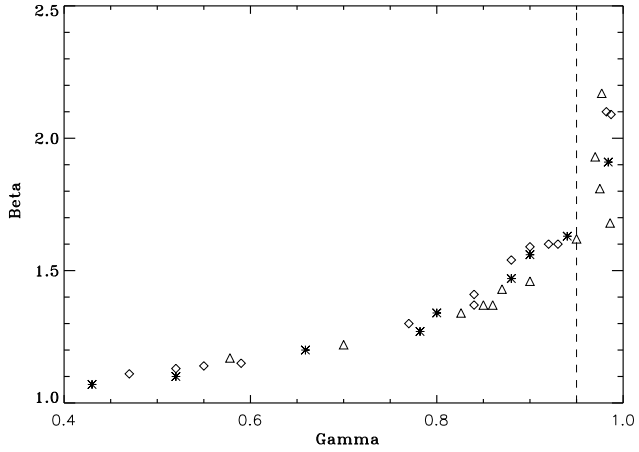

Figure 4.4: The predicted wind velocity structure parameter β versus Γ_e for models approaching the Eddington limit. Symbols are the same as in Fig.4.1.

4.4.2 Γ_e dependence of mass loss

In order to determine the dependence of the mass-loss rate on Γ_e, we could simply fit the data-points to a power law:

$$\dot{M} \propto {\Gamma_e}^p. \tag{4.2}$$

Vink (2006) found p to be equal to ~5, and our dynamically consistent results agree. However, in order to take the *mass* dependence into account, we divide the mass-loss rates by M^q. We show the result in Fig. 4.5 and fit the data with the following power-law:

$$\dot{M} \propto M_\star^q {\Gamma_e}^p. \tag{4.3}$$

Figure 4.5 showcases two mass-loss regimes for $\Gamma_e \lesssim 0.95$, and we identify this boundary at $\Gamma_e \sim 0.7$. This is not only the point where the slope of the mass-loss versus Γ relation changes, but also where β increases and the wind efficiency parameter η surpasses the single scattering limit (see below). Upon further inspection of our models we find that as long as $\Gamma_e \lesssim 0.7$, the winds are optically thin, meaning that the sonic point of the outflowing material lies outside the photosphere, whilst the winds become optically thick – with the photosphere moving outside of the sonic point – for Γ_e values exceeding $\gtrsim$0.7.

We determine two mass-loss recipes for the two separate Γ_e regimes.

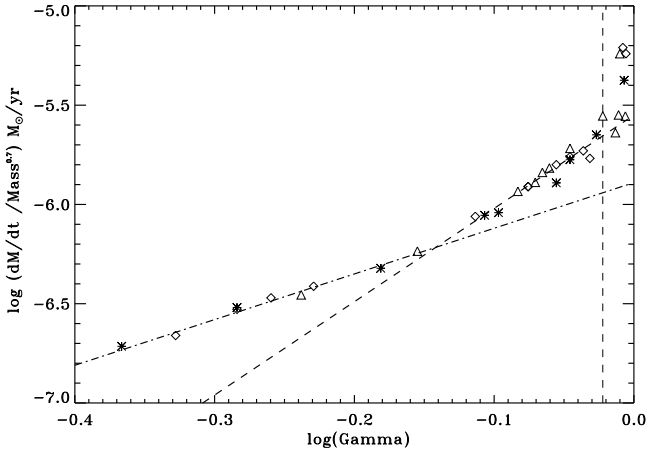

Figure 4.5: The predicted mass-loss rates divided by $M^{0.7}$ versus Γ_e for models approaching the Eddington limit. The dashed-dotted line represents the best linear fit for the range $0.4 < \Gamma_e < 0.7$. The dashed line represents the higher $0.7 < \Gamma_e < 0.95$ range. Symbols are the same as in Fig.4.1.

For $0.4 < \Gamma_e < 0.7$ we find:

$$\begin{aligned} \log\dot{M} &= -5.87(\pm0.08) \\ &\quad +2.2(\pm0.3)\log(\Gamma_e) \\ &\quad +0.68(\pm0.11)\log(M_\star/M_\odot). \end{aligned} \tag{4.4}$$

For $0.7 < \Gamma_e < 0.95$ we determine that:

$$\begin{aligned} \log\dot{M} &= -5.71(\pm0.10) \\ &\quad +4.77(\pm0.46)\log(\Gamma_e) \\ &\quad +0.78(\pm0.04)\log(M_\star/M_\odot). \end{aligned} \tag{4.5}$$

These relationships can easily be transformed using Eq. (4.1). Eq. (4.4) is entirely analogous to $\dot{M} \propto L^{0.68}{\Gamma_e}^{1.52}$ and Eq. (4.5) to $\dot{M} \propto L^{0.78}{\Gamma_e}^{3.99}$. Interestingly, if one subsequently applies a mass-luminosity relationship for classical (He-rich) WR stars of Maeder & Meynet (1987) or for very massive H-rich stars such as that of Yungelson et al. (2008), with $L \propto M^{1.34}$ for both cases, it follows that $\dot{M} \propto M^{2.4}$.

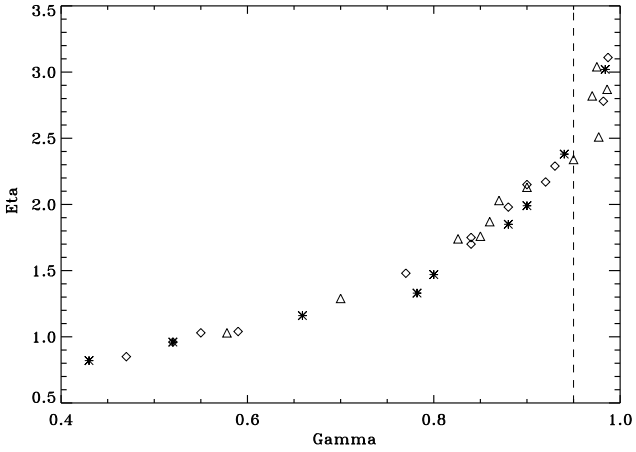

Figure 4.6: The predicted wind efficiency number η versus Γ_e for models approaching the Eddington limit. Symbols are the same as in Fig.4.1.

This appears to be in good accord with the radio mass-loss rate relation $\dot{M} \propto M^{2.3}$ for classical WR stars with measured masses from binaries by Abbott et al. (1986). It is also in agreement with the $\dot{M}$ versus stellar mass relationship of $\dot{M} \propto M^{2.5}$ that has been applied in WR evolution models by Langer (1989).

4.4.3 Increased wind efficiency close to the Eddington limit?

In order to learn whether radiation-driven mass-loss rates continue to increase with increasing Γ_e or reach a maximum in $\dot{M}$ instead, it is insightful to consider the wind efficiency parameter $\eta = \dot{M}v_\infty/(L/c)$. We show the predicted values of η in Fig. 4.6. As the symbols denote different mass ranges, the small scatter on the data-points shows that η is not very sensitive to stellar mass. At values of $\Gamma_e \sim 0.5$ we find wind efficiency numbers η of order 1, in accordance with standard Vink et al. (2000) models. However, when Γ_e approaches unity, η rises in a curved manner to values as high as $\eta \simeq 2.5$. Such large η values are more commensurate with Wolf-Rayet winds than with common O star winds, and these results thus confirm a natural extension from common O-type mass loss to more extreme WR behaviour.

The maximum mass loss in our models up to $\Gamma_e = 0.95$ is log $\dot{M}_{\rm max}$ = -3.8. This is the mass-loss rate retrieved for the most extreme models in our grid. Owocki et al. (2004) investigated the mass loss of stars that formally exceed their Eddington limit and showed – as is implied by our results – that the expected mass loss falls well below the values required to account for the mass that is lost during LBV giant eruptions, such as that of η Carinae in the 1840s. Interestingly, they introduce

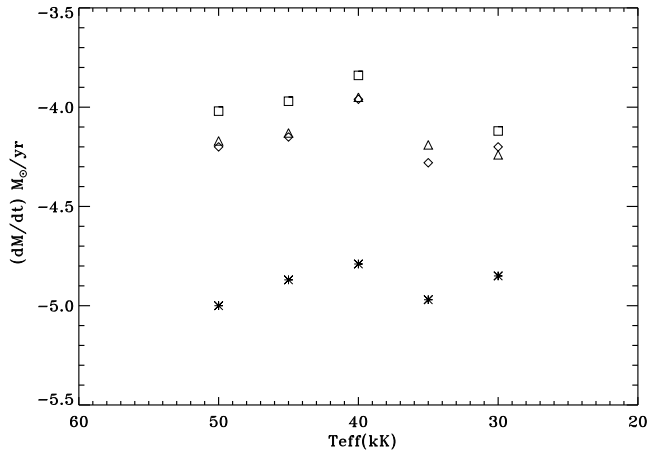

Figure 4.7: The predicted mass-loss rates versus effective temperatures for several values of Γ_e, with from top to bottom Γ_e equal to 0.90 (model 29; open square), 0.87 (model 28; open triangle), 0.83 (model 25; open diamond), and 0.58 (model 23; asterisk) respectively.

a porosity-moderated *continuum* driven mass loss that might account for the huge mass-loss rates associated with LBV eruptions (which may be of order $1 M_{\odot}$/yr).

4.4.4 Effect of $T_{\rm eff}$ on high Γ_e models

In order to establish whether there exists an additional temperature dependence on $\dot{M}$, we varied $T_{\rm eff}$ over the range 50-30 kK for selected Γ_e models, with mass-loss predictions presented in Fig. 4.7 and terminal wind velocities shown in Fig. 4.8. As we wish to stay above the temperature of the bi-stability jump (which starts at $T_{\rm eff}$ values below ∼27.5 kK; see Vink et al. 2000), we restrict our $T_{\rm eff}$ range to a minimum value of 30 kK. We find that for all Γ_e values $\dot{M}$ is not a strong function of temperature. In other words, for high Γ_e models, the influence of effective temperature on the mass-loss rate does not seem to be significant, as long as we refrain from approaching the bi-stability jump. In terms of the terminal velocity dependence, Fig. 4.8 shows a rather steep dependence on temperature, with v_∞ dropping by a factor of two. This is merely a reflection of the fact that the escape velocity drops by a similar factor of two over the temperature range under consideration.

4.4.5 Effect of the helium abundance on high Γ_e models

To establish the existence of a potential helium dependence on $\dot{M}$, we computed additional models across the entire Γ_e region, setting the hydrogen abundance to zero

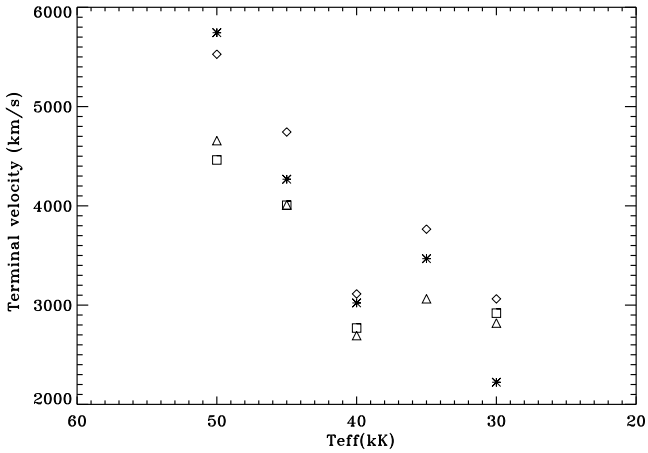

Figure 4.8: The predicted terminal velocities versus effective temperatures for several values of Γ_e, with Γ_e equal to 0.90 (model 29; open square), 0.87 (model 28; open triangle), 0.83 (model 25; open diamond), and 0.58 (model 23; asterisk) respectively.

Table 4.2: Helium enriched mass-loss predictions. All parameters that are not listed are the same as in Table 4.1. The masses have been lowered to keep Γ_e the same.

model number	$M_{\star,\mathrm{old}}$ $[M_\odot]$	$M_{\star,\mathrm{new}}$ $[M_\odot]$	$\log L$ $[L_\odot]$	Γ_e	v_∞ $[\mathrm{km\,s^{-1}}]$	$\log \dot{M}$ $[M_\odot \mathrm{yr}^{-1}]$	β
2He	60	35.8	6.0	0.43	4552	-5.36	1.12
5He	40	23.1	6.08	0.80	3141	-4.86	1.42
10He	85	49.0	6.25	0.55	4567	-5.04	1.21
14He	85	49.0	6.39	0.77	4144	-4.69	1.40
24He	120	69.5	6.50	0.70	4800	-4.70	1.32
26He	180	104.1	6.76	0.85	4759	-4.28	1.53
29He	275	159.5	6.97	0.90	4958	-3.99	1.70
30He	300	175.0	7.03	0.95	4934	-3.88	1.75

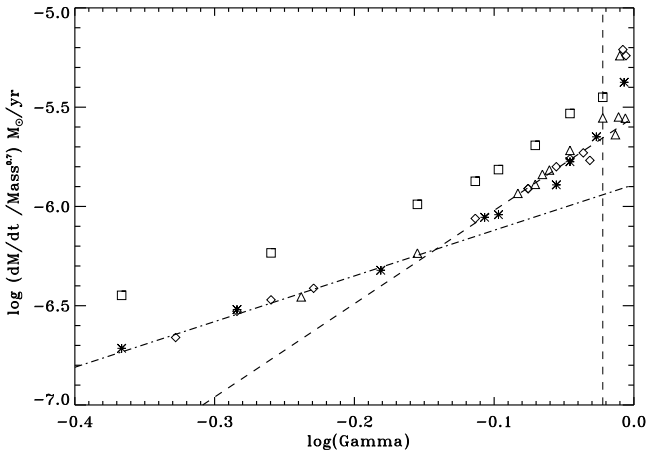

Figure 4.9: Same as Fig. 4.5 but with the He-rich models of Table 4.2 added as open straight squares. The He-rich models form a straight line above the H-rich relationship.

and increasing the helium abundance. The results are listed in Table 4.2 and shown in Fig. 4.9. The mass-loss rates are similar to those of H-rich models for objects with the same Γ_e (see Table 4.1). This is not too surprising given that the indirect effects of different continuum energy distributions for H-rich versus H-poor are rather subtle (Vink & de Koter 2002). However, when the He-rich results are plotted in Fig. 4.9 they lie above the H-rich models. For equal luminosity and Γ_e the masses of the He-rich models are lower since Γ_e is a function of the chemical composition through σ_e (see Eq. 4.1); σ_e is lower for He-rich models therefore the mass must be lowered to keep Γ_e constant. Similar to the H-rich models, there appears to be an upturn in the mass-loss vs. Γ_e dependence for models at about $\Gamma_e \sim 0.7$.

With respect to the terminal velocity and β-dependence, we do not find any significant differences between H-rich and He-rich models (see Table 4.1 versus Table 4.2.).

4.5 Spectral morphology: the characteristic He 4686 Ångström line

In the previous section, we provided evidence for a natural transition in the mass-loss-Γ_e exponent, as well as in the velocity parameter β and wind-efficiency η from moderate Γ_e "optically thin wind" cases to "optically thick wind" cases for objects that find themselves above $\Gamma_e \gtrsim 0.7$. We have inspected our models and confirmed that for $\Gamma_e \lesssim 0.7$, the sonic velocity is reached outside the photosphere, whilst for $\gtrsim$ 0.7 the stars form a pseudo-photosphere.

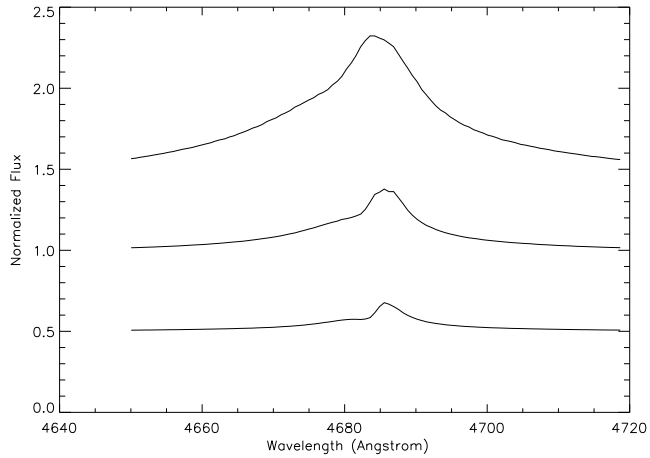

Figure 4.10: The predicted normalized He II λ4686 flux versus wavelength for three values of Γ_e, with from top to bottom Γ_e equal to 0.93 (model 20; $90M_\odot$), 0.84 (model 15; $100M_\odot$), 0.70 (model 24, $120M_\odot$) respectively. Note that wind clumping has not been taken into account.

We expect that the occurrence of a pseudo-photosphere has a consequence for the spectral morphology of the stars in question. We might suspect that the transition $\Gamma_e = 0.7$ is the point where the spectral morphology of normal O stars changes from the common O and Of-types into a WN-type spectrum. The spectral sequence involving the Of/WN stars has a long history (e.g. Conti 1976, Walborn et al. 1992, de Koter et al. 1997, Crowther & Dessart 1998) but it has yet to be placed into theoretical context. Figure 4.10 shows a sequence for the predicted He II 4686Å lines for three gradually increasing values of Γ_e: 0.70 (model 24), 0.84 (model 15), and 0.93 (model 20) respectively. These models have been selected to be objects with a constant luminosity of $\log(L/L_\odot) = 6.5$ and we have simply lowered the mass from $120M_\odot$ to $100M_\odot$, to $90M_\odot$. It is insightful to note that although the first spectrum below the transition Γ_e already shows filled-in emission – characteristic for Of stars – the line-flux is rather modest in comparison to that found for the next two cases with Γ_e values exceeding the critical value of 0.7. These objects show very strong and broad He II 4686Å emission lines that are characteristic for full-blown Wolf-Rayet stars of the nitrogen sequence (WN).

These models thus indicate that the observed spectral transition from Of to WN corresponds to a transition from relatively low Γ_e to high $\Gamma_e$values (and larger β) for WN stars. This assertion is not only based on the larger predicted mass-loss rates themselves, but also on the finding that at $\Gamma_e = 0.7$ the mass-loss behaviour (as a function of Γ_e) changes.

4.6 Comparison with empirical mass-loss rates and wind velocities

Comparing our new mass-loss predictions against observed mass-loss rates is a non-trivial undertaking as high Γ_e objects are scarce. The largest sample of such potentially high Γ_e objects that involves state-of-the-art modelling analysis is probably that of the Arches cluster by Martins et al. (2008). They provided stellar and wind properties (accounting for wind clumping) of 28 of its brightest members from K-band spectroscopy. Roughly half of their sample comprises O4-O6 supergiants whilst the other half includes H-rich WN7-9 stars.

It is not possible to quote direct mass-loss predictions, as the Martins et al. analysis did not yield object masses. However, on the basis of the high stellar luminosities, with $\log(L/L_\odot)$ up to 6.3, these objects were suggested to be consistent with initial masses of up to $\sim 120 M_\odot$. For the O4-6 supergiant population, luminosity values are in the range $\log(L/L_\odot) = 5.75$–6.05, consistent with initial masses $M \simeq 55 - 95 M_\odot$. For this mass and luminosity range, $\Gamma_e \simeq 0.2$ – comfortably within our low-Γ_e regime. Assuming the current mass of these objects is about the same as their initial mass, our mass-loss formula yields values of $\log \dot{M} \simeq -6.1$, which is in good agreement with the lower end of the Martins et al. mass-loss rates for their O4-O6 I objects.

The second group of Martins et al. objects comprise the WN7-9 objects. If we again assume their current masses can directly be inferred from the observed luminosities, we find $\Gamma_e \simeq 0.4$ and mass-loss rates $\log \dot{M} \simeq -5.3$. Even if the helium abundances of these objects are increased, these properties would not result in a pronounced emission profile of the He II λ4686 line, i.e. a profile shape that is typical for late-WN stars. For this to happen the mass-loss rates need to be higher by at least a factor of a few. This seems to require a high Γ. In the framework of our models this could be achieved by lowering the mass. However as the non-electron contribution in our models is not self-consistently treated in the high Γ_e regime, and because Crowther et al. (2010) have challenged the stellar parameters of Martins et al., we refrain from providing quantitative assessments.

As the O4-O6 supergiants from the Martins et al. (2008) analysis have effective temperatures in the range 32-40 kK, we expect v_∞ to fall in the range 2500-3500 km s^{-1} (see Fig. 4.8), which is in reasonable agreement with the upper end of the Arches O4-O6 supergiant stars. However, for the late WN stars, the v_∞ values presented by Martins et al. drop to values as low as 800 km s^{-1} which is significantly lower than we predict. We identify two possible reasons for this discrepancy. The first option could be that as a result of our model assumptions (1D, smooth winds, etc.) we over-predict the wind terminal velocity. A second possibility is that the K-band spectral fits of Martins et al. (2008) yield terminal velocities that are too low (note that no ultra violet P Cygni blue edges are available for these obscured objects).

4.7 Discussion

In this section we compare our results with alternative model predictions. In the above we have investigated the mass-loss behavior at high Γ_e for an extensive grid of models, and we obtained two mass-loss regimes. Moreover, we found that the mass-loss rate is dependent on Γ_e and stellar mass, and that the shape of the dependence is well-described by a power law.

4.7.1 Comparison to CAK and other O-type star mass-loss models

In classical CAK theory, the mass-loss rate is proportional to:

$$\dot{M} \propto L \left(\frac{\Gamma_e}{1 - \Gamma_e} \right)^{\frac{1-\alpha}{\alpha}}, \tag{4.6}$$

where α is a force multiplier parameter expressing the importance of optically thin lines to the total ensemble of lines. It is generally assumed that α is ~2/3 for galactic O-type stars (Puls et al. 2008) and constant throughout the atmosphere. In reality α is however depth-dependent (Vink 2000, Kudritzki 2002, Muijres et al. 2010b) which is better captured with an alternative representation of the line acceleration (Müller & Vink 2008). Nevertheless, the classical CAK formalism as described by Eq. 4.6 already shows a dependence on both L and Γ_e, and one could rewrite this mass-loss dependence as a function of M and Γ_e using a mass-luminosity relation.

In the standard Vink et al. (2000) mass-loss parametrization $\dot{M} \propto L^{2.2}\ M^{-1.3}\ (v_\infty/v_{\rm esc})^{-1.2}$, which can be re-organized to $\dot{M} \propto {\Gamma_e}^{1.9}\ M^{1.2}$. This is the type of mass-loss parametrization that is currently employed in modern evolutionary computations (see e.g Meynet & Maeder 2003, Palacios et al 2005, Limongi & Chieffi 2006, Eldridge & Vink 2006, Brott et al. 2009, and Vink et al. 2010). In other words, stellar models do include the important effect of positive mass-loss feedback (contrary to recent claims by Smith & Conti 2008), which describes how the mass-loss rate gradually increases whilst – as a result of mass loss – the stellar mass decreases. Having noted this, as we here find a much steeper $\dot{M}$ vs. mass dependence, in agreement with our earlier steeper $\dot{M} \propto M^{-1.8}$ for constant-luminosity LBVs (Vink & de Koter 2002, Smith et al. 2004), it is likely that the mass-loss feedback effect currently employed in the stellar evolution models is not strong enough over all areas of the Hertzsprung-Russell diagram. We therefore concur with the notion of Smith & Conti (2008) that new stellar evolution computations that take this effect properly into account are needed.

For the "low" Γ_e range considered here, we found $\dot{M} \propto {\Gamma_e}^{2.2}\ M^{0.68}$, which is given the somewhat different Γ_e range and difference in underlying approach (global energy versus local dynamical consistency) quite similar. However for the "high" Γ_e

regime we considered here ($0.7 < \Gamma_e < 0.95$) we found $\dot{M} \propto {\Gamma_e}^{4.77}\ M^{0.78}$ which is a much steeper dependence on Γ_e than any previous radiation-driven wind model has delivered (see also Vink 2006).

4.7.2 Comparison to alternative Wolf-Rayet mass-loss models

We now compare our models to the optically thick wind models for Wolf-Rayet stars by Nugis & Lamers (2002) and Gräfener & Hamann (2008). As there is a significant qualitative difference between our Monte Carlo approach and these optically thick wind approaches, a meaningful quantitative comparison is a non-trivial undertaking (see section 4.3.1).

First we quantitatively compare our $\dot{M}$ versus Γ_e dependence to the WNL star mass-loss dependence recently suggested by Gräfener & Hamann (2008). For the models in our grid at $T_{\rm eff} = 50$ kK, we find very good agreement with the Gräfener & Hamann (2008) mass-loss rates and also find that the power-law slope of our dependence is very similar. However, the onset of WR-type behaviour occurs earlier, i.e. for lower Γ_e in the models by Gräfener & Hamann.

In Sect. 4.3, we discussed the possibility of such a shift in Γ_e, because the actual Eddington parameter Γ is expected to be affected by free-free and bound-free contributions and peaks in the iron opacity. By comparison with OPAL opacity tables (Iglesias & Rogers 1996), we estimate an increase of Γ by $\sim 20\%$ in the region of the sonic point, assuming the location of the sonic point remains unaffected. This value corresponds roughly to a $\sim 25\%$ shift in Γ_e between our relation and that by Gräfener & Hamann for typical parameters of Galactic WNL stars ($T_{\rm eff} = 45$ kK, $\log(L/L_\odot) = 6.3$). Note that this could be considered a maximum shift since we may overestimate the line force near the sonic point by applying the Sobolev approximation (Pauldrach et al. 1986). However, a change in Γ affects the atmospheric structure and therefore the location of sonic point, consequently the effect on $\dot{M}$ is hard to establish.

The Gräfener & Hamann mass-loss rates also display a strong temperature dependence, with $\dot{M} \propto T_{\rm eff}^{-3.5}$ (and an additional strong dependence on the clump filling factor). The actual size of the shift in Γ_e is thus strongly dependent on the specific stellar parameters. Our Monte Carlo models suggest a much smoother dependence on $T_{\rm eff}$ (see Fig. 4.7) as long as we stay above the location of the predicted bi-stability jump, where the mass-loss properties jump drastically (Vink et al. 1999, Pauldrach & Puls 1990). What we wish to stress is that both modelling approaches show a $\dot{M}$ versus Γ_e dependence that is *much* stronger than any additional mass or luminosity dependence. Where the two distinct mass-loss prescriptions differ is in the Γ_e value for the onset of WR-type mass loss behaviour. The exact location of this transition is of paramount importance for the evolution of the most massive stars. Ultimately, this should be testable with comparisons to observational data when sufficient objects are

available in the appropriate Γ_e range. This will be a crucial aim of the Very Large Telescope (VLT) Tarantula survey (Evans et al. 2010).

4.8 Summary

We presented mass-loss predictions from Monte Carlo radiative transfer models for very massive stars in the mass range 40-300$M_\odot$ and with Eddington factors Γ_e in the range 0.4–1.0. An important outcome is that when winds become optically thick their (physical) properties change. This transitional behaviour can be summarized as follows:

(I) Our modelling suggests a *natural transition* from common O-type stars to more extreme Wolf-Rayet behaviour when Γ_e exceeds a critical value, which is found to be $\simeq$0.7.

(II) The way in which the mass-loss rate depends on Γ_e in the range $0.4 \lesssim \Gamma_e \lesssim 0.7$ is $\dot{M} \propto M_\star^{0.68}\Gamma_e^{2.2}$, where rates are found to be consistent with the standard Vink et al. (2000) mass-loss rates.

(III) At $\Gamma_e \simeq 0.7$ the $\dot{M}$ dependence shows a "kink", i.e. the slope is steeper for objects closer to the Eddington limit. Here the slope becomes $\dot{M} \propto M_\star^{0.78}\Gamma_e^{4.77}$. This slope is in agreement with WNL models by Gräfener & Hamann (2008).

(IV) When Γ_e approaches unity, the wind efficiency number η *rises in a curved manner to values as high as* $\eta \simeq 2.5$. Such large η values are more commensurate with Wolf-Rayet winds than with common O stars winds, and these results thus confirm a natural extension from common O-type mass loss to more extreme WR behaviour.

(V) This transitional behaviour is also found in terms of the wind acceleration parameter β*, which naturally reaches values as high as 1.5*

(VI) The spectral morphology of the He II line at 4686Å changes gradually as a function of Γ_e. This links the spectral sequence O-Of-Of/WN-WN to a transition of optically thin to optically thick winds.

(VII) The mass-loss rate is found to be only modestly dependent on the effective temperature for the range of 30 to 50 kK.

5 Predictions of the mass-loss rates for evolved very metal-poor massive stars

L. Muijres, Jorick Vink, A. de Koter, N. Langer, and S.-C. Yoon

to be submitted to Astronomy & Astrophysics

Abstract

The first generations of stars are expected to have been massive, of order $10^2\,M_\odot$, and to have played an important role in galaxy formation and early chemical enrichment of the universe. Part of these objects may have ended their lives in pair-instability supernovae or gamma-ray bursts. The stellar winds of these metal-free and/or metal-poor massive stars may have played an important role in all of these processes.

Winds of massive stars are driven by radiation pressure on spectral lines, and their strengths are therefore expected to be a function of chemical composition; the lower the metal content, the weaker the winds. So far, almost all predictions of the strengths of the winds of metal-poor stars assume a scaled-down solar abundance pattern. However, evolutionary tracks of rotating massive stars in the early universe show surface enrichment, through rotational mixing, of CNO processed material as even metal-free stars switch to CNO-burning quite early-on in their evolution. We address the question whether the surfacing of such material has an important impact on their mass-loss properties.

We use Monte Carlo simulations to establish the local line-force and solve for the momentum equation of the stellar outflow, testing whether an outflow can actually be established by assessing the net acceleration at the sonic point of the flow. Constraints from stellar evolution models of rotating metal-poor stars are used to specify the surface chemical composition, focussing on the phases of early enrichment.

We find the mass-loss rates of these stars can be strongly reduced compared to assessments using a scaled-down solar abundance pattern. Metal-poor stars in the metallicity range investigated here (with an initial metallicity $Z \lesssim 10^{-4}$) and hotter than ~50 000 K do not feature an outflow at all, as the high-ionization species of the CNO elements have too few strong lines to drive the wind. We provide a heuristic formula that allows to estimate the mass-loss rates of CNO-dominated winds.

The winds of massive metal-poor stars, albeit they are CNO enriched or not, are very weak and do not contribute significantly to the overall mass and/or angular momentum loss. If other mass-loss mechanisms, for instance in η Carinae type of eruptions, do not occur for such objects, their supernova explosions are expected to be responsible for the major part of the early nucleosynthetic enrichment.

5.1 Introduction

Massive stars in the present-day universe may loose a substantial fraction of their initial mass in a stellar wind, from which they suffer from the moment they form up to the moment they end their lives as supernovae (SNe). These stellar winds are driven by radiation pressure on spectral lines, consequently they are expected to depend on the chemical composition. At low abundances, the lines are weaker, and the mass-loss $\dot{M}$ lower. The dependence of mass-loss on metallicity, $\dot{M}(Z)$, has been studied in detail, both observationally (Puls et al. 1996, 1998b; Mokiem et al. 2007) and theoretically (Vink et al. 2001; Kudritzki 2002; Krtička & Kubát 2004; Vink & de Koter 2005; Gräfener & Hamann 2005). For a recent review, see e.g. Puls et al. (2008).

Studies of star formation in the early universe suggest that the typical stellar mass was $\sim 10^2\ M_\odot$ for zero metallicity (Abel et al. 2002; Bromm et al. 2002; Nakamura & Umemura 2002; Bromm & Larson 2004; Loeb et al. 2008). Very massive stars of zero metallicity are considered to be the prime candidates for the re-ionization of the universe (Haehnelt et al. 2001; Wyithe & Loeb 2003, e.g.) at redshifts above six (Becker et al. 2001). Therefore, it is particularly interesting to ponder on the question of how much mass these first generation(s) of stars might have lost through stellar winds, prior to their supernova explosion. If the time integrated mass-loss is small, or even negligible, they may have left intermediate mass black holes (of masses $\sim 10^2\ M_\odot$), that may have been the building blocks of the supermassive black holes detected in the centers of galaxies today (Kawakatu et al. 2005). Moreover, it is proposed that long-duration gamma-ray bursts (GRBs) may originate from rapidly rotating massive single stars of low metal content (Yoon & Langer 2005; Woosley & Heger 2006), if the winds are weak enough to prevent significant angular momentum loss.

Therefore, there exist many reasons to study $\dot{M}(Z)$. Kudritzki (2002) and Krtička

& Kubát (2004) found that massive *zero*-metallicity objects may drive only very weak winds or no winds at all. Evolutionary predictions for very metal poor stars, especially if they are rapidly rotating, show the surfacing of sometimes large quantities of primary produced carbon, nitrogen and oxygen (e.g Yoon & Langer 2005; Meynet et al. 2006; Yoon et al. 2006; Hirschi 2007). One may wonder whether the surfacing of such material may cause (dramatic) changes in the mass-loss behavior of these objects. This question is the topic of this study. We present tailored mass-loss predictions for evolutionary stages of metal-poor stars in which substantial amounts of CNO processed material is expected to have surfaced. These predictions therefore differ from the theoretical studies mentioned in the first paragraph, in which scaled solar metallicities are used for O-stars.

The first investigation in this direction was performed by Vink & de Koter (2005) who studied the winds of CNO-enhanced atmospheres at low iron metallicities (down to 10^{-5}). The discovered enhanced wind driving by CNO-elements was reason to wonder whether primary carbon or nitrogen in the atmospheres of extremely metal-poor massive stars might boost the mass-loss rates, and potentially prevent the occurrence of pair-instability supernovae (Vink 2006). Such complete stellar disruptions are hypothesized to occur for initial masses in the range $M = 140 - 260\,M_{\odot}$ if mass loss is negligibly small (Heger et al. 2003; Langer et al. 2007). Krtička & Kubát (2009) investigated the winds of enriched metal-poor stars, describing the physics of line-driven winds following Castor et al. (1975, hereafter CAK). One interesting aspect of their work is that during the initial hot phase ($> 50\,000$ K) of the evolution of metal-poor stars with initial mass above $\sim 30\,M_{\odot}$ also CNO-enriched stars fail to produce a stellar wind. Overal, it was concluded that the surfacing of primary CNO does not produce stellar winds strong enough to have a major impact on the evolution of metal-poor massive stars.

Our predictions are based on a newly developed self-consistent dynamical treatment of stellar winds by Müller & Vink (2008) and Muijres et al. (2010b) based on a description of the line force that results from a Monte Carlo simulation. In Sect. 5.2 we introduce this method and discuss the evolutionary tracks on which the adopted chemical compositions are based. Section 5.3 presents the results. These are discussed in Sect. 5.4, as well as compared to the results of Vink et al. (2001) – often applied in evolutionary calculations – and Krtička & Kubát (2009). We end with conclusions.

5.2 Method

In this section we present our method for predicting mass loss rates for massive stars at very low metallicity. Distinctive for these computations is that a tailored chemical composition of the surface layers is used to compute the radiative line driving. The

adopted surface abundance patterns are motivated using evolutionary tracks for rotating metal-poor stars. In sections 5.2.1 and 5.2.2 we present and discuss our wind models. Consulted evolutionary tracks are discussed in Sect. 5.2.3. The adopted grid is presented in Sect. 5.2.4.

5.2.1 Wind models

To determine mass-loss rates, we use an iterative method, as developed by Müller & Vink (2008) and Muijres et al. (2010b), in which ISA-WIND model atmospheres (de Koter et al. 1993) are used to describe the model atmosphere and MC-WIND models (de Koter et al. 1997) to treat the wind dynamics. The latter uses a Monte Carlo approach based on the method developed by Abbott & Lucy (1985). Advantageous aspects of this approach are that multiple photon scatterings are taken into account, that excitation/ionisation changes of the gas are treated self-consistently, and that one can quite easily dissect the relative contributions of individual species to the line force. Essential aspects of the wind dynamics are summarized in Sect. 5.2.2. First, we briefly summarize the main assumptions of the model atmospheres. For further details we refer the reader to the above references.

We assume the wind to be homogeneous, spherically symmetric and stationary. Our model atmospheres extend from the base of the photosphere to approximately 20 stellar radii. For hydrogen, helium, carbon, nitrogen, oxygen, and silicon, we solve the ionization state and the occupation numbers of the levels in non-local thermodynamical equilibrium (NLTE). The other elements are treated using a modified nebular approximation. The radiative transfer in lines is calculated using the Sobolev method (Sobolev 1960).

To compute the line force we make a selection of the strongest lines from the line-list in Kurucz & Bell (1995). This line list is essentially complete for the ions that play an important role in driving the winds studied here. Transitions of the CNO elements of ionization species C V, N VI and O VI or higher are not considered. These ions with one or few bound electrons have only few lines in the part of the spectrum that coincides with the flux maximum of the stellar radiation. As ionization of all these species depends on the radiation field in the He II continuum above 54.4 eV they would remain trace species in our models. Shocks in the outflows of massive stars (see Kudritzki & Puls (2000) for a discussion/review) may heat a fraction of the gas to higher temperatures and produce non-thermal emission at soft X-ray wavelength. Such effects may increase the importance of transitions of these highly ionized species, though it is unlikely that an associated increase in line force is significant. We therefore do not expect that the lack of these lines has an important impact on our mass loss predictions. For completeness, we are missing part of the transitions of N VI. However, because of the same argument we do not think that this affects our results in a notable way.

5.2.2 Wind dynamics

The main problem faced in determining the structure of a line driven stellar wind is the strong, but delicate, interaction between radiation, line force and atmospheric structure: The radiation field and the density (or velocity) structure set the excitation/ionisation state of the gas. The line force results from the structure and the state of the gas, while, in turn, the line force sets the structure, therefore indirectly also the radiation field. We try to tackle this problem through an iterative process. By assuming a velocity law and a mass-loss rate we can determine the excitation/ionization structure. Next, the line force is calculated. Based on a fit to the line force the velocity law is re-determined. A model is considered converged once the fit parameters of the line force fit function and the mass-loss rate do not change significantly from one iteration step to the next.

The procedure followed is based on the method described by Müller & Vink (2008) and Muijres et al. (2010b), that improve on the treatment as developed by de Koter et al. (1997), and applied in a series of papers by Vink et al. (e.g. 2000, 2001) Actually, the Müller & Vink and Muijres et al. studies present two approaches to deal with the equation of motion. In the one solution, referred to as best-β method, the velocity law is assumed to be a β-law (Castor et al. 1975; Lamers & Morton 1976). A fit function to the line force is constructed that is used to find the most appropriate terminal velocity v_∞ and measure for the rate of acceleration in the lower part of the wind, expressed by β. In the other solution the fit function to the line force is used to numerically solve the equation of motion, referred to as the hydrodynamical method. Both methods are compared in Muijres et al. (2010b), where it is found that the derived mass-loss rates do not differ more than about 25 percent and that the terminal wind velocities agree within 20 percent.

The hydrodynamical method is dynamically consistent but is sensitive to the quality of the fit to the line force at the base of the wind, and therefore less stable. In the range of parameter space investigated in this article, we anticipate this to be more problematic than for the main sequence O-stars studied by Muijres et al. (2010b). For this reason we apply the best $\beta-$method.

The best β-method is, strictly speaking, not dynamically consistent. This warrents caution. Muijres et al. (2010b) discuss this issue in detail. They identify the solution to be physically correct only if the effective gravity $g_{\rm eff}$ – i.e. the Newtonian gravity corrected for forces due to continuum radiation pressure – is approximately equal to the line force $g_{\rm line}$ at the location of the sonic point $r_{\rm s}$, i.e.

$$g_{\rm line}(r_{\rm s}) \simeq g_{\rm eff}(r_{\rm s}). \tag{5.1}$$

The sonic point corresponds to the radial distance where the flow velocity reaches the local sound speed. We compare the line force as simulated by the Monte Carlo

code to the effective gravity and conclude that if the latter differs from the line force by more than 20 percent the wind can not be driven by line radiation pressure alone. Phrased differently: in this case our model does not drive a wind.

The condition Eq. 5.1 is more sophisticated than the one applied by Krtička & Kubát (2009). In their approach they apply a test to establish whether a wind is driven that does not involve solving the equation of motion, and requires specification of the wind mass-loss rate.

5.2.3 Evolutionary tracks

Evolutionairy tracks for rotating metal-poor massive stars have been computed by Yoon & Langer (2005), Meynet et al. (2006), Yoon et al. (2006) and Hirschi (2007). The set of models by Yoon & Langer are for initially 12 to 60 $M_\odot$ stars. They span the metallicity range $Z = 10^{-5}$ to 2×10^{-3} and cover initial equatorial rotation velocities between zero and 80 percent of the Keplerian value. In these tracks, transport of angular momentum is due to Eddington-Sweet circulations, shear instability, Goldreich-Schubert-Fricke instability, and magnetic torques, and is approximated by diffusion. In most cases, magnetic torques dominate, that are described in the context of the Spruit-Tayler dynamo (Spruit 2002), as explained by Heger et al. (2005). The tracks by Hirschi (2007) are for initial masses between 20 and 85 $M_\odot$ and cover metal fractions $Z = 10^{-8}$ to 0.02 and rotational velocities from zero to 800 km s^{-1}. Instabilities accounted for by Hirschi are meridional circulation and secular and dynamical shear instabilities.

Typical examples of the two sets of tracks are shown in Fig. 5.1. Interestingly, the rapidly rotating tracks of Yoon & Langer (2005) and Yoon et al. (2006) evolve more or less along the zero age main sequence (ZAMS) toward higher luminosities. Hence, these stars stay hot and compact. The tracks of Hirschi (2007) evolve away from the ZAMS, into the cool range of the Hertzsprung-Russell diagram. This striking difference between the evolutionary tracks of the two groups should be investigated and might be due to the difference in the inclusion and treatment of transport processes.

Different prescriptions are used to account for mass loss. Yoon & Langer (2005) and Yoon et al. (2006) use results by Kudritzki et al. (1989), assuming a metallicity dependence $\dot{M} \sim Z^{0.69}$ from Vink et al. (2001). For Wolf-Rayet phases they use results by Hamann et al. (1995), reduced by a factor 10, and a metallicity dependence as proposed by Vink & de Koter (2005). An *ad hoc* recipe for the effect of the increased CNO abundances on the mass loss is used. Hirschi (2007) adopt the mass-loss recipes from Nugis & Lamers (2000) for Wolf Rayet phases. For O- and B-star phases, they use Vink et al. (2001). For stars cooler than 12 500 K they use de Jager et al. (1988). An artifact of the recipe of de Jager et al. is that for luminous but cool stars (below $\sim$ 10 kK - 20 kK dependent on luminosity), outside of the range of validity of the fitting function, a 20-term Chebychev polynomial, unrealistically

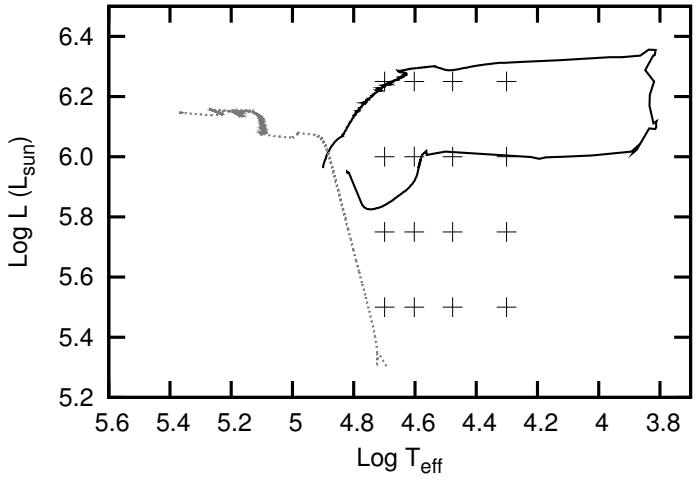

Figure 5.1: Evolutionary tracks for metal-poor stars. The grey track is for $M_{\rm init} = 40\,M_\odot$, $Z = 10^{-5}$ and for a rotational velocity that is $v_{\rm rot} = 555\,{\rm km\,s^{-1}}$ (Yoon et al. 2006). This rotational velocity is so large that their model is evolving homogeneously. The black track is for $M_{\rm init} = 85\,M_\odot$, $Z = 10^{-8}$ and $v_{\rm rot} = 800\,{\rm km\,s^{-1}}$ (Hirschi 2007). The plusses denote (L,$T_{\rm eff}$) combinations for which mass-loss rates have been computed using abundance patterns that are typical for the surface composition of the evolutionary tracks.

large mass-loss rates are produced (of order $10^{-2}\ M_\odot{\rm yr}^{-1}$). This rapidly strips stars of their outer envelope, causing the tracks of Hirschi (2007) to become excessively enriched in this part of the HRD. A feedback occurs, as the metallicity associated with the enriched surface causes a high mass loss once they evolve back to higher temperatures. This implies that the surface enrichment in the blue-ward tracks of Hirschi is strongly dependent on the (unrealistic) mass-loss history.

5.2.4 Grid

We limit the grid of models to the temperature range from 20 kK to 50 kK and the luminosity interval from $10^{5.5}$ to $10^{6.25}\,L_\odot$. The reason why we did not try hotter models – though predicted by Yoon et al. (2006) – is explained below. Essentially, for such high temperatures in combination with a low iron group metal content we do not find sufficient line driving to sustain a stellar wind. We encounter convergence problems of the model atmospheres for temperatures close to 10 000 K because convection is not accounted for. To avoid that convection becomes an issue, we adopt 20 kK as the low end of the investigated temperature range.

For the surface abundance of carbon, nitrogen and oxygen combined, $Z_{\rm CNO}$, as

Table 5.1: Adopted abundance patterns: X and Y values are always consistent with the adopted $Z_{\rm CNO}$, but are given here for the case $Z_{\rm CNO} = 0.04$.

Case	Track type	X	Y	C	N	O	$Z_{\rm iron}$
1	Hirschi	0.56	0.40	42 %	38 %	20 %	1×10^{-8}
2	Hirschi	0.56	0.40	55 %	25 %	20 %	1×10^{-8}
3	Yoon et al.	0.56	0.40	57 %	10 %	33 %	1×10^{-5}
4	Yoon et al.	0.05	0.91	57 %	10 %	33 %	1×10^{-5}

well as the relative abundances of these three elements we assumed values that are typical – but, deliberately, not tailored – for the predictions of Yoon et al. (2006) and Hirschi (2007). Having said this, the abundance choices best fit the $85\,M_\odot$, $Z = 10^{-8}$ and $v_{\rm rot} = 800\,{\rm km\,s^{-1}}$ track for the case of Hirschi and the $40\,M_\odot$, $Z = 10^{-5}$ and $v_{\rm rot} = 555\,{\rm km\,s^{-1}}$ track for the Yoon et al. case. These are the tracks that are shown in Fig. 5.1. For the Hirschi case we selected two compositions, one that is characteristic for the start of the surfacing of CNO processed material (termed Case 1) by rotational mixing and one that is typical for the end of this mixing phase (termed Case 2), but *before* the phase of extreme mass loss as discussed in Sect. 5.2.3. The stars computed by Yoon et al. evolve on a chemically homogeneous track and are helium stars at the point they are enriched with hydrogen burning products. We adopt a relative CNO abundance that is typical for the start of enrichment (termed Case 4). To separate the effects of the H/He ratio from CNO abundance effects we introduce an intermediate Case 3 in which the H/He ratio was assumed to be equal to the H/He ratio from the Hirschi track. An overview of these abundance patterns is provided in Table 5.1.

For all these cases we adopt three values of $Z_{\rm CNO}$, i.e. 0.002, 0.02 and 0.04. For abundances of other elements, we adopt the solar values from Anders & Grevesse (1989) and scale them down to the metallicities as listed in Table 5.1. We point out that these other elements do not contribute to the wind driving.

5.3 Results

5.3.1 Mass-loss behavior

The overall trends in the behavior of the predicted mass-loss rates are as follows: For iron-group metallicities below $\sim 10^{-4}$ (in line with Vink et al. (2001)) and no primary

enrichment of the atmosphere with carbon, nitrogen and oxygen we find that we can not drive an outflow. Only for $Z_{\rm CNO} \sim 10^{-3}$ or higher, the CNO elements can drive a stellar wind – if circumstances are favorable. For temperatures of 50 kK or higher the CNO elements are highly ionized. These ionic species – such as C v, N v and O v – have relatively simple atomic level configurations, resulting in only few lines near the flux maximum of the emergent spectrum. The cumulative radiation pressure of these lines, supplemented with a contribution by hydrogen and helium lines that is diminishing for increasing temperature, is insufficient to power a wind. Therefore, we do not predict stars hotter than ∼50 kK to have a line driven outflow.

Table 5.3 presents the $\dot{M}$, v_∞, and β predictions for our grid. For these models, characterized by a line driving that is on the brink of being sufficient to drive a wind, numerical uncertainties as well as the accuracy of the physical solution requirement Eq. 5.1 may play a role in whether or not a solution is found. Typical uncertainties in the (iterative) numerical method itself are 0.1–0.2 dex in the mass-loss rate and ∼30 % in the terminal velocity. To avoid over-interpretation of individual models, we opt to present the results in terms of their overall characteristics. Moreover, to provide a frame of reference we compare the computed mass-loss rates with predictions based on the recipe of Vink et al. (2001). These reference rates are referred to as $\dot{M}_{\rm V}$ and are also provided in Table 5.3.

The Vink et al. recipe has been derived for a chemical composition of all elements apart from hydrogen and helium (i.e. the metallicity in the astrophysical context) that is scaled to the solar composition as given by Anders & Grevesse (1989). We compare our mass loss $\dot{M}$ with $\dot{M}_{\rm V}$ by identifying $Z_{\rm CNO}$ of the models presented here as the metallicity Z as intended by Vink et al.. Clearly, as a general trend we may expect that the Vink et al. recipe predicts larger mass-loss rates compared to the values computed here, as iron-group elements are more efficient in driving the wind through the sonic point than are lines of CNO only.

The $\dot{M}_{\rm V}$–recipe is valid for stars that are not too close to their Eddington limit. In terms of the ratio of the radiation pressure on free electrons to the Newtonian gravity, i.e. $\Gamma_{\rm e} = g_{\rm e}/g_{\rm N}$, all $\dot{M}_{\rm V}$ predictions are for $\Gamma_{\rm e} \lesssim 0.4$. An extension of these predictions for stars close to their Eddington limit by Vink et al. (2010b) shows that for $\Gamma_{\rm e} \lesssim 0.7$ the standard $\dot{M}_{\rm V}$-recipe remains unaltered. The largest value of $\Gamma_{\rm e}$ in the computations presented in this study are $\Gamma_{\rm e} \sim 0.5$ for models in which the luminosity $\log L/L_\odot = 6.25$. We conclude that effects of approaching the Eddington limit do not complicate the comparision of our results to the $\dot{M}_{\rm V}$ predictions.

The outcome of the comparison is shown in Fig. 5.2, for the three different values of $Z_{\rm CNO}$, together with a power-law fit. The coefficients of these fits are listed in Table 5.2. In all cases the behavior is approximately

$$\dot{M}(Z_{\rm CNO}) = a\,\dot{M}_{\rm V}^{\alpha}(Z = Z_{\rm CNO}) \sim \frac{1}{300}\dot{M}_{\rm V}^{0.7}(Z = Z_{\rm CNO}), \tag{5.2}$$

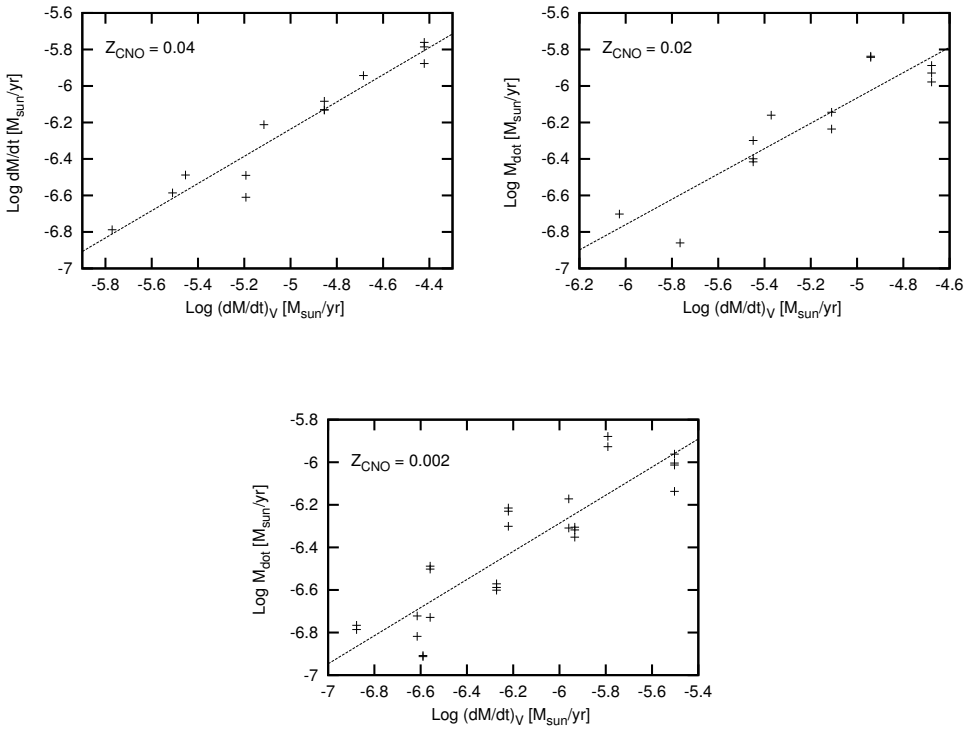

Figure 5.2: Derived mass-loss rates versus predictions by Vink et al. (2001) (denoted $\dot{M}_{\rm V}$) for $Z = 0.04$ (top left panel), $Z = 0.02$ (top right panel) and $Z = 0.002$ (bottom panel). The coefficients of the power law fits are given in Table 5.2.

where the mass-loss rates are in units of $M_{\odot}{\rm yr}^{-1}$. The error in this relation is typically a factor of three. We point out that this relation is only valid if the iron-group mass fraction is extremely low, i.e. below a few times $10^{-4}Z_{\odot}$, and the temperature is in the range from 20 kK to ~50 kK. For higher temperatures, as pointed out above, we do not drive an outflow.

Let us appraise some aspects of Eq. 5.2. For a Vink et al. mass loss of $10^{-6}\,M_{\odot}{\rm yr}^{-1}$, our models imply a mass loss that is 0.3 dex lower for $Z_{\rm CNO} = 0.002$; 0.8 dex lower for $Z_{\rm CNO} = 0.02$, and 1.0 dex lower for $Z_{\rm CNO} = 0.04$. So, for progressively higher CNO enrichments the discrepancy with $\dot{M}_{\rm V}$ increases. This reflects that the driving power of the CNO lines is topped once the relevant driving lines become saturated. An increase of the iron-group metal content to high metallicities of 0.02-0.04 does not suffer from this effect as most of the iron lines that drive the wind are relatively weak. Consequently, the mass-loss rate of a wind in which the gas composition scales to the solar abundance pattern continues to rise with increasing metallicity. The fact that the

Table 5.2: Fit parameters, expressing our predicted mass-loss rates for winds driven by carbon, oxygen and nitrogen lines, in terms of the mass-loss rates $\dot{M}_{\rm V}$ as predicted by Vink et al. (2001): $\dot{M} = a \times \dot{M}_{\rm V}^{\alpha}$. The coefficients are almost independent of Z, and can be summarized according to Eq. 5.2.

Fit Parameters		
$Z_{\rm CNO}$	a	α
0.04	-2.51 ± 0.31	0.745 ± 0.062
0.02	-2.60 ± 0.49	0.694 ± 0.095
0.002	-2.33 ± 0.43	0.660 ± 0.070

main CNO driving lines are saturated in the $Z_{\rm CNO}$ range explored here implies that the absolute mass-loss rates of metal-poor stars enriched with primary CNO must be essentially independent of $Z_{\rm CNO}$. Indeed, this is what we find.

5.3.2 Hydrogen rich versus helium rich stars

We find that overall it is more difficult for helium rich stars to drive a wind, if all other stellar parameters (notably stellar mass) remain unaltered. We identify two reasons for this. First, helium does not provide as many free electrons as does hydrogen. Therefore the contribution of the free electrons to the radiative force is less. Second, the contribution of the helium lines to the radiative force is at maximum on the order of the contribution of the hydrogen lines but in many cases less. The latter effect is most relevant for the 20 kK models, where the neutral hydrogen fraction (though small in an absolute sense) is the highest.

The mass loss is found to be independent of H/He ratio. This could, however, only be assessed for the case $Z_{\rm CNO} = 0.002$. Please note that though Cases 3 and 4 are representative for the homogeneously evolving tracks of Yoon et al. (2006), they need not be representative for strongly enriched modestly rotating WNL (that may have $Z_{\rm N} > 0.15$) or WC stars (that may have $Z_{\rm C} > 0.50$). Models representative for such 'classical' type of Wolf-Rayet stars have been computed by Vink & de Koter (2005).

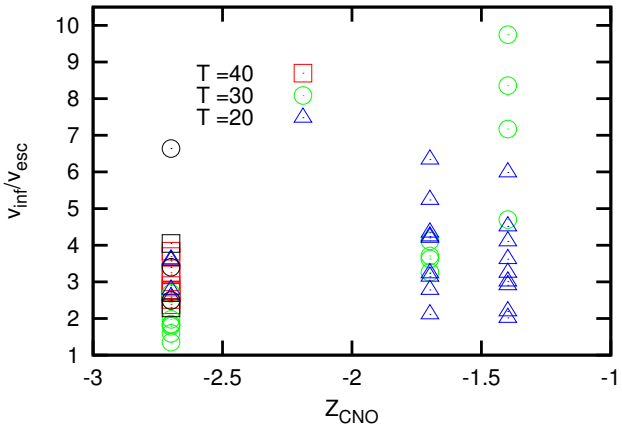

Figure 5.3: Predicted terminal velocities v_∞ for all models normalized to the effective escape velocity at the stellar surface v_{esc}. Symbols and color codings indicate temperature; black symbols represent the H-poor models. Including the outliers towards high v_∞/v_{esc}, the average of the H-rich models increases with Z_{CNO}, from 2.6 to 3.9 to 4.7 for Z_{CNO} = 0.002, 0.02 and 0.04, respectively.

5.3.3 Terminal velocity behavior

Figure 5.3 shows the ratio of the terminal velocity to the effective surface escape velocity as a function of Z_{CNO}, for all converged models in our grid. As for the mass-loss properties we also focus on the overall trends in the terminal flow characteristics. In line-driven winds the nature of the driving lines (both in terms of chemical composition and ionization) is reflected in the ratio v_∞/v_{esc} (see e.g. Castor et al. 1975; Kudritzki & Puls 2000), therefore we discuss our results in these terms.

For the H-rich stars in our grid (Cases 1 through 3) the trend is that v_∞/v_{esc} is increasing with Z_{CNO}. To be quantitative, the ratio increases from 2.7 ± 0.7 to 3.9 ± 1.1 to 4.7 ± 2.4 for Z_{CNO} = 0.002, 0.02 and 0.04, respectively. Notice that the scatter in v_∞/v_{esc} is quite large for the highest metallicity, and that for this case the models of 20 000 K only yield a mean v_∞/v_{esc} that is substantially lower, i.e. 3.5 ± 1.2.

The acceleration of the flow in the supersonic part of the wind is – as in galactic O- and early B-stars – controlled by strong lines of CNO. In galactic OB-stars the observed ratio of terminal velocity to escape velocity is ~2.6 for stars hotter than 22 000 K and about 1.3 for cooler objects (Lamers et al. 1995). Predictions of this ratio for normal O-stars by Muijres et al. (2010b) for the best-β method (see Sect. 5.2.2) yield v_∞ values that are typically 30% higher than observed. Correcting for this, we still find higher outflows speeds. The reasons why the CNO enriched metal-poor

stars produce higher terminal velocities than do galactic stars is a combination of a lower mass-loss rate and a more efficient driving in the supersonic part of the outflow, due to the high abundances of CNO. Relative changes in the abundances of carbon, nitrogen and oxygen (as implied by Cases 1, 2 and 3) have a rather modest effect on v_∞, given the uncertainty in the predictions of the terminal velocity (~30%), this is not significant.

The converged He-rich models (Case 4) at 30 000 K tend to have higher $v_\infty/v_{\rm esc}$ ratios than do comparable H-rich models. In the He-rich case the continuum flux in the region where the main driving lines are located is larger, therefore these lines are more efficient, leading to larger v_∞.

5.4 Discussion

5.4.1 Comparison to other studies

The mass-loss from luminous metal-poor stars enriched with primary CNO has also been studied by Krtička & Kubát (2009), using stellar parameters from the evolutionary tracks for First Stars, formed from metal-free gas clouds in the early universe, by Marigo et al. (2001, 2003). There are similiarities and differences in our treatment of the stellar atmosphere and wind and that by Krtička & Kubát. In both methods the state of the gas is treated in NLTE and the Sobolev approximation is used to describe the transfer of radiation in spectral lines. Krtička & Kubát, however, treat the photosphere – from where the continuum radiation originates – and wind separately. They adopt an emergent flux taken from H-He model atmospheres, where we treat the photosphere and wind in a self-consistent, unified way. Moreover, in our Monte Carlo treatment we self-consistently account for multiple scattering effects, which are ignored in the Krtička & Kubát approach. For the type of models discussed here, these differences are not likely to cause major differences. More important is the difference pointed out already in Sect. 5.2.2. Krtička & Kubát apply a test in order to assess whether a wind can be sustained that is much simpler than the method applied here. The advantage of their criterium is that it allows one to *a priori* determine whether a star can drive a wind. However, such a test does not fully capture the feedback between line driving and wind density, nor does it fulfill the requirement of dynamical consistency.

A quantitative comparison of our results with those of Krtička & Kubát (2009) can only be made for a limited number of models, because of (too large) differences in stellar parameters and surface $Z_{\rm CNO}$ abundances. In any case, accounting for the uncertainty introduced by their model grid spacing Krtička & Kubát find a similar $T_{\rm eff}$ boundary for which stars in the same luminosity range can drive a wind: stars must be cooler than ~60–50 kK. Accepting a ~10% difference in the stellar mass,

we find a very similar mass-loss rate for the model with $Z_{\rm CNO} = 0.02$, $T_{\rm eff}$= 20 kK and $\log L/L_\odot = 5.9$ (their model M500-3): the difference is ~0.2 dex. However, we obtain a terminal velocity that is 20–40 percent lower, depending on the exact choice of chemical pattern.

For the most luminous objects, we can compare models at both 30 kK and 20 kK, again for $Z_{\rm CNO} = 0.02$ (their models M999-1 and M999-2). Here we find a mass-loss rate that is ~0.3-0.7 dex lower, while terminal velocities are lower by ~20 percent. Here it should be noted that Krtička & Kubát adopt a mass of $100\,M_\odot$, while the tracks on which we rely suggest $\sim 80\,M_\odot$.

This very limited comparison suggests that we predict roughly similar mass-loss rates for stars of initially 50–75 $M_\odot$, but that for more massive stars, in the range of 75–100 $M_\odot$ our mass-loss rates are lower by a factor of a few.

5.4.2 How to apply $\dot{M}(Z_{\rm CNO})$

Vink et al. (2001) point out that their recipe is valid for a scaled solar metallicities as low as $1/30\,Z_\odot$ for luminosities less than a million solar luminosities, and $1/100\,Z_\odot$ for more luminous objects. Their adopted solar values are from Anders & Grevesse (1989), in which $Z_\odot = 0.019$. In exploring the line-driving at their lowest metal contents, Vink et al. (2001) already detect an increasing relative importance of CNO. Moreover, they point out that the occurrence of the bi-stability jump at about 25 000 K at very low metal content due to the recombination of ions of a CNO element, i.e. C IV to C III. We tested whether neglecting the up-turn in mass-loss for stars cooler than 25 000 K in the present-day universe in the $\dot{M}_{\rm V}$-recipe improved or degraded the correlation presented in Fig. 5.2 and Table 5.2. This significantly degrades the correlation.

To provide a simple recipe to adjust the Vink et al.-recipe for models that show primary enrichment, we propose the heuristic formula:

$$\dot{M} = \dot{M}(Z_{\rm CNO}) + \dot{M}_{\rm V}(Z_{\rm initial}), \tag{5.3}$$

where $Z_{\rm initial}$ is the initial metal content of the star and $Z_{\rm CNO}$ is the primary CNO abundance. $\dot{M}(Z_{\rm CNO})$ is given by Eq. 5.2. In the $\dot{M}_{\rm V}$-recipe, the bi-stability jump should remain to be applied. Equation 5.3 is valid for $T_{\rm eff} < 50$ kK. For hotter temperatures and abundances below $Z \sim$ a few 10^{-4} (Vink et al. 2001), we do not predict stars to loose mass in a line driven wind. The validity of the $\dot{M}_{\rm V}$ formula extends to temperatures as low as 12 500 kK. The new $\dot{M}_{\rm CNO}$ predictions have been computed down to 20 000 kK. A modest extrapolation may be applied, though, most certainly not below 15 000 kK. The highest $Z_{\rm CNO}$ abundance in our computations is 0.04. Again, some extrapolation may be acceptable. However, for chemical compositions that are more typical for evolved Wolf-Rayet objects ($Z_{\rm CNO} \gtrsim 0.1$), we refer to Vink & de Koter

(2005). The lowest $Z_{\rm CNO}$ abundance in our computations is 0.002. The minimum $Z_{\rm CNO}$ for which a wind may be driven is a function of luminosity, proximity to the Eddington limit, and, to a lesser extend, detailed chemical abundance pattern. However, the mass-loss rates associated with such low CNO abundances will not impact the overall mass-loss and/or angular momentum loss of these stars (see Sect. 5.4.3). This largely removes a practical need to define the limit below which metal-poor stars may or may not drive a wind.

We point out that in terms of proximity to the Eddington limit, the stars investigated show Eddington factors $\Gamma_{\rm e}$ up to ~0.5. We therefore do not exclude that metal-poor stars very close to their Eddington limit may still drive a wind through line radiation pressure, as discussed by Kudritzki (2002); Vink & de Koter (2005); Krtička & Kubát (2006); Gräfener & Hamann (2008).

5.4.3 Implications for the evolution of metal-poor stars

Though the surfacing of CNO-cycle products may make the difference in whether or not a metal-poor star can produce a line-driven wind or not, the actual mass-loss rate such stars feature is only modest. Absolute values of $\dot{M}$ for the grid of stars presented here are in the range 10^{-6}–$10^{-7}\,M_{\odot}{\rm yr}^{-1}$. Though substantial surface enrichment may only occur after a significant part of the lives of metal-poor massive stars, even when simply assuming this would happen shortly after reaching the main-sequence the cumulative mass-loss is only $\sim 1\,M_{\odot}$ for a $30\,M_{\odot}$ star and $\sim 10\,M_{\odot}$ for a $80\,M_{\odot}$ star. So, at most a few percent of the initial mass, but likely less than that. This is similar to the conclusion reached by Krtička & Kubát (2009).

Purely by line-driven winds, metal-poor and initially metal-free stars may inject at total of the order of $10^{-3} - 10^{-1}\,M_{\odot}$ of CNO processed material into their (primordial) surroundings. This is substantially less than the enrichment with CNO and other metals that is to be expected in the (pair-instability) supernova that ends their lives. Still, it may be too early to conclude that a shift from a top-heavy initial mass function (IMF), predicted in simulations of the first star-forming regions (Bromm et al. 1999; Nakamura & Umemura 2002), to a Salpeter (1955) IMF, is due to dust grains formed from *supernovae* material. This outcome is based on the fact that a line-driven wind is the only mass-loss mechanism a metal-poor or First Star may suffer. As already pointed out, rotation close to critical, perhaps in combination with approaching the Eddington limit (Meynet et al. 2006) and/or pulsations (Baraffe et al. 2001) may boost the mass-loss rate of these objects. Mass-loss eruptions in a post-main sequence phase, as for instance suffered by the massive star η Carinae (Humphreys & Davidson 1994), might play a role in the early universe as well. So, far the exact nature of these eruptions eludes us (see Owocki et al. 2004), and possibly mechanism does not depend on the chemical composition. If so, this type of mass-loss may have played relatively an important role early-on in the universe.

The low mass-loss rates of massive metal-poor stars imply that up to a CNO surface abundance of $Z_{\rm CNO} \sim 0.1$ such objects are not likely to loose significant angular momentum. A lack of loss of angular momentum is favorable for the proposition that very rapidly rotating stars at low metallicity may result in long-duration gamma-ray bursts (Yoon & Langer 2005; Woosley & Heger 2006).

5.5 Conclusions

We present calculations of the mass-loss rates of metal-poor massive stars that, as a result of rotational mixing, become enriched at their surfaces with products of primary CNO burning. From predictions of the evolution of such stars we adopt several characteristic CNO enriched abundance patterns, and for these chemical patterns we perform tailored computations of the mass-loss rate in line driven winds. The formal requirement to drive a wind is that the gravity equals the radiative forces at the sonic point of the flow.

On the basis of the results, we provide a heuristic formula to estimate the mass-loss rates of such metal poor stars, for the parameter range $L \gtrsim 10^{5.5}\,L_\odot$, $T_{\rm eff} \gtrsim 15\,000\,{\rm K}$ and $\Gamma_{\rm e} \lesssim 0.5$, and we propose to apply this formula (Eq. 5.3) – expressed as a scaling to the often applied Vink et al. (2001)-recipe – in evolutionary predictions of such objects.

The main conclusions we obtain are:

(I) The mass-loss predictions $\dot{M}_{\rm V}$ (Vink et al. 2001) are not tailored for massive metal-poor ($Z \lesssim 1/100\,Z_\odot$), but CNO enriched stars. Applying this formula, by equalizing the CNO enriched chemical pattern to Z, will overestimate the actual CNO driven mass-loss rate. The mass-loss rates we find for the most massive objects ($M \gtrsim 75 M_\odot$) are up to a factor of a few lower than those by Krtička & Kubát (2009) and roughly comparable for stars of lower mass.

(II) Metal-poor and surface CNO enriched massive stars hotter than 50 000 K do not feature a line driven wind; highly ionized carbon, nitrogen and oxygen ions provide too few efficient driving lines. This result is similar to that obtained by Krtička & Kubát (2009), within the uncertainties in the $T_{\rm eff}$ resolution of our and their grid computations. It implies that homogeneously evolving stars (which remain very hot during their entire life) do not have line-driven winds in the initial metallicity range investigated here ($Z \lesssim 10^{-4}$).

(III) In the range of $Z_{\rm CNO} = 0.002$-0.04, the mass-loss rate is not a strong function of the ratio of C to N to O.

(IV) The terminal wind velocities of CNO enriched metal-poor stars are higher than those of massive stars in the present-day universe. For $Z_{\rm CNO} \sim 0.02$–0.04 they

are 25-50% higher. The reasons for this behavior are a combination of the lower mass-loss rate and a more efficient driving in the supersonic part of the outflow, due to the high abundance of CNO.

(V) The winds of massive very metal-poor stars ($Z \lesssim 10^{-4}$), whether they are CNO enriched or not, are so weak that they do not significantly impact the total mass and/or angular momentum loss during their evolution. If other mass-loss mechanisms, such as η Carinae type of mass eruptions, do not occur for such objects, their supernova explosions are expected to be responsible for the major part of the early nucleosynthetic enrichment.

5.6 Appendix: Grid of wind properties of metal-poor stars with primary enrichment of C, N, and O

Table 5.3: Adopted model parameters and predicted wind properties. Both the models for which a wind solution is achieved and those for which this is not the case are listed. The chemical compositions (column 7) correspond to the coding as given in Table. 5.1. Typical errors on the theoretical mass-loss rates are 0.1–0.2 dex; the errors on the terminal velocities are ∼30%. For models in which the abundance pattern is followed by a semi colon the errors are larger. The reference mass-loss rates $\dot{M}_{\rm V}$ are as given by Vink et al. (2001), if we employ $v_\infty = 2.6\, v_{\rm esc}$. Beware that in order to compute $\dot{M}_{\rm V}$ we have set the value of $Z_{\rm CNO}$ equal to the metallicity value Z, which is not intended by the $\dot{M}_{\rm V}$–recipe, in which Z refers to the initial iron abundance. Small changes in the effective escape velocity from the stellar surface (column 10) are due to abundance effects on $\Gamma_{\rm e}$.

Model Parameters							Wind properties			
L	M	$T_{\rm eff}$	R	$Z_{\rm CNO}$	$\dot{M}_{\rm V}$	Abund.	$\dot{M}$	v_∞	$v_{\rm esc}$	β
$\log(L_\odot)$	$M_\odot$	kK	$R_\odot$		$\log(M_\odot/{\rm yr})$	pattern	$\log(M_\odot/{\rm yr})$	$\rm km\,s^{-1}$	$\rm km\,s^{-1}$	
5.50	30.0	50.0	7.5	0.04	-5.496	–	–	–	–	–
				0.02	-5.752	–	–	–	–	–
				0.002	-6.602	–	–	–	–	–
		40.0	11.7	0.04	-5.484	–	–	–	–	–
				0.02	-5.740	–	–	–	–	–
				0.002	-6.590	3	-6.908	2330	852	0.72
				0.002	-6.590	4	-6.913	2060	900	0.64
		30.0	20.9	0.04	-5.771	2	-6.788	5406	647	1.12
				0.02	-6.027	1	-6.702	2100	644	0.78
				0.002	-6.877	1:	-6.766	1150	644	0.66
						3	-6.786	1193	646	0.64
		20.0	47.0	0.04	-5.510	2:	-6.586	956	436	0.67
				0.02	-5.765	1:	-6.860	2750	434	1.23
				0.002	-6.615	1:	-6.818	1550	434	0.84
						2:	-6.722	1126	436	0.72

Table 5.3: Continued ...

Model Parameters							Wind properties			
L	M	$T_{\rm eff}$	R	$Z_{\rm CNO}$	$\dot{M}_{\rm V}$	Abund.	$\dot{M}$	v_∞	$v_{\rm esc}$	β
$\log(L_\odot)$	$M_\odot$	kK	$R_\odot$		$\log(M_\odot/{\rm yr})$	pattern	$\log(M_\odot/{\rm yr})$	km s^{-1}	km s^{-1}	
5.75	45.0	50.0	10.0	0.04	-5.179	–	–	–	–	–
				0.02	-5.435	–	–	–	–	–
				0.002	-6.285	–	–	–	–	–
		40.0	15.6	0.04	-5.167	–	–	–	–	–
				0.02	-5.422	–	–	–	–	–
				0.002	-6.272	1	-6.571	2080	875	0.67
						2	-6.588	2204	875	0.71
						3	-6.601	2377	875	0.70
		30.0	27.8	0.04	-5.454	3	-6.488	3130	666	0.84
				0.02	-5.709	–	–	–	–	–
				0.002	-6.559	1	-6.488	1060	665	0.66
						2:	-6.502	900	665	0.60
						4	-6.729	4800	723	0.95
		20.0	62.4	0.04	-5.193	1	-6.490	2030	450	0.86
						3	-6.610	2694	450	1.09
				0.02	-5.449	1	-6.399	1250	450	0.69
						2:	-6.299	950	450	0.80
						3	-6.416	1412	450	0.81
				0.002	-6.299	–	–	–	–	–

Table 5.3: Continued …

Model Parameters							Wind properties			
L	M	$T_{\rm eff}$	R	$Z_{\rm CNO}$	$\dot{M}_{\rm V}$	Abund.	$\dot{M}$	v_∞	$v_{\rm esc}$	β
$\log(L_\odot)$	$M_\odot$	kK	$R_\odot$		$\log(M_\odot/{\rm yr})$	pattern	$\log(M_\odot/{\rm yr})$	$\mathrm{km\,s^{-1}}$	$\mathrm{km\,s^{-1}}$	
6.00	65.0	50.0	13.3	0.04	-4.840	–	–	–	–	–
				0.02	-5.096	–	–	–	–	–
				0.002	-5.946	–	–	–	–	–
		40.0	20.8	0.04	-4.828	–	–	–	–	–
				0.02	-5.084	–	–	–	–	–
				0.002	-5.934	1	-6.305	2500	863	0.72
						2	-6.318	2400	863	0.71
						3	-6.352	2752	863	0.75
		30.0	37.0	0.04	-5.115	1	-6.212	4740	661	1.06
				0.02	-5.371	1:	-6.160	2450	661	0.78
				0.002	-6.221	2	-6.215	1305	660	0.64
						3:	-6.230	1205	659	0.63
						4	-6.301	2500	736	0.76
		20.0	83.3	0.04	-4.854	1	-6.132	1625	449	0.80
						2:	-6.130	1350	449	0.71
						3:	-6.084	905	449	0.65
				0.02	-5.110	1:	-6.236	1950	449	0.96
						2:	-6.144	1450	449	0.82
				0.002	-5.960	1	-6.172	1250	449	0.76
						2:	-6.309	1620	449	0.87

Table 5.3: Continued ...

Model Parameters							Wind properties				
L	M	$T_{\rm eff}$	R	$Z_{\rm CNO}$	$\dot{M}_{\rm V}$	Abund.	$\dot{M}$	v_∞	$v_{\rm esc}$	β
$\log(L_\odot)$	$M_\odot$	kK	$R_\odot$		$\log(M_\odot/{\rm yr})$	pattern	$\log(M_\odot/{\rm yr})$	km s^{-1}	km s^{-1}	
6.25	80.0	50.0	17.8	0.04	-4.410	–	–	–	–	–
				0.02	-4.666	–	–	–	–	–
				0.002	-5.516	–	–	–	–	–
			27.8	0.04	-4.398	–	–	–	–	–
				0.02	-4.653	–	–	–	–	–
				0.002	-5.503	1	-5.962	2310	711	0.76
						2	-6.004	2616	709	0.80
						3:	-6.013	2721	709	0.81
						4	-6.137	3400	840	0.75
		30.0	49.3	0.04	-4.685	2	-5.943	5400	554	1.16
				0.02	-4.941	2:	-5.837	2274	552	0.84
						3	-5.843	2000	552	0.77
				0.002	-5.791	2	-5.879	1483	552	0.74
						4	-5.927	1667	669	0.65
		20.0	111.0	0.04	-4.422	1	-5.786	1110	382	0.74
						2:	-5.877	1567	382	0.81
						3:	-5.761	1240	382	0.81
				0.02	-4.678	1	-5.978	2000	382	0.91
						2	-5.888	1615	381	0.93
						3:	-5.929	1600	381	0.83
				0.002	-5.528	–	–	–	–	–

Samenvatting in het Nederlands

Ons heelal is ongeveer veertien miljard jaar oud. Het is ontstaan in een snelle expansie van de ruimte zelf, die de populaire benaming “oerknal” heeft gekregen. Vlak na deze oerknal zag het heelal er heel anders uit dan tegenwoordig. Het bestond uit een soep van materie en energie waaruit na enige minuten de elementen waterstof, helium, lithium en berilium gevormd werden. Uit dit gas, gedomineerd door de twee lichtste elementen, ontstonden onder invloed van de zwaartekracht na enige honderden miljoenen jaren de eerste sterren.

Sterren ontstaan door de ineenstorting van een gaswolk die te zwaar is om tegen zijn eigen zwaartekracht te vechten. Deze wolk stort in elkaar totdat het binnenste van de samengeperste gasbol heet genoeg is om kernfusie te starten. Bij kernfusie komt energie vrij. Deze wordt naar buiten getransporteerd en door de bol van gas uitgestraald in de vorm van licht (fotonen). Een ster is geboren.

Tijdens het leven van een ster worden door de kernfusie in het sterinwendige elementen gevormd die zwaarder zijn dan waterstof en helium. Eerst wordt uit waterstof helium gemaakt en dan uit helium zwaardere elementen zoals koolstof, stikstof, en zuurstof via een heel stappenplan. De verschillende fusiefases kunnen we zien als verschillende fases in het leven van een ster. Dit leven wordt door sterrenkundigen de evolutie van de ster genoemd.

Op een gegeven ogenblik is de brandstof op. De ster kan dan geen energie meer produceren door fusie en stort in elkaar. Hoe dat precies gaat en wat er verder met de ster gebeurt hangt af van de geboortemassa. Als de ster geboren wordt met een massa van maximaal acht keer die van de zon dan zal ze in elkaar storten tot er een kleine kern achterblijft die bijna geen licht meer geeft. Dit wordt een witte dwerg genoemd. Als een ster zwaarder is dan acht keer de massa van de zon zal ze de ineenstorting omzetten in een explosie die we supernova noemen en zal de kern van de ster in elkaar storten tot een neutronenster, zwart gat of zal de ster helemaal niets achterlaten. Bij dit soort explosies komt heel veel energie vrij en worden de buitenste lagen van de ster weggeblazen. Dit gas komt in de interstellaire ruimte en verandert de compositie van de aldaar aanwezige gaswolken.

Nieuwe sterren die uit deze gaswolken gevormd worden, zullen een iets andere samenstelling hebben dan die van de generatie ervoor. Als dit proces zich vaak genoeg

herhaalt, zijn er zoveel elementen gemaakt dat tijdens de stervorming ook planeten kunnen ontstaan, en op één van die planeten leven wij.

De sterren die minimaal acht keer zwaarder zijn dan de zon, zware sterren, vervuilen hun omgeving met de elementen die ze tijdens hun leven hebben geproduceerd. Ze doen dat zoals eerder beschreven aan het eind van hun leven tijdens de supernova-explosie maar kunnen dit ook tijdens hun leven doen in de vorm van een sterrewind. De sterrewinden van zware sterren zijn het onderwerp van dit proefschrift.

Een sterrewind is niets anders dan de uitstromende atmosfeer van een ster. Het licht dat de ster uitstraalt, kan een naar buiten gerichte kracht op de buitenste lagen van de atmosfeer uitoefenen die groter is dan de naar binnen gerichte zwaartekracht. Daardoor versnelt de atmosfeer en zal ze uitstromen als een sterrewind.

Het sterlicht oefent een kracht uit op de atmosfeer omdat fotonen door de daar aanwezige gasdeeltjes worden geabsorbeerd. Er zijn veel verschillende manieren waarop dat kan maar voor de wind van deze sterren is één proces erg belangrijk: een atoom bestaat uit een kern met elektronen er om heen. Elk verschillend atoom heeft een bepaalde structuur met een bepaald aantal energieniveaus waarin de elektronen zich kunnen bevinden. De elektronen kunnen in een hoger energieniveau rondom het atoom gebracht worden door een foton te absorberen. Om geabsorbeerd te kunnen worden, moet het foton precies de juiste energie hebben om zo'n overgang tussen energieniveaus te bewerkstelligen. De fotonenergie die het deeltje ziet, is afhankelijk van de snelheid van dit deeltje ten op zichte van de ster. Als het deeltje versnelt, zal het fotonen absorberen met een andere energie dan in rust. Dat betekent dat de hoeveelheid energie die geabsorbeerd wordt afhankelijk is van de versnelling, hoeveel verschillende soorten atomen er zijn, de hoeveelheid van deze atomen, en de complexiteit van de set beschikbare energieniveaus die de atomen hebben. In het algemeen geldt, des te meer ingewikkelde atomen zoals koolstof, stikstof, zuurstof en ijzer de ster bevat des te makkelijker de atmosfeer van de ster versnelt.

Door de sterrewind verliest de ster langzaam massa. Het afnemen van haar massa heeft een belangrijke invloed op het leven van een ster. Het is daarom belangrijk om te bepalen wat het massaverlies is als functie van de eigenschappen van de ster. Zoals hierboven beschreven hangt de hoeveelheid massa die een ster verliest af van de compositie van de atmosfeer. Daarom zal het effect bij de eerste zware sterren die in het universum gevormd werden, en die bijna alleen uit waterstof en helium bestonden, anders zijn geweest dan bij de zware sterren in ons Melkwegstelsel die al heel veel verschillende soorten atomen bevatten.

In dit proefschrift wordt het massaverlies als functie van de eigenschappen van sterren bestudeerd. Dit wordt gedaan door uit te rekenen wat de structuur van de atmosfeer van een ster is. Er worden enkele fysische aspecten van sterrewinden besproken. Ook wordt er gekeken naar het massaverlies van de eerste sterren die in het heelal gevormd zijn.

Hieronder wordt kort beschreven wat het onderwerp van elk hoofdstuk is:

In hoofdstuk 2 worden de effecten van inhomogeniteiten in de sterrewind op de overdracht van energie van de fotonen op het atmosferische gas beschreven. Een niet homogeen gas is in het algemeen minder efficiënt in het absorberen van licht. We vinden dat de totale hoeveelheid energie die van de fotonen op de sterrewind wordt overgedragen afneemt in vergelijking met een homogene wind. Dit betekent dat de hoeveelheid massa die een ster per jaar verliest afneemt en/of dat de uitstroomsnelheid kleiner wordt.

In eerdere bepalingen van het massaverlies met de methode die in dit proefschrift wordt toegepast, werd de vergelijking die de uitstroom van het gas beschrijft niet opgelost. In hoofdstuk 3 worden twee manieren beschreven om dit wel aan te pakken. Er worden nieuwe massaverliezen uitgerekend voor een grid van hete zware sterren die dezelfde samenstelling hebben als de meeste sterren in ons Melkwegstelsel. Het resultaat is dat we ongeveer dezelfde massaverliezen vinden als met de oude methode voor sterren die meer dan 160000 keer zo lichtsterk zijn als de zon. Voor sterren die minder lichtsterk zijn, vinden we dat ze geen massa verliezen. Ook waarnemingen laten zien dat er iets heel drastisch met de sterrewind gebeurt bij deze grenslichtkracht. Wij denken dat het sterk afnemen van het empirisch gevonden massaverlies voor sterren die licht zwakker zijn dan 160000 zonslichtkrachten te maken heeft met het onvoldoende kunnen versnellen van de uitstroom.

Superzware sterren die ongeveer 50 tot 100 keer zwaarder zijn dan de zon blazen zichzelf bijna op. Ze kunnen heel veel massa verliezen. Het gedrag van het massaverlies van deze sterren is niet goed bekend. In hoofdstuk 4 wordt dit bestudeerd. Ook de overgang van het massaverlies van zware naar superzware sterren wordt beschreven.

In het vroege heelal werden waarschijnlijk voornamelijk zware sterren gevormd. Deze sterren verloren in eerste instantie weinig massa omdat ze geen zware elementen met ingewikkelde sets van energieniveaus bevatten. Tijdens hun evolutie, kunnen door mengingsprocessen de in de kern geproduceerde elementen koolstof, stikstof en zuurstof naar de buitenste lagen van de ster worden getransporteerd. De efficiëntie van de menging hangt af van de rotatiesnelheid van de ster. Als de ster snel roteert, zijn deze processen zo efficiënt dat de hoeveelheid koolstof, stikstof en zuurstof aan het oppervlak zo groot kan worden dat de ster wel veel massa kan verliezen. Hoeveel massa de ster dan kan verliezen, is het onderwerp van het hoofdstuk 5.

Bibliography

Abbott, D. C. 1982, ApJ, 259, 282
Abbott, D. C., Beiging, J. H., Churchwell, E., & Torres, A. V. 1986, ApJ, 303, 239
Abbott, D. C. & Lucy, L. B. 1985, ApJ, 288, 679
Abel, T., Bryan, G. L., & Norman, M. L. 2002, Science, 295, 93
Anders, E. & Grevesse, N. 1989, Geochim. Cosmochim. Acta, 53, 197
Asplund, M., Grevesse, N., & Sauval, A. J. 2005, in Astronomical Society of the Pacific Conference Series, Vol. 336, Cosmic Abundances as Records of Stellar Evolution and Nucleosynthesis, ed. T. G. Barnes, III & F. N. Bash, 25
Babel, J. 1995, A&A, 301, 823
Babel, J. 1996, A&A, 309, 867
Baraffe, I., Heger, A., & Woosley, S. E. 2001, ApJ, 550, 890
Barlow, M. J., Smith, L. J., & Willis, A. J. 1981, MNRAS, 196, 101
Becker, R. H., Fan, X., White, R. L., et al. 2001, AJ, 122, 2850
Belkus, H., Van Bever, J., & Vanbeveren, D. 2007, ApJ, 659, 1576
Bouret, J., Lanz, T., & Hillier, D. J. 2005, A&A, 438, 301
Bouret, J., Lanz, T., Hillier, D. J., et al. 2003, ApJ, 595, 1182
Bromm, V., Coppi, P. S., & Larson, R. B. 1999, ApJ, 527, L5
Bromm, V., Coppi, P. S., & Larson, R. B. 2002, ApJ, 564, 23
Bromm, V. & Larson, R. B. 2004, ARA&A, 42, 79
Brott, I., Hunter, I., de Koter, A., et al. 2009, Communications in Asteroseismology, 158, 55
Cantiello, M., Langer, N., Brott, I., et al. 2009, A&A, 499, 279
Castor, J. I., Abbott, D. C., & Klein, R. I. 1975, ApJ, 195, 157
Chiosi, C. & Maeder, A. 1986, ARA&A, 24, 329
Conti, P. S. 1976, Memoires of the Societe Royale des Sciences de Liege, 9, 193
Crowther, P. A. & Dessart, L. 1998, MNRAS, 296, 622
Crowther, P. A., Hillier, D. J., Evans, C. J., et al. 2002, ApJ, 579, 774
Crowther, P. A., Schnurr, O., Hirschi, R., et al. 2010, MNRAS, 1103
Davies, B., Oudmaijer, R. D., & Vink, J. S. 2005, A&A, 439, 1107
Davies, B., Vink, J. S., & Oudmaijer, R. D. 2007, A&A, 469, 1045
de Jager, C., Nieuwenhuijzen, H., & van der Hucht, K. A. 1988, A&AS, 72, 259

de Koter, A. 2006, in Astronomical Society of the Pacific Conference Series, Vol. 353, Stellar Evolution at Low Metallicity: Mass Loss, Explosions, Cosmology, ed. H. J. G. L. M. Lamers, N. Langer, T. Nugis, & K. Annuk, 99
de Koter, A., Heap, S. R., & Hubeny, I. 1997, ApJ, 477, 792
de Koter, A., Schmutz, W., & Lamers, H. J. G. L. M. 1993, A&A, 277, 561
de Koter, A., Vink, J. S., & Muijres, L. 2008, in Clumping in Hot-Star Winds, ed. W.-R. Hamann, A. Feldmeier, & L. M. Oskinova, 47
Dessart, L. & Owocki, S. P. 2003, A&A, 406, L1
Dessart, L. & Owocki, S. P. 2005, A&A, 437, 657
Drew, J. E., Hoare, M. G., & Denby, M. 1994, MNRAS, 266, 917
Eldridge, J. J. & Vink, J. S. 2006, A&A, 452, 295
Evans, C. J., Bastian, N., Beletsky, Y., et al. 2010, in IAU Symposium, Vol. 266, IAU Symposium, ed. R. de Grijs & J. R. D. Lépine, 35–40
Evans, C. J., Smartt, S. J., Lee, J., et al. 2005, A&A, 437, 467
Eversberg, T., Lepine, S., & Moffat, A. F. J. 1998, ApJ, 494, 799
Feldmeier, A. 1995, A&A, 299, 523
Feldmeier, A. 1999, in Lecture Notes in Physics, Berlin Springer Verlag, Vol. 523, IAU Colloq. 169: Variable and Non-spherical Stellar Winds in Luminous Hot Stars, ed. B. Wolf, O. Stahl, & A. W. Fullerton, 285
Feldmeier, A., Oskinova, L., & Hamann, W. 2003, A&A, 403, 217
Figer, D. F. 2005, Nature, 434, 192
Figer, D. F., Najarro, F., Gilmore, D., et al. 2002, ApJ, 581, 258
Figer, D. F., Najarro, F., Morris, M., et al. 1998, ApJ, 506, 384
Fullerton, A. W., Massa, D. L., & Prinja, R. K. 2006, ApJ, 637, 1025
Gayley, K. G., Owocki, S. P., & Cranmer, S. R. 1995, ApJ, 442, 296
Glatzel, W. & Kiriakidis, M. 1993, MNRAS, 263, 375
Gräfener, G. & Hamann, W. 2005, A&A, 432, 633
Gräfener, G. & Hamann, W. 2008, A&A, 482, 945
Grosdidier, Y., Moffat, A. F. J., Joncas, G., & Acker, A. 1998, ApJ, 506, L127
Haehnelt, M. G., Madau, P., Kudritzki, R., & Haardt, F. 2001, ApJ, 549, L151
Hamann, W. & Koesterke, L. 1998, A&A, 335, 1003
Hamann, W., Koesterke, L., & Wessolowski, U. 1995, A&A, 299, 151
Harries, T. J., Howarth, I. D., & Evans, C. J. 2002, MNRAS, 337, 341
Heger, A., Fryer, C. L., Woosley, S. E., Langer, N., & Hartmann, D. H. 2003, ApJ, 591, 288
Heger, A. & Langer, N. 1996, A&A, 315, 421
Heger, A., Langer, N., & Woosley, S. E. 2000, ApJ, 528, 368
Heger, A., Woosley, S. E., & Spruit, H. C. 2005, ApJ, 626, 350
Herrero, A., Kudritzki, R. P., Vilchez, J. M., et al. 1992, A&A, 261, 209
Hillier, D. J. 1991, A&A, 247, 455

Hillier, D. J., Lanz, T., Heap, S. R., et al. 2003, ApJ, 588, 1039
Hirschi, R. 2007, A&A, 461, 571
Hirschi, R., Meynet, G., & Maeder, A. 2005, A&A, 443, 581
Hjorth, J., Sollerman, J., Møller, P., et al. 2003, Nature, 423, 847
Howarth, I. D. & Prinja, R. K. 1989, ApJS, 69, 527
Howarth, I. D., Siebert, K. W., Hussain, G. A. J., & Prinja, R. K. 1997, MNRAS, 284, 265
Humphreys, R. M. & Davidson, K. 1994, PASP, 106, 1025
Iglesias, C. A. & Rogers, F. J. 1996, ApJ, 464, 943
Ignace, R., Quigley, M. F., & Cassinelli, J. P. 2003, ApJ, 596, 538
Ishii, M., Ueno, M., & Kato, M. 1999, PASJ, 51, 417
Kaper, L., Henrichs, H. F., Nichols, J. S., et al. 1996, A&AS, 116, 257
Kawakatu, N., Saitoh, T. R., & Wada, K. 2005, ApJ, 628, 129
Kippenhahn, R. & Weigert, A. 1990, Stellar Structure and Evolution, ed. Kippenhahn, R. & Weigert, A.
Krtička, J. 2006, MNRAS, 367, 1282
Krtička, J. & Kubát, J. 2000, A&A, 359, 983
Krtička, J. & Kubát, J. 2004, A&A, 417, 1003
Krtička, J. & Kubát, J. 2006, A&A, 446, 1039
Krtička, J. & Kubát, J. 2007, A&A, 464, L17
Krtička, J. & Kubát, J. 2009, A&A, 493, 585
Krtička, J., Owocki, S. P., Kubát, J., Galloway, R. K., & Brown, J. C. 2003, A&A, 402, 713
Krtička, J., Puls, J., & Kubát, J. 2008, in Clumping in Hot-Star Winds, ed. W.-R. Hamann, A. Feldmeier, & L. M. Oskinova, 111
Kudritzki, R. & Puls, J. 2000, ARA&A, 38, 613
Kudritzki, R. P. 2002, ApJ, 577, 389
Kudritzki, R. P., Pauldrach, A., & Puls, J. 1987, A&A, 173, 293
Kudritzki, R. P., Pauldrach, A., Puls, J., & Abbott, D. C. 1989, A&A, 219, 205
Kudritzki, R. P., Puls, J., Lennon, D. J., et al. 1999, A&A, 350, 970
Kurucz, R. & Bell, B. 1995, Atomic Line Data (R.L. Kurucz and B. Bell) Kurucz CD-ROM No. 23. Cambridge, Mass.: Smithsonian Astrophysical Observatory, 1995., 23
Lamers, H. J. G. L. M. & Cassinelli, J. P. 1999, Introduction to Stellar Winds (Introduction to Stellar Winds, by Henny J. G. L. M. Lamers and Joseph P. Cassinelli, pp. 452. ISBN 0521593980. Cambridge, UK: Cambridge University Press, June 1999.)
Lamers, H. J. G. L. M. & Leitherer, C. 1993, ApJ, 412, 771
Lamers, H. J. G. L. M. & Morton, D. C. 1976, ApJS, 32, 715
Lamers, H. J. G. L. M., Snow, T. P., & Lindholm, D. M. 1995, ApJ, 455, 269

Langer, N. 1989, A&A, 220, 135
Langer, N. 1991, A&A, 248, 531
Langer, N. 1998, A&A, 329, 551
Langer, N., Norman, C. A., de Koter, A., et al. 2007, A&A, 475, L19
Lépine, S. & Moffat, A. F. J. 1999, ApJ, 514, 909
Lépine, S. & Moffat, A. F. J. 2008, AJ, 136, 548
Limongi, M. & Chieffi, A. 2006, ApJ, 647, 483
Loeb, A., Ferrara, A., & Ellis, R. S. 2008, First Light in the Universe, ed. Loeb, A., Ferrara, A., & Ellis, R. S.
Lucy, L. B. 2010, A&A, 512, A33
Lucy, L. B. & Abbott, D. C. 1993, ApJ, 405, 738
Lucy, L. B. & Solomon, P. M. 1970, ApJ, 159, 879
Maeder, A. 1981, A&A, 99, 97
Maeder, A. 1987, A&A, 178, 159
Maeder, A. & Meynet, G. 1987, A&A, 182, 243
Maeder, A. & Meynet, G. 1994, A&A, 287, 803
Maeder, A. & Meynet, G. 1996, A&A, 313, 140
Maeder, A. & Meynet, G. 2000, A&A, 361, 159
Marcolino, W. L. F., Bouret, J., Martins, F., et al. 2009, A&A, 498, 837
Marigo, P., Chiosi, C., & Kudritzki, R. 2003, A&A, 399, 617
Marigo, P., Girardi, L., Chiosi, C., & Wood, P. R. 2001, A&A, 371, 152
Markova, N., Puls, J., Repolust, T., & Markov, H. 2004, A&A, 413, 693
Martins, F., Hillier, D. J., Paumard, T., et al. 2008, A&A, 478, 219
Martins, F., Schaerer, D., & Hillier, D. J. 2005a, A&A, 436, 1049
Martins, F., Schaerer, D., Hillier, D. J., & Heydari-Malayeri, M. 2004, A&A, 420, 1087
Martins, F., Schaerer, D., Hillier, D. J., et al. 2005b, A&A, 441, 735
Massa, D., Fullerton, A. W., Sonneborn, G., & Hutchings, J. B. 2003, ApJ, 586, 996
Meynet, G., Ekström, S., & Maeder, A. 2006, A&A, 447, 623
Meynet, G. & Maeder, A. 2003, A&A, 404, 975
Moffat, A. F. J. & Robert, C. 1994, ApJ, 421, 310
Mokiem, M. R., de Koter, A., Puls, J., et al. 2005, A&A, 441, 711
Mokiem, M. R., de Koter, A., Vink, J. S., et al. 2007, A&A, 473, 603
Muijres, L., de Koter, A., Vink, J. S., et al. 2010a, A&A, accepted (ch. 2)
Muijres, L., Vink, J. S., de Koter, A., Müller, P. E., & Langer, N. 2010b, A&A, submitted (ch. 3)
Müller, P. E. 2001, Ph.D. Thesis, Univ. of Heidelberg, Germany, www.ub.uni-heidelberg.de/archiv/1422
Müller, P. E. & Vink, J. S. 2008, A&A, 492, 493
Nakamura, F. & Umemura, M. 2002, ApJ, 569, 549

Nugis, T. & Lamers, H. J. G. L. M. 2000, A&A, 360, 227
Nugis, T. & Lamers, H. J. G. L. M. 2002, A&A, 389, 162
Oey, M. S. & Clarke, C. J. 2005, ApJ, 620, L43
Oey, M. S. & Massey, P. 1995, ApJ, 452, 210
Oskinova, L. M., Hamann, W.-R., & Feldmeier, A. 2007, A&A, 476, 1331
Owocki, S. P. 1994, Ap&SS, 221, 3
Owocki, S. P. 2008, in Clumping in Hot-Star Winds, ed. W.-R. Hamann, A. Feldmeier, & L. M. Oskinova, 121
Owocki, S. P., Castor, J. I., & Rybicki, G. B. 1988, ApJ, 335, 914
Owocki, S. P. & Cohen, D. H. 2006, ApJ, 648, 565
Owocki, S. P., Gayley, K. G., & Shaviv, N. J. 2004, ApJ, 616, 525
Owocki, S. P. & Puls, J. 1996, ApJ, 462, 894
Owocki, S. P. & Puls, J. 1999, ApJ, 510, 355
Owocki, S. P. & Puls, J. 2002, ApJ, 568, 965
Palacios, A., Arnould, M., & Meynet, G. 2005, A&A, 443, 243
Panagia, N. & Felli, M. 1975, A&A, 39, 1
Pauldrach, A., Puls, J., & Kudritzki, R. P. 1986, A&A, 164, 86
Pauldrach, A. W. A., Hoffmann, T. L., & Lennon, M. 2001, A&A, 375, 161
Pauldrach, A. W. A. & Puls, J. 1990, A&A, 237, 409
Petrovic, J., Pols, O., & Langer, N. 2006, A&A, 450, 219
Press, W. H., Teukolsky, S. A., Vetterling, W. T., & Flannery, B. P. 1992, Numerical recipes in FORTRAN. The art of scientific computing, ed. Press, W. H., Teukolsky, S. A., Vetterling, W. T., & Flannery, B. P.
Prinja, R. K., Barlow, M. J., & Howarth, I. D. 1990, ApJ, 361, 607
Prinja, R. K. & Massa, D. L. 1998, in Astronomical Society of the Pacific Conference Series, Vol. 131, Properties of Hot Luminous Stars, ed. I. Howarth, 218
Puls, J. 1987, A&A, 184, 227
Puls, J., Kudritzki, R., Herrero, A., et al. 1996, A&A, 305, 171
Puls, J., Kudritzki, R., Santolaya-Rey, A. E., et al. 1998a, in Astronomical Society of the Pacific Conference Series, Vol. 131, Properties of Hot Luminous Stars, ed. I. Howarth, 245
Puls, J., Markova, N., Scuderi, S., et al. 2006, A&A, 454, 625
Puls, J., Springmann, U., & Lennon, M. 2000, A&AS, 141, 23
Puls, J., Springmann, U., & Owocki, S. P. 1998b, in Cyclical Variability in Stellar Winds, ed. L. Kaper & A. W. Fullerton, 389
Puls, J., Vink, J. S., & Najarro, F. 2008, A&A Rev., 16, 209
Repolust, T., Puls, J., & Herrero, A. 2004, A&A, 415, 349
Runacres, M. C. & Owocki, S. P. 2002, A&A, 381, 1015
Runacres, M. C. & Owocki, S. P. 2005, A&A, 429, 323
Salpeter, E. E. 1955, ApJ, 121, 161

Schaerer, D. & de Koter, A. 1997, A&A, 322, 598
Schmutz, W. 1991, in NATO ASIC Proc. 341: Stellar Atmospheres - Beyond Classical Models, 191
Shaviv, N. J. 1998, ApJ, 494, L193
Shaviv, N. J. 2000, ApJ, 532, L137
Smith, N. & Conti, P. S. 2008, ApJ, 679, 1467
Smith, N., Vink, J. S., & de Koter, A. 2004, ApJ, 615, 475
Sobolev, V. V. 1960, Moving envelopes of stars, ed. V. V. Sobolev
Springmann, U. 1994, A&A, 289, 505
Springmann, U. W. E. & Pauldrach, A. W. A. 1992, A&A, 262, 515
Spruit, H. C. 2002, A&A, 381, 923
Sundqvist, J. O., Puls, J., & Feldmeier, A. 2010, A&A, 510, A11
Tenorio-Tagle, G. & Bodenheimer, P. 1988, ARA&A, 26, 145
van der Sluys, M. V. & Lamers, H. J. G. L. M. 2003, A&A, 398, 181
van Marle, A. J., Owocki, S. P., & Shaviv, N. J. 2008, MNRAS, 389, 1353
Vink, J. S. 2000, PhD thesis, Universiteit Utrecht
Vink, J. S. 2006, in Astronomical Society of the Pacific Conference Series, Vol. 353, Stellar Evolution at Low Metallicity: Mass Loss, Explosions, Cosmology, ed. H. J. G. L. M. Lamers, N. Langer, T. Nugis, & K. Annuk, 113
Vink, J. S., Brott, I., Gräfener, G., et al. 2010a, A&A, 512, L7
Vink, J. S., Davies, B., Harries, T. J., Oudmaijer, R. D., & Walborn, N. R. 2009, A&A, 505, 743
Vink, J. S. & de Koter, A. 2002, A&A, 393, 543
Vink, J. S. & de Koter, A. 2005, A&A, 442, 587
Vink, J. S., de Koter, A., & Lamers, H. J. G. L. M. 1999, A&A, 350, 181
Vink, J. S., de Koter, A., & Lamers, H. J. G. L. M. 2000, A&A, 362, 295
Vink, J. S., de Koter, A., & Lamers, H. J. G. L. M. 2001, A&A, 369, 574
Vink, J. S., Muijres, L., Anthonisse, B., et al. 2010b, A&A, in preparation (ch. 4)
Walborn, N. R., Ebbets, D. C., Parker, J. W., Nichols-Bohlin, J., & White, R. L. 1992, ApJ, 393, L13
Weidner, C. & Kroupa, P. 2004, MNRAS, 348, 187
Woosley, S. E. & Heger, A. 2006, ApJ, 637, 914
Wright, A. E. & Barlow, M. J. 1975, MNRAS, 170, 41
Wyithe, J. S. B. & Loeb, A. 2003, ApJ, 586, 693
Yoon, S. & Langer, N. 2005, A&A, 443, 643
Yoon, S., Langer, N., & Norman, C. 2006, A&A, 460, 199
Yungelson, L. R., van den Heuvel, E. P. J., Vink, J. S., Portegies Zwart, S. F., & de Koter, A. 2008, A&A, 477, 223

List of publications

Refereed journal paper

- **Muijres, L.**; de Koter, A.; Vink, J. S.; Krtička, J.; Kubát, J.; Langer, N., "Predictions of the effect of clumping on the wind properties of O-type stars", accepted by **A&A**.

In preparation

- **Muijres, L.**; Vink, J. S.; de Koter, A.; Müller, P. E.; Langer, N., "Predictions for mass-loss rates and terminal wind velocities of massive O-type stars", submitted to **A&A** 2010.

- Vink, J. S.; **Muijres, L.**; Anthonisse, B.; de Koter, A.; Gräfener, G.; Langer, N., "Wind models for very massive stars up to 300 solar masses", *to be submitted* to **A&A** 2010.

- **Muijres, L.**; Vink, J. S.; de Koter, A.; Langer, N.; Yoon, S.-C., "Predictions of the mass-loss rates for evolved very metal-poor massive stars", *to be submitted* to **A&A** 2010.

Conference proceedings

- de Koter, A.; Vink, J. S.; **Muijres, L.**, "Constraints on wind clumping from the empirical mass-loss vs. metallicity relation for early-type stars". Proceedings

of the workshop “Clumping in Hot-Star Winds”. Edited by W.-R. Hamann, A. Feldmeier, and L. M. Oskinova. 2008., p.47

- Krtička, J.; **Muijres, L.**; Puls, J.; Kubát, J.; de Koter, A., “The influence of inhomogeneities on hot star wind model predictions”. Proceedings of the IAU Symposium “The Art of Modeling Stars in the 21st Century”. Edited by L. Deng and K. L. Chan. 2008., p.283

- **Muijres, L.**; de Koter, A., “The Effect of Clumping on Predictions of the Mass-Loss Rate of Early-Type Stars”. Proceedings of “First Stars III Conference”. Edited by B. W. O’Shea and A. Heger. 2008.,p.209

Acknowledgements

For the Quest is achieved, and now all is over. I am glad you are here with me. Here at the end of all things, Sam.

J.R.R. Tolkien

Like Frodo's epic journey to Mordor, the path to the production of a thesis is fortunately not a lonely one. It would have been impossible for me to achieve this goal alone. There are many people that contributed to this work. First of all, I would like to thank Alex de Koter, who had to put up with "I have one more question" for four years. Thank you for answering all of them so patiently! I enjoyed our many scientific discussions and, perhaps even more, our political ones. I hope that by the time that this thesis is printed we will finally have a government honouring the liberal tradition of our country and our constitution. We will see. Jorick Vink, I really got inspired by our meetings in Amsterdam and Armagh. Our discussions were occassionally very heated but I must say that I still get really scared when Alex and you discuss football. You even remember details of matches from your childhood – respect! Thanks for your great sense of humour! I still say that I am vegetarian, even though I will never convince you of the truth. Norbert Langer, during the last half of my journey, we had very frequent meetings in Bonn. This really helped me to gain a deeper understanding of the field of stellar evolution. I enjoyed it a lot. Thanks!

I had a great time at the Astronomical Institute "Anton Pannekoek" of the University of Amsterdam. The atmosphere is very friendly and I made many friends. Evghenii, you once advised me never to trust Russians that I meet on the street. I guess that trusting you was a crazy undertaking but one of the best of my life. I really enjoy our friendship. Dominik, you are definitely crazy! Thanks for your humour! Lucinda, I hope to continue our many discussions on our favourite subject. Maithili, thank you for our late night chats and remember that Mister Longbottom is mine. Paolo, still the unbeaten Italian of the year, grazie di tutto. Dave, that bottle of wine

I stole from you on the plane was just not enough, but thanks a lot! Valeriu, the vampire, I enjoyed our dancing classes together. Alessandro, next time I will really poison you at dinner. Samia my Theist-Christian-Muslim friend. Rudy, bedankt voor al je steun. Joop, het was een genoegen met jou te discussiëren! Yuri, your help with the typesetting of this document was great. Joke, Salome and Marc, Nathalie, Eduardo, Bart, Theo, Montse, Diego, John and Daniela, Hanno, Ken, Asaf, Gemma, Kostadinos, Patrick, Richard, Atish, Ramanpreet and Aadi, Gijs, Thijs, Casey and Jessica, Anna, Anastasia, Lucas, Peter Polko, Hugues, Maciej, Mihkel, Gerrit, Rens, Jaap, Carsten, Huib, Lex, Evert, Martin, and also Ines from the University of Utrecht, thanks to all of you for the nice times. Mehtap, I hope we continue our crazy plans. Nabi, tashakor mikoni for all your help with Farsi. Minou, Lidewijde, Esther, Eva, and Milena, thanks for all your support! Thanks to all the APIs!

The journey of my PhD started a long time before I came to work at API. Living in Brasil and working as a volunteer I started to think about it. This experience helped me to become more firm. I saw an aspect of the world that is hidden from most people here in the Netherlands. My Brazilian friends taught me how to really enjoy life the most:

A vida não é só trabalho. A minha vida me levou até Diamantina, Minas Gerias, Brasil, até um cantinho esquecido do mundo onde o tempo parece ter parado.
Agradeço muito aos meus amigos brasileiros: Eloiza, Soraia, Sandra, Éricka, Ana Luiza, Flávio, Assis, Regina, Rogério, Henrique, Fernanda, Dona Joaquina, Senhor Arlindo, e todos os outros da família Farias, Ney, Rodrigo, Marcelo, Paulo, Valdirene, e Samuel. A gente dançou até amanhecer, a gente nadou nas cachoeiras frias de Minas Gerias, a gente tomou cerveja, a gente tomou mais cerveja e cachaça, a gente riu, a gente chorou, a gente foi na praia, a gente viveu a vida boa. Obrigada por tanta alegria.

Aos meus alunos brasileiros, só queria dizer: o tempo compartilhado foi curto, muito curto, mas mudou a minha vida. Nos meus pensamentos sempre estarei com vocês: subindo os cerros de Diamantina, vocês falando demais e eu correndo rapido para não chegar tarde. Tia, me dá a mão, tia, me leva, tia, tia... Vocês tem a liberdade de fazer alguma coisa com as suas vidas. Nunca desistam! Obrigada pela confiança, pela amizade.

Vladímir, gracias por insistir tanto que visitara Bucaramanga. Te agradezco mucho por contarme: “Hace dos semanas la guerilla dejó volar este puesto de peaje.”, justo al pasar. Si lo hubiese sabido antes, no hubiera ido a Colombia. Roberto, mi querido hermano chileno, he pensado mucho en esos días que paseábamos juntos por Santiago, nuestro Santiago querido. Espero volver pronto, ojalá. Erika gracias por acompañarme tantas veces en una de las épocas más grises de mi vida.

Nina, vielen Dank für die Zeit, die wir zusammen im Bonn verbracht haben. Ich habe mich immer auf meine Reisen nach Bonn gefreut, weil ich gewusst habe, dass

wir uns wieder treffen werden.

Catalina, Axel, and Vincent, thanks for the music, nice dinners, and the parties here and in Chile.

Saskia en Willem, bedankt voor alle steun door de jaren heen, dank voor jullie onvoorwaardelijke vriendschap. Remco, bedankt voor alle discussies over ons werk!

Manon, al die jaren ben ik niet van je afgekomen, basisschool, middelbare school en universiteit. Als ik naar Zuid-Amerika ging, jij ook. Hopelijk duurt het nog heel lang voordat ik je eindelijk kwijt raak.

Tot slot wil ik graag mijn hele familie bedanken. Het leven geeft ons niet altijd dat wat we willen maar gelukkig zijn het de mooie mooie herinneringen die blijven. Els, mijn lieve buurvrouw, graag zou ik willen dat je nog bij ons kon zijn. Je was mijn steun en toeverlaat, altijd... Mijn oma Tiny en oma Mia (ook al ben jij er helaas niet meer bij): bedankt voor alle verhalen over vroeger die me geleerd hebben om mijn leven in een heel ander licht te zien! Mijn vader Math en moeder Marly: ooit kreeg ik van jullie een techniek-kit cadeau, ik denk dat dat het begin van mijn interesse in de natuurwetenschappen was. Bedankt voor alle aanmoediging! Bedankt dat jullie me de vrijheid gegeven hebben om te zijn wie ik ben! Mijn zus Marill: bedankt voor de gezelligheid en soms een luisterend oor! Danny: bedankt voor het mooie ontwerp op de boekenlegger! Mijn broer Michiel: eindelijk heb ook jij je weg gevonden! Daar ben ik blij om en de resultaten mogen er zijn! Bedankt voor de mooie bijdrage aan de kaft van mijn thesis!

Lianne